Synthesis and Characterization of Si, Ge, and Si_xGe_{1-x} Nanowires by Fiber Drawing

Adam R Floyd

Thesis submitted to the faculty of the Virginia Polytechnic Institute and State University in partial fulfillment of the requirements for the degree of

Masters of Science

In

Materials Science and Engineering

Gary R. Pickrell- Chair
David E. Clark
William T. Reynolds

May 13, 2019
Blacksburg, VA

Keywords: Silicon, germanium, SiGe alloys, nanowires, optical fiber

Synthesis and Characterization of Si, Ge, and Si_xGe_{1-x} Nanowires by Fiber Drawing

Adam R Floyd

ABSTRACT

This research provides a method of using a mixed powder in tube approach for producing and characterizing large quantities of highly oriented, high aspect ratio semiconductor nanowires in an inherently safe and contained manner. This work modifies the previously used mixed powder method to produce significantly smaller features below 100nm in diameter. For the first time SiGe alloys are produced in optical fiber from a mixture of the two powders across the entire compositional range.

A discussion of the properties of silicon and germanium and their alloys is given with emphasis on the differences between properties at the bulk scale and at the nanoscale. The limitations of silicon and germanium for photonic applications, due to their indirect band gap nature, is removed when these materials are reduced to the nanoscale. A brief discussion of ways that these properties can be modified is given with size, composition, and strain all being viable factors of control.

The optical and electrical properties of these nanowire arrays is evaluated as a function of the size, number of wires, and composition. A clear dependence between size and quantity of wires was observed with respect to composition. The nanowires were found to have complex interactions with light showing high absorption as well as unique transmission characteristics. Arrays of these fibers were able to create a measurable photocurrent and provide potential uses for detection of light and other photonic applications.

An understanding of the etching necessary to both expose these nanowires for analysis as well as completely remove them from the glass matrix was developed. Etch rates in these areas was

observed to be higher than reported etch values. Etching with dilute solutions was found to allow removal of the wires cleanly and allow recovery of them for other applications.

Synthesis and Characterization of Si, Ge, and Si_xGe_{1-x} Nanowires by Fiber Drawing

Adam R Floyd

General Audience Abstract

This research provides a method of using a mixed powder in tube approach for producing and characterizing large quantities of highly oriented, high aspect ratio semiconductor nanowires in an inherently safe and contained manner. These wires are over 1000 times smaller than thickness of a human hair are made using traditional fiber drawing methods or pulling at high temperatures. These fibers differ from traditional optical fibers in that they are produced from a tube filled with powder instead of a solid glass rod. This is similar to the same method used to produce wires in other materials such as copper. The use of the glass to contain the semiconductor material allows us to increase the temperature it is pulled at above the melting point. The liquid material is then drawn into the very small sizes using pores in the glass powder it is mixed with. This allows these wires to be produced in much longer lengths, larger quantities, and easier than previous methods.

These nanowires are produced from silicon and germanium, which are two of the most important materials currently used in electronics. These semiconductors are used in most electronics, solar cells, and LEDs that are used in everyday life. Silicon and germanium while very important materials have limitations in photonic applications, interactions with light. The properties of the materials for these applications can be improved by reducing them in size to the nanoscale.

The wires produced in this research were evaluated to determine if they possessed the more ideal properties. The wires were found to have detectable photocurrent, electricity generated from light. This is the primary property that is needed in solar cells. The wires produced in this method are an important early step to improving solar cells efficiency and reliability. These

wires have benefits over other forms of silicon because they are produced with protective glass coating in a single step.

Acknowledgements

I would like to thank my advisor, Dr. Gary Pickrell, for his support and guidance in carrying out this work. I am extremely grateful for his patience during the learning process and help navigating the challenging issues that I encountered developing the processes needed for this work.

I would also like to thank Dr. Dan Homa for his guidance and training in operation of the optical fiber draw tower. Dan's experience with traditional optical fiber processing and equipment was invaluable in helping me learn to develop and carry out this research.

Table of Contents

Table of Figures

List of Tables

Introduction

Semiconductors have found ever-increasing use in light generation and detection as well as other photonic applications. These applications are traditionally best fulfilled by the compound III-V semiconductors (e.g. GaP, GaAs, InP, InAs) and some II-VI semiconductors.[1] These semiconductors are used due to their direct band gap nature and due to the tunable nature of the band gap in some cases. This nature of the band gap is also what has limited the use of silicon and germanium in these applications. Silicon and germanium unlike the compound semiconductors have indirect band gaps and as a result are limited in their efficiency in producing or collecting light. III-V semiconductors are very advantageous due to their direct nature and optical properties but are limited by their integration with silicon-based systems and their cost. Development of methods to control the type and energy of the band gap provides a useful way to greatly improve these materials in photonic applications. The direct band gap provides for improved absorption characteristics in light detecting applications and allows for increased light generation capabilities.

Development of germanium and silicon nanostructures has led to the discovery of changes in the band gap behavior. Silicon and germanium are desired for photonic applications due to the ease of integration into existing silicon-based electronics. Manipulation of the bandgap using a variety of techniques has been shown to be possible. Nanowires in particular have shown great promise due to the tunable nature of the bandgap with size and even the change to direct behavior is possible. Currently nanowires are produced using a variety of growth mechanisms that require significant substrate preparation and controlled conditions.[2] These methods are useful in

producing nanowires but integration of these structures into existing applications has been costly and challenging.

Integration of electronic and optical devices has also been limited and is desired for ideal photonic applications. Light detection or generation currently takes place outside of optical fibers and then has to be coupled into or out of fibers before being useful. An ideal system would allow for the integration of these features directly into an optical fiber and would be a significant step forward in optoelectronic applications. Several semiconductors have already been directly integrated and drawn into optical fibers including both silicon and germanium as well as compound semiconductors.[3-7] A continuation of producing both silicon and germanium in optical fibers is producing them in a way that allows for more useful photonic properties.

Work done by Ayers[8] developed a method for producing arrays of metallic wires in glass fibers by using a mixed powder method. This process was used to produce large arrays of different metallic materials such as germanium, copper, and some iron alloys. This method was shown to produce arrays of wires with sizes ranging from 0.1-6 microns and lengths in the centimeter range.

Using this mixed powder in tube method to produce nanowires is possible by controlling the powder sizes and composition as well as the preform dimensions and draw conditions. This research focuses on understanding the conditions needed to produce wires of silicon and germanium and their alloys to produce large numbers of wires with diameters below 100nm. One of the goals of this research is to understand how to produce wires small enough to alter the band gap behavior from the indirect behavior exhibited by the bulk materials. Features of silicon and

germanium nanostructures have been shown to be different from the bulk, especially with respect to the band gap properties.

Production of these nanowires in the optical fiber allows for potential use in more photonic applications while utilizing the well-studied and cheaper silicon and germanium systems, which have already been successfully integrated into optical fibers. The array of wires also opens the possibility for multiple structures in the fiber to be manipulated independently with post processing versus the single core semiconducting structures that have already been produced.

The limiting size of features produced is not well understood for this method, nor are the factors that directly control the drawdown of the semiconducting particles. The size of the features produced directly affects the mechanical stability of the fiber due to the high stress states created by the volume expansion of these semiconductors during solidification. The size of the wires produced is controlled not only by the size of the molten droplets of semiconductor present but also by the pore sizes of the glass powder particles present in the region. It is influenced by the draw down ratio (size of the starting preforms versus the final fiber size), draw speed, composition of the molten semiconductor and glass regions, and potential coalescence of the semiconductor regions. The composition of the glass and semiconductor has a major effect on drawing due to changes in the viscosity and surface tension of these systems. Micron sized features of these materials have been observed to be polycrystalline but it is unclear whether that behavior is still present when size is below 100nm.

This research focuses on understanding the drawing conditions necessary to produce nanowires in the range of alloys across the full composition range of the Silicon-Germanium system. It also

focuses on understanding the powder size and composition necessary to produce sufficiently small wires and sizes capable of being produced. Furthermore, this work investigated the properties of the nanowires focusing on crystallinity, composition, and band gap. Characterization of the optical absorption properties of the semiconductor allows for the behavior and value of the bandgap to be studied. Light generation capabilities are also studied to determine the potential use of these arrays of nanowires in these applications.

Background

1.1 Properties of Silicon and Germanium

One of the most important properties of semiconductors in photonic applications is the bandgap. This key property of semiconductors arises due to the bonding and structure resulting in the valence and conduction band being separated by a small bandgap. In semiconductors at 0K the valence band is completely filled with electrons while the conduction band is completely void of electrons. At temperatures above 0K, thermal energy can provide the necessary energy to move an electron from the valence band into the conduction band. This process generates both the electron in the conduction band as well as a corresponding hole in the valence band. Both electrons and holes contribute to electrical conduction processes in semiconductors. Periodically electrons that are present in the conduction band in a semiconductor crystal encounter holes in the valence band. A process known as recombination occurs at this point and involves the electron dropping from the conduction band and filling the hole in the valence band. The process of an electron dropping to a lower energy state in the valence band expends excess energy in various forms depending on the type of bandgap in the semiconductor.[1]

Two different types of band gaps exist in semiconductors, direct and indirect, and are dependent on the band structure. The differences in these types of semiconductors arise from the conservation of momentum of an electron. The easiest method for determining the bandgap nature of a semiconductor is to examine an E-k diagram. E-k diagrams are plots of energy versus crystal momentum. A simplified plot for both an indirect and a direct bandgap semiconductor is shown below in Figure 0-1.

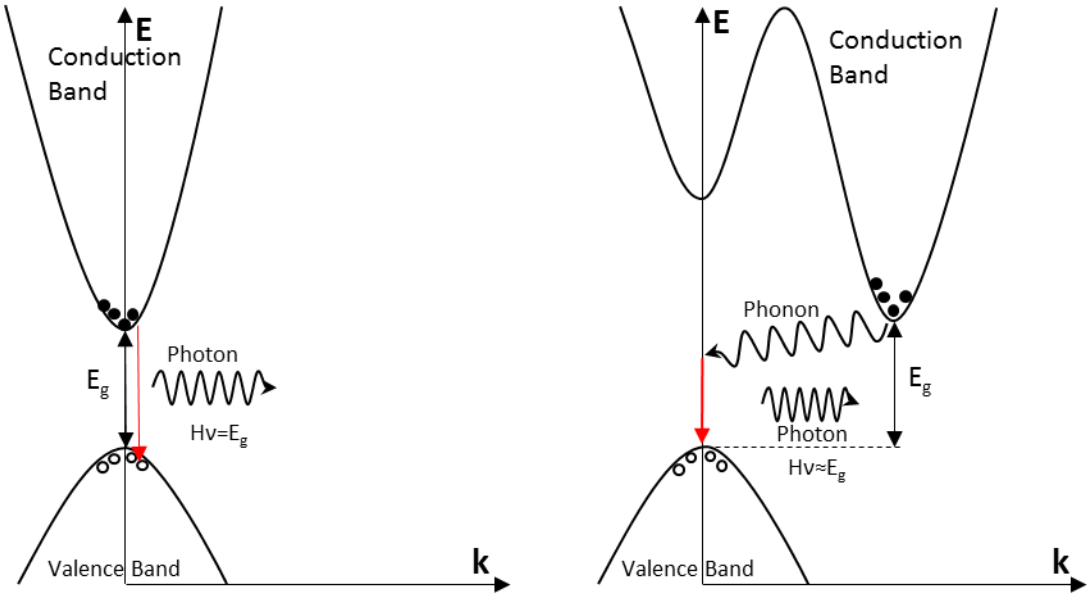

Figure 0-1: E-k plot of Direct and Indirect bandgap type materials demonstrating Photoluminescence.

The feature from the plots that determines whether a bandgap has direct behavior depends on the location of the minimum energy point in the conduction band in relation to the maximum energy value in the valence band. When the minimum and maximum value line up in the k vector, the behavior is direct as is the case in Figure 0-1 for GaAs. When the minimum and maximum do not match up along the k-vector, the behavior is indirect, meaning that recombination cannot occur without a phonon to conserve momentum. In the case of light generating applications, recombination must occur frequently enough for efficient use. This limits the use of any indirect bandgap semiconductor in these applications. This limitation has greatly diminished the usefulness of silicon and germanium, which are both indirect in their bulk forms.

Importance of the bandgap lies not only with the nature of the bandgap but also with the value of it. The energy of the bandgap is the same quantity of energy as that of the photon that is emitted during recombination. The energy of the photon corresponds to the wavelength of light that is

emitted. The bandgaps for Silicon and Germanium are 1.12eV and 0.66eV respectively. These values correspond to the energy of photons generated as well as the maximum wavelength of light that can provide enough energy to excite the electron. In this case, the wavelengths of light corresponding to these bandgaps are 1.11 microns for silicon and 1.87 microns for germanium.[1] These wavelengths are within the infrared region of light, which is useful to the telecommunications industry at wavelengths of 1.3 and 1.55 microns, which are commonly used today to transmit information.

For silicon and germanium to be of true use for light generating applications, the bandgap behavior needs to be modified to be direct as well as be able to be tuned to more usable values. Research has shown multiple ways for modifying and tuning the bandgap in both silicon and germanium. Quantum confinement [9-11], alloying [12-15], and strain [12, 14, 16, 17] have all been shown capable of changing the bandgap structure of silicon and germanium. These methods show the potential of creating silicon and germanium devices for many different photonic applications and improving integration into existing systems. Silicon nanowire structures have already been successfully created to produce appreciable generation of light in the visible spectrum.[18] These nanowires, which were less than five nanometers in diameter, successfully produced light when encapsulated in a dielectric material and coupled to an AC electric field. This light was generated as a broad peak at 600nm indicating a significant shift in the bandgap from the 1.1-micron wavelength that corresponds to the bulk band gap. It has also been shown that the diameter as well as crystal orientation has a large effect on the bandgap of both silicon and germanium.[11, 19] Finally strain has also been successfully shown to modify the bandgap as well.[16, 20, 21] These experiments have shown that the while silicon and germanium are not

traditionally useful in photonic applications due to their indirect bandgap; recent developments have shown that several different methods are possible for modifying the bandgap.

Alloys of Germanium and Silicon present interesting opportunities in bandgap tuning. The phase diagram for silicon-germanium is shown below in Figure 0-2.

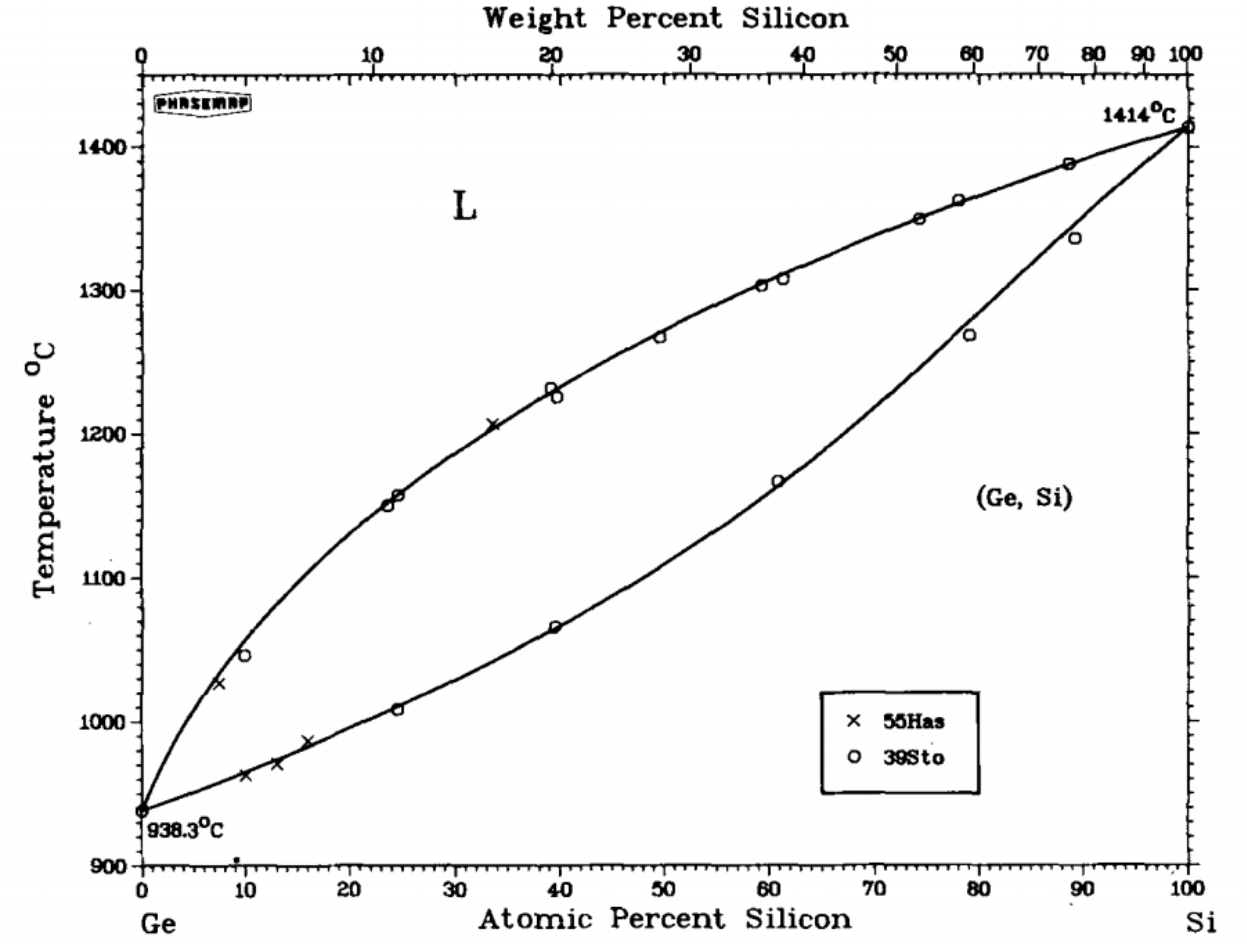

*Figure 0-2: Phase Diagram of Silicon-Germanium. Reprinted from "The Ge–Si (Germanium-Silicon) system." R. W. Olesinki and G.J. Abbaschian, 1984, Bulletin of Alloy Phase Diagrams **5**(2): 180-183. Copyright 1984 Springer. Reprinted with Permission.[22]*

The phase diagram shows that a solid solution is formed across the entire composition range. This is beneficial as the bandgap is a function of the composition and can be varied over the

entire range. Nanowires have been synthesized using CVD methods across the entire composition range in the work done by Yang.[15] This work showed that nanowires could be produced in a variety of sizes and compositions. The bandgap has been observed to be tunable in nanowires over the range of 0.68 to 2.25eV.[15] This showed that with alloying the bandgap can be varied from the mid-IR well into the visible range of light. The bandgap has been shown to vary across the composition range as well as with the diameter of the nanowires. This work measured the fundamental bandgap across all samples by measuring the optical absorption edge. The composition was calculated based on the XRD peak of the (111) plane. These experiments show that composition is an effective method for tuning the bandgap of nanowires from the near IR region into the visible light spectrum.

Strain has also been shown to be very useful in modifying the bandgap structure of both germanium and silicon.[17, 20, 23-25] These experiments have shown experimentally the strain is capable of changing the bandgap structure of these materials and in some cases can cause the material to behave in a direct manner. Bandgap changes arise from strain alterations in the lattice parameter and both tensile and compressive strains can alter the value and behavior of the bandgap. Biaxial tension has been modeled and shown to greatly increase light output in germanium nanomembranes.[17] This work has also shown that 2% strain can be generated which is above the predicted value needed to induce the change to direct behavior. Additionally strain effects on silicon nanowires have been theoretically modeled and this has shown that both tensile and compressive strains have varying effects depending on crystal orientation.[20] Strain effects on the bandgap can greatly increase the ability to tune and modify bandgap in these

semiconductors. Applications of tensile strain are of particular interest due to the aligned in-fiber nature of nanowires produced for this work.

In addition to these methods of bandgap modification, doping also plays a role in the optical properties of these semiconductors. Doping plays an irreplaceable role in silicon and germanium-based electronics. These benefits primarily focus around the increased in charge carriers provided by the doping elements. In some cases, this doping can also aid in providing appreciable light generation. In particular, heavy n-type doping in germanium has shown significant improvement in the light generating efficiency when combined with strain. Figure 0-3 below shows the bandgap structure of germanium as well as the changes strain and doping have.

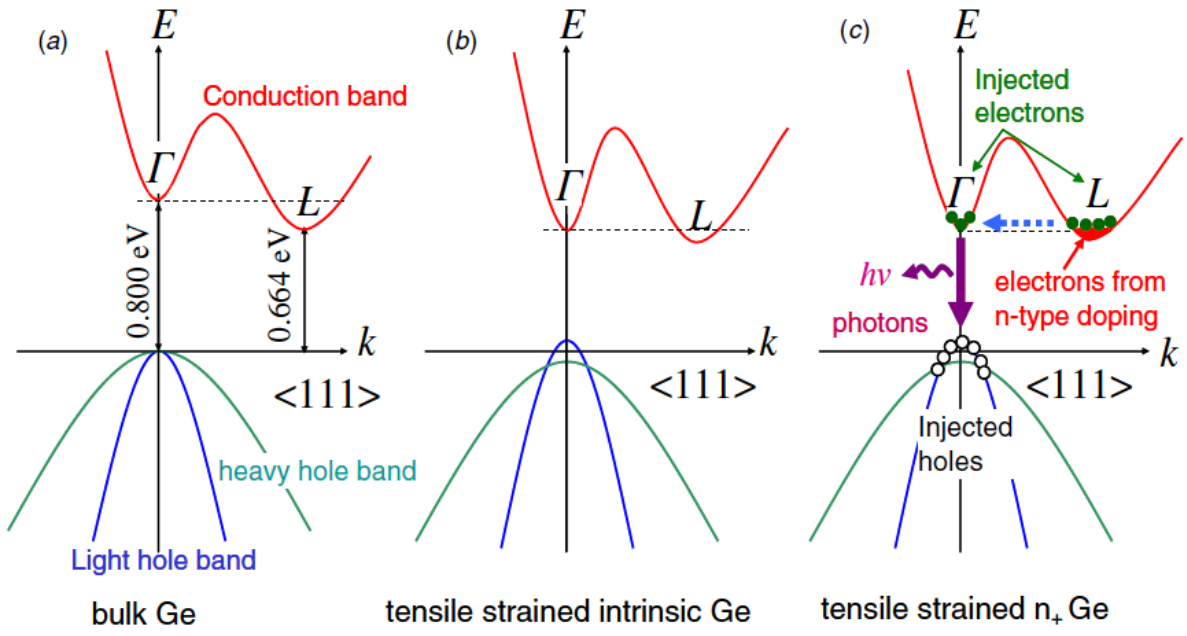

Figure 0-3: Bandgap Structure of Germanium demonstrating the lowering of the Gamma valley by strain and the effects of n-type doping.[23]

Figure 0-3 a) shows the bandgap structure of bulk germanium along with the values for both the direct (Γ-valley) and the indirect (L-valley) gaps. In b) it shows that the applied strain is capable of producing a lowering of the direct bandgap energy. The strain provided brings the direct gap energy lower and is capable of producing a direct band gap transition with no other means needed. In c) this shows the effect of strain on a heavily n-type doped germanium. The electrons provided by the doping fill the bottom of the L-valley causing the injected electrons to be forced into the Γ-valley and recombine with holes undergoing a direct transition.[23]

In addition to the bandgap, several other properties of these semiconductors are very important to this research. The resistivity and absorption characteristics of these semiconductors are relevant to applications of these wires and have been shown to have differences at the nanoscale from their bulk values. The absorption characteristics in silicon nanowires has been studied for its use in solar applications. [26] This work has primarily focused on evaluating and comparing arrays of nanowires to bulk thin films to determine optimal optical properties for the solar cell application. The work done by Hu and Chen (2007) found that reflection was drastically reduced for these nanowire arrays with significantly higher absorbance that depended both on length and width of the nanowires. The resistivity of semiconductor nanowires has also been studied and observed to be orders of magnitude lower than their bulk counterparts. The resistivity of doped and undoped silicon as well as germanium has been measured.[27-30] In all this work the resistivity was measured to be several orders of magnitude lower than the established bulk values for germanium and silicon.

Several other properties of the semiconductors are of importance to the drawing behavior and stability of the fibers as a whole. Surface tension between the molten semiconductor and the

glass surface, volume expansion during solidification, and elastic properties of the solid semiconductor all greatly affect how the wires draw and the mechanical stability of the drawn fiber.

1.2 Semiconductor Fiber Production

Optical fibers in the traditional sense consist of fused quartz cladding with a doped fused quartz core to give it a higher refractive index. In recent years, new core materials have been investigated to provide a variety of improved properties including longer transmission windows. Production of semiconductor core fibers has been attempted with a variety of materials and methods.[3] The information below covers some of the relevant materials that have been successfully used as cores in fibers and the methods used to produce them. It also then covers some of the common problems and properties of these semiconductor materials that have been observed in previous research.

Fibers that have both silicon and germanium cores as well as compound semiconductors have been produced with fused quartz claddings. In these cases, the core is comprised of a single solid semiconductor in the micron size range. In the cases of fibers produced both at Virginia Tech and at Clemson, the semiconductor core material is provided by either a core drill hole filled with a solid rod of semiconductor or powder sources.[4, 31] In these cases, the fiber is heated until the semiconductor is in a molten state and the silica fiber becomes soft enough to pull. Some fibers produced in these methods exhibited cracking at the interface of the semiconductor and the glass cladding. The loss of mechanical stability and damage to the glass matrix can be explained by looking at the high stress environment created by the solidification of the

semiconductors. Silicon and germanium both have lower densities in the solid state than in liquid and the percent difference is shown below in Equation 1 and 2.

$$\%\ Density_{Si} = \frac{\rho_{l,Si} - \rho_{s,Si}}{\rho_{l,Si}} x100 = \frac{2.57\frac{g}{cm^3} - 2.329\frac{g}{cm^3}}{2.57\frac{g}{cm^3}} x100 = 9.4\% \quad (1)$$

$$\%\ Density_{Ge} = \frac{\rho_{l,Ge} - \rho_{s,Ge}}{\rho_{l,Ge}} x100 = \frac{5.6\frac{g}{cm^3} - 5.323\frac{g}{cm^3}}{5.323\frac{g}{cm^3}} x100 = 5.2\% \quad (2)$$

These equations show that the solid state of the semiconductors is around 5% and 10% less dense than their liquid states respectively. This change in density directly correlates to an increase in the volume of the solid state of these semiconductors. This volume expansion creates a high stress state in the glass leading to the cracking that is observed. Fused silica has a very high theoretical ideal strength >18GPa and has been observed in real world fiber tests near 5GPa.[32] The primary cause of loss of strength in silica glass is defects and the presence of water vapor which aids in crack propagation. The glass is expected to have a very high strength at the surface to the semiconductor. This surface is produced next to a liquid in a vacuum environment which should produce a surface with minimal defects and eliminate the presence of water vapor. These factors indicate that for cracking to occur high stresses must be caused by the pressure of the solidifying semiconductor. The semiconductor cores in these experiments were found to be pure semiconductor with no unexpected contamination or oxidation.[4, 33] The absence of contaminants combined with the large volume increase upon solidification illustrate the cause of cracking observed in the glass around the features. Smaller features of semiconductor have been observed without cracking in the glass indicating that a trapped stress state is present in the semiconductor and surrounding glass.

Further analysis on semiconductor fibers was carried out to understand the properties of the semiconductors. Some of these experiments used both x-ray diffraction (XRD) and electron backscatter diffraction (EBSD) to study the crystal structure of the semiconductor core fibers. The results from XRD studies in germanium have shown that the fiber appears single crystal over long lengths with a (111) orientation.[33] EBSD on silicon samples has shown that the fiber is polycrystalline with grains that extend across the entire diameter of the core and are several microns in length.[4]

Semiconductor fibers exhibit different drawing behavior compared to fibers produced entirely of glass. In these fibers, small glass tubes are created as the glass powder matrix is drawn creating capillaries that the semiconductor then fills. This phenomenon was observed in previous research with a single semiconductor core where the glass could be observed to draw as a tube until a critical pressure sucked the semiconductor down the tube. This behavior is expected to continue as the size scale is reduced. Capillary pressure is governed by the Young-Laplace equation shown below as Equation 3 and rewritten for liquid moving through a capillary tube in Equation 4.

$$\Delta p = \gamma \left(\frac{1}{r_1} + \frac{1}{r_2} \right) \tag{3}$$

$$\Delta p = \gamma \left(\frac{2 \cos \theta}{R} \right) \tag{4}$$

These equations show that the capillary pressure is controlled by the contact angle between the materials, the radius of the capillary, and the surface tension of the liquid. These variables shown schematically in Figure 0-4 below.

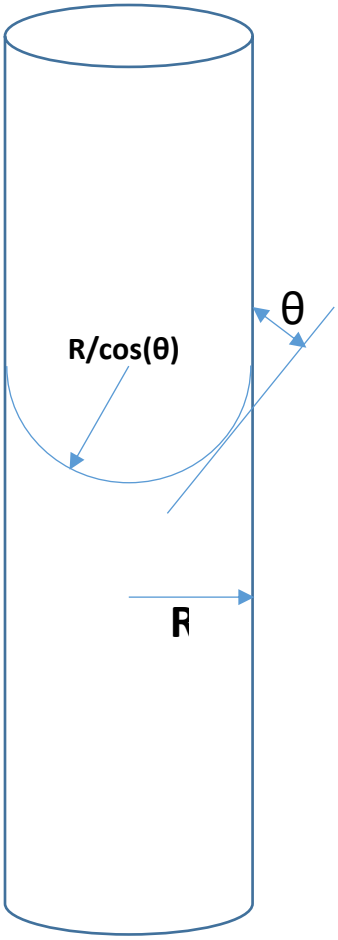

Figure 0-4: Schematic of liquid being drawn in a capillary tube with variables from Equation 4

The surface tension and wetting angle are 700-850mN/m and 85° for silicon and 575-650 mN/m and 150° for germanium.[34-36] Plugging these values into Equation 4 shows that germanium will experience much higher capillary pressure than silicon and exhibit much better drawing. The high wetting angle combined with lower melting temperature and lower volume expansion indicate that germanium should produce longer smaller wires than silicon.

In addition to producing semiconductor core fibers in a traditional fiber pulling method with a molten core approach, semiconductor core fibers have also been made via CVD methods. In

these methods a fused silica tube is drawn down to dimension and semiconductor cores are deposited using a high pressure CVD process.[37] These fibers were produced by the high-pressure CVD process using silane and germane as precursors. Quartz tubes were drawn down to micron size tubes and semiconductor was deposited through the tapered length of the tubes. This leads to a semiconductor tube deposited on the inside surface of the glass tube. These experiments also showed that by controlling the decomposition temperature of the precursor gases you could deposit both amorphous and crystalline thin films.

1.3 Powder Packing

Understanding the nature and behavior of the powder is important to understand and control the drawing characteristics to produce wires of the desired size. The primary factor used for understanding the drawing is the drawdown ratio. The drawdown ratio of a fiber is defined as the ratio of the starting diameter of the preform to the final diameter of the fiber produced. In traditional optical fiber this ratio is the same for the core and cladding regions. The work previously done on mixed powder based preforms showed that the drawdown ratio of the core region differed considerably from the drawdown ratio of the outer diameter of the preform.[8] The difference in these drawdown ratios is a result of powder material being used and the void space present in a powder.

The powder sizes, shapes, and packing density govern the nature of the core and the starting point for the drawing conditions to be determined. The powder composition and packing are the two most important factors in understanding the core nature prior to drawing. Packing factor determines the amount of void space present in the core. The packing factor is determined

predominately by the shape of the particles that make up the powder. The highest packing factors are obtained by using a mixture of particle sizes but in this work, a mixture of powder sizes is not used.

When considering packing of monosize powders, ordered arrangements are possible and allow for densities ranging from 0.524 for cubic arrangement up 0.740 for a rhombohedral arrangement similar to the arrangement for an FCC material.[38] In practice powders do not achieve the ordered arrangements and tend to have a more random packing structure. This random packing is categorized as either loose random packing or dense random packing. The loose packing characterizes a poured density while the dense packing represents a tap density. The dense packing is achieved by pouring the powder into a container and then vibrating to achieve the highest possible density in a random arrangement. The densities for the loose random packing and the dense random packing are usually calculated to be about 0.52 and 0.64 respectively.[38, 39] The low packing density of the random packing leaves a large amount of space that must be collapsed in the preform prior to drawing and allows the molten semiconductor to move in the preform prior to the drawing. The collapse and removal of the void space is necessary to allow the molten semiconductor droplets to be drawn into wires.

Sieving allows the powder to be limited in size and approach more of the monosize behavior. The sieving does not limit the shape or roughness of the powder particles. The rougher the particle and the greater the deviation from a spherical shape, the further the decrease in the packing density of the powder mix.

The initial powder sizes and composition (among other things) affect the size of the wire capable of being drawn by dictating the amount of semiconductor present for drawing as well as the pore sizes present for the semiconductor to be drawn in. Starting pore sizes has a large impact on the size of the features that can be obtained. While the pore sizes in ordered arrangements are easily understood and calculated, determining the pore sizes present in a random arrangement are more difficult. Theoretical calculations have been performed to determine the relative pore sizes possible in both loose and dense random packing. Work done by Nolan and Kavanagh[39] calculated different pore sizes possible in random packing arrangements and found the mean relative pore size to particles for the loose and dense random arrangements to be 0.463 and 0.338 respectively. This pore size represents the starting semiconductor feature size not the starting powder size, as the molten semiconductor is free to move in the preform.

1.4 Etch Chemistries

The materials used in this research SiO_2, Si, and Ge have been extensively studied in their behavior due to their importance to the electronics industry. As a result of this importance, extensive research has been carried out for these materials in a wide variety of etchants.[40, 41] The significant body of work done by Williams et al. have produced well documented etch rates for these materials allowing for determination of an ideal etchant for modifying these nanowire glass structures. Using the information provided in this work allows for the determination of an HF based etchant for removing glass from these samples. Concentrated HF has been shown to have rapid etching in the micron/min range on silica with minimal to no etching of the semiconductor features. Additionally, the etch rate can be slowed by diluting with water to provide very tunable etch rates of SiO_2.

Experimental Procedures

A method for producing large quantities of high aspect ratio-oriented semiconductor nanowires in a safe and scalable method has been developed. This section describes in detail the process for producing both the source preforms as well as the conditions necessary for drawing those preforms to target fiber sizes for integration in current fiber systems. Analysis of the optical and electrical properties of these nanowire arrays was conducted to understand and evaluate potential uses of these nanowires.

1.5 Semiconductor NW Fiber Production

1.5.1 Preform Fabrication

The fabrication of preforms is the first step in producing optical fibers and in this case consists of the production of the powders for the core region and the production of the glass cladding material. The cladding material ranges from directly using a stock purchased tube for fibers on the lathe to multiple over cladding steps to making a custom thick-walled tube for use on the tower. These initial preforms allowed fibers to be directly produced on the lathe but suffered from size and speed limitation of the lathe that provided a finite limitation on draw down and thus the length and size of the nanowires produced. These lathe produced fibers were capable of producing some nanowires but the majority of the semiconductor features were above the target 100nm diameter size and extremely inconsistent fibers in both length and diameter resulted. To overcome these limitations fiber production was shifted to the draw tower, which allows for much larger preforms and much higher draw speeds. While the size of the preforms differs greatly depending on the target diameter of the fiber and the method of drawing, the production of the core material is constant across all preforms and only differs in the compositional content.

The production of the core material is common to all the preforms and so is covered first, and then the differences in cladding regions are covered afterwards.

In addition to these powder-filled preforms a secondary type of preform was also developed. This preform consists of a stacked tube approach and allows for more precise control of location of semiconductor features as well as combining semiconductor features with traditional optical fiber cores and materials. The stacked approach can be achieved by taking thicker sections of fiber produced in the range of 1-2mm in diameter and arranging them inside a glass tube with a doped core region. These rods can consist of single silicon features similar to those produced in other work done by our group[4] or of rods that contain multiple features produced in this work.

Core Material

In all preforms, the core was composed of a mixed powder of fused silica and the desired semiconductor powders. Due to the limited purities in commercially available powders of target sizes, all powders used were produced in the lab. Powders were produced in the lab by grinding using an alumina mortar and pestle. Sieving was used to control and limit the particle sizes in the preforms. Four different sieves were used to control the sizes of particle used, No. 100, 120, 325, and 635. These meshes correspond to particle sizes of 150, 125, 45, and 20 microns respectively. The source materials and sizes used for the various preforms are summarized in Table 0-1.

Table 0-1: Source Material used for Core Region Powders

Material	Source	Purity	Sizes Used
Silica	GE Type 214 Fused Quartz Cladding Tubes	Trace Impurities <1ppm OH^- Content <5ppm	125-150µm <45µm <20µm
Silicon (Undoped)	Alfa Aesar virgin poly fines	99.999%	<20µm
n-type Silicon	<111> n-type Wafer	Phosphorous Doping	<45µm <20µm

p-type Silicon	<110> p-type Wafer	Boron Doping	<45µm <20µm
Germanium	Alfa Aesar -100mesh Powder	99.999%	<45µm <20µm

The sizes were chosen to provide particles that would draw down to nano size based on the draw down ratios possible with both the lathe as well as the draw tower. The smallest size of 635 mesh was also the smallest commercially available standard sieve size. The larger 100 and 120 mesh sizes were then selected to provide particles sizes that provided interstitial spaces the size of the smaller 20-micron particles.

These powders were used to make a variety of compositions of semiconductor-glass powders. Compositions were investigated ranging from 5-30% wt. semiconductor in glass and mixed using a rolling jar mill for 1 hour.

Cladding Material

In all preforms, the outer tube used was GE Type 214 Fused Quartz tubing. This tubing was used, as it is suitable purity for use in optical applications. Initial preforms used on the lathe were produced using stock sizes of tubes available from the supplier. For the larger preforms necessary to be used on the draw tower, the cladding regions were produced in the lab. The glass lathe used to produce these preforms as well as fibers is shown below in Figure 0-1.

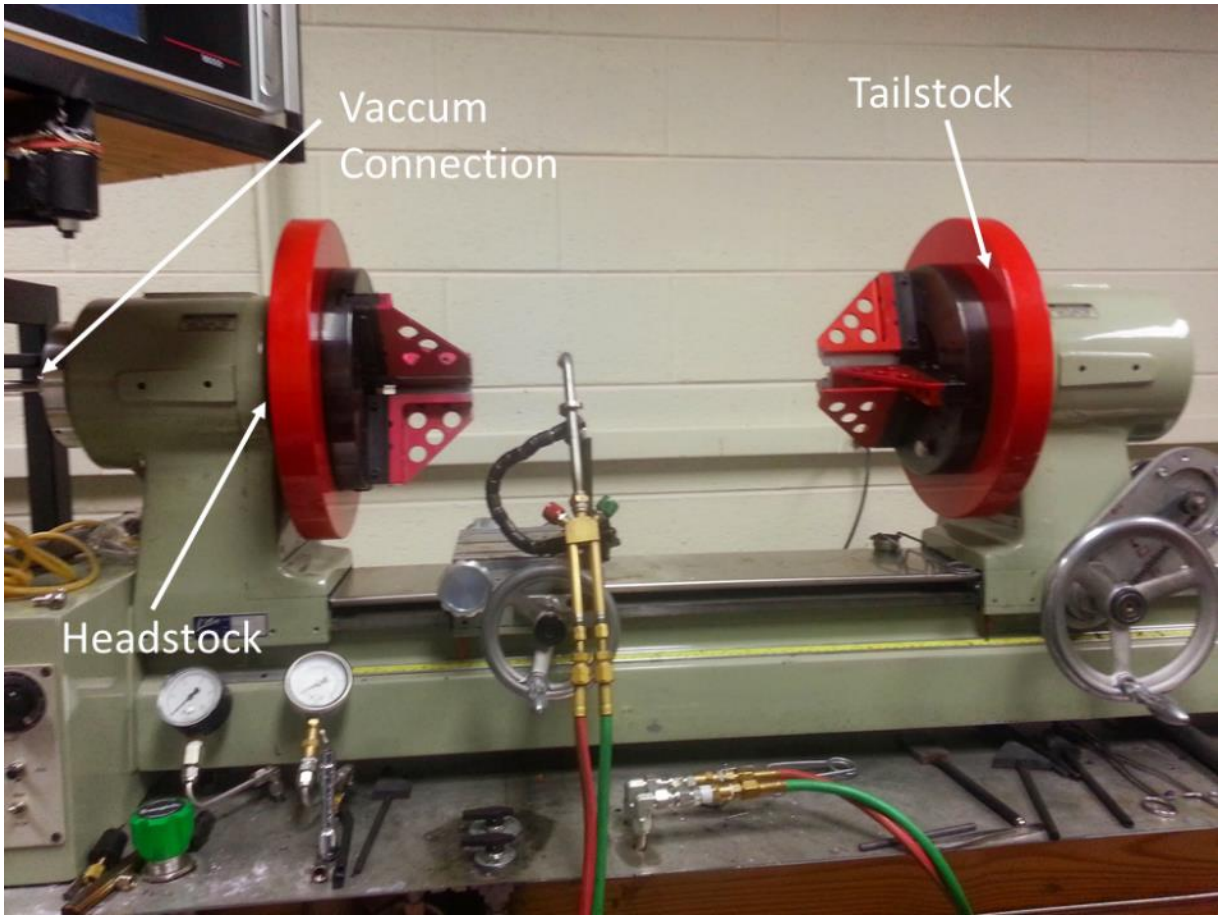

Figure 0-1: Glass Lathe used for initial fiber drawing and later preform production for the draw tower.

These tubes were produced by using a series of close-fitting tubes bought from the manufacturer and then over cladding the tubes to the desired sizes. This process was done on the glass lathe and is completed in the following series of steps.

1. Seal the end of the smaller inner tube.
2. Mount the smaller tube to the tailstock chuck.
3. Mount the larger overclad tube to the headstock chuck.
4. Using the lathe controls insert the smaller tube into the desired length of the preform being overclad.
5. Attach vacuum line to the end of the larger tube on the headstock side.

6. Heat the open end of the larger tube near the tailstock end allowing it to naturally consolidate and collapse onto the smaller tube.
7. Once the outer tube has collapsed and attached to the smaller tube around the entire circumference the vacuum is then turned on.
8. The torch is then slowly traversed (5-30mm/min) down the length of preform collapsing the outer tube onto the inner tube.

The use of the vacuum allows the process to be done much quicker than waiting for the natural collapse as well as allowing for a uniform clean interface between the two tubes. This process is then repeated continuing until the desired size of the preform is reached. For most of the preforms used for the draw tower, this process is done 2-3 times. This process allows for virtually any size of preform to be created and provides very repeatable sizes with similar tolerances in sizes to those received directly from the manufacturer. Table 0-2 below summarizes a list of tubes used to make the preforms.

Table 0-2: Typical set of tubes used to create a thick walled preform for use on the draw tower.

Tube	ID (mm)	OD (mm)
1	4	8
2	10	16
3	16	20
4	21	25

This set of tubes creates a preform with an outer diameter approximately 23mm. This large outer diameter allows for much larger draw down ratios and thus the ability to create significantly smaller features in the fiber than those of smaller preforms.

The final step in creating the preforms is to fill the core region with the desired target powder composition. When inserting the powders into the tubes a static charging problem was observed

between the powders and the glass tubes. This problem made powder insertion difficult and was eliminated by using a funnel made from aluminum foil. Continually tapping of the preform was done to aid the powder in settling, provide the highest packing possible, and limit the void spaces present. After the tube is filled to the desired level, a small amount of fused silica wool is inserted in the tubes to act as a filter and limit any powder movement during the vacuum assisted drawing process. Figure 0-2 below shows several preforms produced both for lathe drawing as well as for tower drawing. All of these preforms are shown after the drawing process.

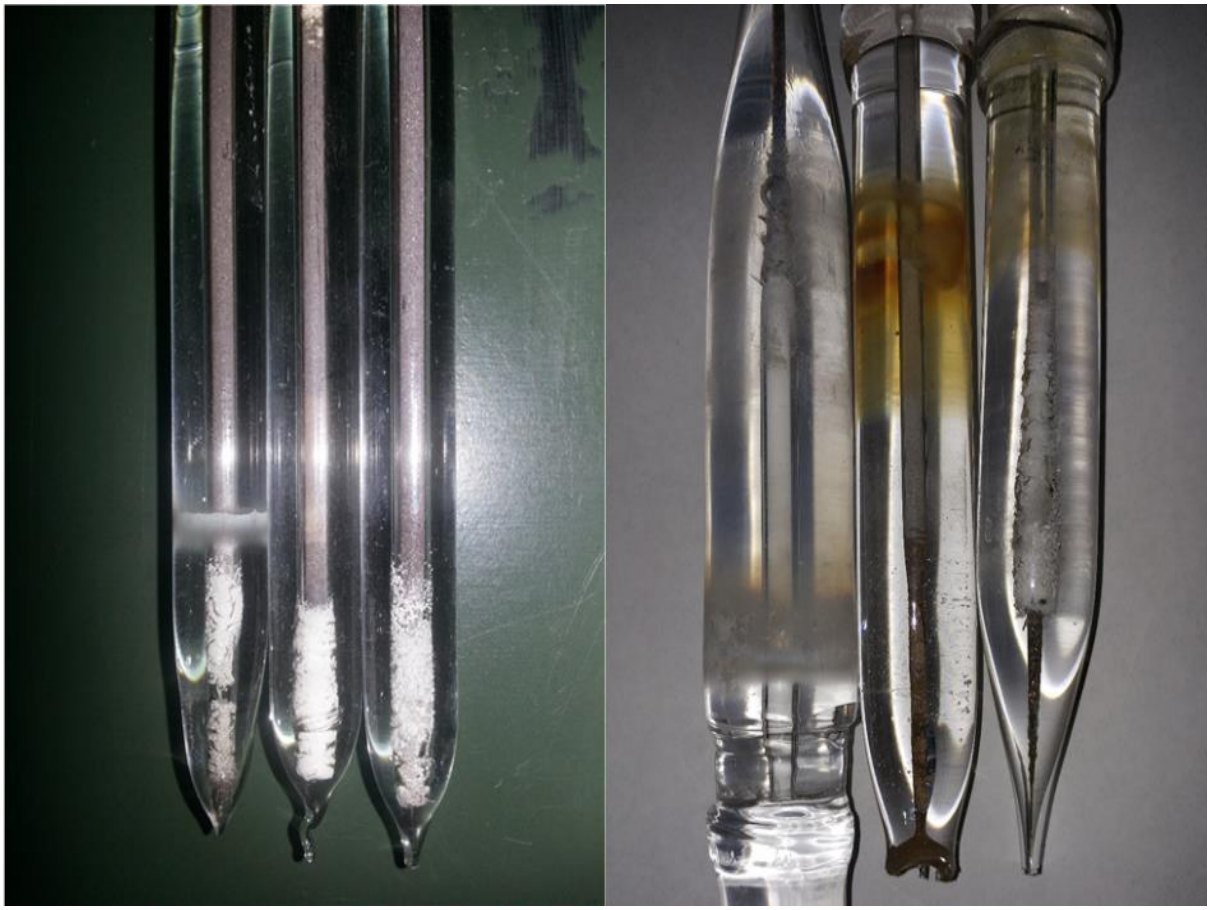

Figure 0-2: Image of preforms used on the lathe with an approximate OD of 8mm(left) and preforms used on the draw tower with an approximate OD ranging from 19-24mm(right).

1.5.2 Fiber Drawing via Lathe

Fiber production was initially completed using the lathe to provide preliminary results and small-scale evaluation. The glass lathe provides motorized control of both the pulling tailstock as well as the torch carriage. This allows for draw and feed speeds ranging from 0-5000mm/min. Heating for the lathe is provided by an oxy-hydrogen torch with rotation to provide a uniform heating profile. Based on the draw and feed speeds capable on the lathe, the maximum diameter of preform capable of producing a fiber of the target 125 microns is 8mm. Initial cladding tubes for fiber production on the lathe were stock tubes with an OD of 8mm and an ID of 3mm. This size was chosen as it provided the thickest wall and did not exceed the max size.

Producing fibers from the small preforms directly on the lathe suffered from several limitations. The oxy-hydrogen torch heat source provided an uneven heat profile that was partially alleviated by rotation of the preform during drawing. This uneven heat source and horizontal orientation led to pooling and movement of the molten semiconductor material present. This caused fibers produced to have inconsistent sizes as well as regions with no core material present. The lathe also limited the max length of fiber produced and the draw down. Additionally, a blow out of a gaseous species in the heated preforms was frequently observed.

1.5.3 Fiber Drawing via Tower

The majority of fiber drawing was completed using the draw tower located at the Fiber Optic Draw Tower Facility on Prices Fork Rd. The draw tower provides considerably increased capabilities in producing fibers. The tower is 6m tall, capable of continuously producing kilometer lengths of acrylate-coated fibers and is shown below in Figure 0-3. This tower is

equipped with a resistive element graphite furnace capable of rapidly heating to and operating at a maximum temperature of 2400°C. This furnace operates in an inert nitrogen atmosphere and provides a uniform heating profile for optimal fiber drawing. The tower also provides real time diameter measurements using a pair of laser micrometers to measure both the drawn fiber size as well as the fiber size after being coated with an acrylate coating. The draw tower is capable of feed speeds ranging from 1-50mm/min and draw speeds of 10-100cm/sec. These speeds allow for a much larger range of preforms to be drawn with the only limit on size being provided by the 25mm opening of the furnace.

Figure 0-3: Draw Tower Facility located at Prices Fork Rd.

Development of the drawing process was ongoing with the goal of producing long uniform fibers with continuous sections of nanowires present in the core region. Preforms for use on the draw tower underwent additional steps that were not needed for drawing on the lathe. The first step added a “drop” to the bottom end of the preform. The drop consists of a fused quartz rod 2-5cm in length of similar diameter as the preform being added to the end of the preform. This drop is added to provide additional mass to minimize waste of preform at startup of the draw on the tower. The additional mass allow for draws to be started quicker and at a lower temperature. This drop is added prior to filling the preform with powder to prevent any unwanted heat effects on the powder. After the preform is then filled with powder, it is returned to the lathe for a handle tube to be attached. This handle tube is a long ID 19mm OD 25mm tube attached to allow a long enough sample to be mounted on the draw tower and connected to the operating vacuum. The process for mounting and starting a draw on the tower is summarized below.

1. Preform is inserted into the mounting chuck at the top of the tower with at least 400mm of preform present below the chuck.
2. Process vacuum is then connected to the top of the preform using Teflon tape to provide a seal between steel vacuum tube and the glass preform.
3. Process vacuum is turned on ensuring that fiber filter is prevent powder from being removed from the preform.
4. Preform is then lowered into the furnace so that the drop is located just below the hot zone approximately 180mm from the top of the furnace.
5. The furnace is purged with nitrogen gas and maintains continually flowing nitrogen during drawing.

6. The furnace is then rapidly heated to draw temperature of approximately 2000°C in 30-40 minutes.
7. Upon reaching temperature, the weight of the drop assists in the causing drawing to begin. The bottom furnace gate is opened to allow the passage of the drop and closed back around the fiber diameter.
8. Once the drop is clear of the furnace it is removed from the fiber and the fiber is hand pulled down the tower passing through the pressure coating system and the UV curing lamp.
9. The fiber is then inserted into the drawing capstan going at its minimum speed and feed of the preform is turned on.
10. Temperature, draw speed, and feed speed are then controlled to reach the target fiber size and to control the tension present in the fiber during the draw.
11. Once target sizes are achieved acrylate coating is applied and cured to provide strength and protect the fiber.
12. Fiber is then fed to the spooler and continuous drawing can begin.

The primary method of controlling size on the draw tower is done by draw speed with the feed speed being left primarily at its minimum value for most draws. The draw is initially started at a higher temperature then lowered to increase the viscosity of the glass being drawn and provide a higher tension draw. The high tension is desirable to increase the force applied to the liquid semiconductor particles and aide in the formation of wires during drawing. Figure 0-4 below schematically shows the drawing process of a preform on the tower.

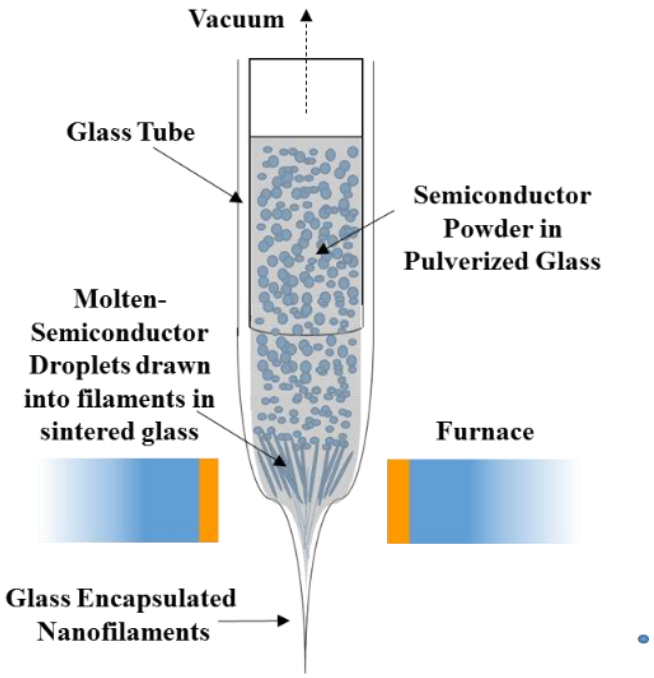

Figure 0-4: Schematic showing the drawing process of mixed semiconductor glass powder into fiber.

1.5.4 Gaseous Products during Drawing

During drawing of fibers on both the lathe and the draw tower, gas formation was observed. This gas formation is unable to be completely removed by the vacuum process during drawing and leads to the drawing of capillary tubes and ultimately blowout of the preform. This gas formation was very detrimental to production of nanowires and slowed down the drawing process by interrupting draws with blowouts. The thicker walled preforms reduced the occurrence of blowouts but still allowed for large sections of fiber to consist of capillary tubes with no core material present.

Two possible causes of the gas formation were determined to be formation of volatile monoxides of Silicon and Germanium and carbon contamination present in the powders. Formation of the monoxides is possible when silicon and germanium are heated in oxygen deficient environments

and sublimates below the melting temperatures of the semiconductors. This should have minimal effect on the blowout, as the gas is present below the softening point of the silica tube and should no longer be produced once the semiconductors have reached their molten states. This leaves the likely culprit of gas production to be carbon contamination. This is further confirmed by the presence of a yellowish-brown residue observed in the capillary tube sections produced that is consistent with carbon contamination observed in other fiber drawing projects. In work on photonic crystal fiber preforms carbon contamination is removed from the glass tubes via burnout with torch. This leads to the development of a furnace treatment to remove the carbon from the powders prior to their placement in preforms. A furnace treatment of 760°C for 2 hours in air was used to eliminate carbon contamination of powders. The powders were spread out in fused quartz boats into thin layers to aid in providing the surface area to remove the contaminant. The temperature of 760°C was determined based on common treatments used for carbon burnout in ceramic materials as well as being above the recommended oxidation temperature of carbon in ASTM7542-15. Preforms produced with powders post heat treatment virtually eliminated blowout and completely removed the yellow contamination and hollow regions present in the fibers.

1.6 Characterization of NW Containing Fibers

Characterization of these fibers containing nanowire features was performed using a variety of methods to fully understand the morphology created and how they relate to the starting sizes of the powders. The electrical and optical properties of these fibers were evaluated by measuring the transmission of light both broad spectrum and laser light of various wavelengths. The electrical properties were evaluated using a DC power source and picoammeter. Specific

relations between the optical and electrical properties were evaluated by looking for any light generated by electroluminescence as well as looking for potential photocurrent generated by these samples.

1.6.1 Characterization of NW Sizes

Characterization of the NW arrays was done using both optical microscopy as well electron microscopy. Optical microscopy was performed using both transmitted as well as reflected light techniques on an Olympus BX51 microscope. Samples for optical microscopy were cleaved on both ends using an optical fiber cleaver to provide a flat smooth surface on both ends. The samples were cleaved to a length of approximately 1 cm. This length was chosen to provide an easy to handle length that could be mounted and allow the transmission light source to be coupled into the bottom of the fiber. The optical microscope was equipped with 100W halogen light sources in both the transmission and reflected directions. Additionally, the microscope was equipped with a mercury halide lamp in reflection to provide a higher intensity source as well as providing strong UV peaks for fluorescence work. Optical microscopy was performed to provide an overview of the entire fiber structure as well as to produce side views of the features.

Scanning Electron Microscopy (SEM) was used to provide high-resolution images of the samples. Two different electron microscopes were used in this work to provide the most information. The Leo 1550 field emission SEM was used as the primary imaging tool due to its in-lens detector, which is capable of providing excellent resolution down to the 2-5nm range. The FEI Quanta 600 FEG environmental SEM was used to analyze samples using backscatter electrons to provide contrast based on atomic number. The FEI scope is also equipped with a higher sensitivity detector for performing Energy Dispersive Spectroscopy (EDS). EDS is used

to provide detailed chemical information of a sample with a resolution in the range of 1% atomic. While EDS is limited to a minimum analysis region of approximately one cubic micron, which is considerably larger than the features produced, it is possible to get chemical analysis by removing part or the entire glass matrix surrounding the nanowires.

Evolution of Sample Mounting

Sample preparation for SEM requires an additional step to just the cleaving for optical microscopy. Due to the insulating nature of the glass, samples for SEM must be very flat and then coated with a metal to provide a conductive pathway. Initial samples followed the traditional materials sample prep of mounting the fibers vertically in epoxy then grinding and polishing until a smooth surface was achieved. Grinding started with 120grit paper and was then incrementally polished down to a size of 0.3μm alumina polish. These samples were then coated with a gold palladium film using a sputter coater to ensure electrical conduction. Samples prepared with this initial process proved difficult to analyze and provided very little contrast for the nanowires. Samples polished also suffered from significant particle contamination present on the surface despite being rinsed in an ultrasonic bath.

Etching with hydrofluoric acid was used to remove the glass matrix, expose the nanowires, and provide better contrast for imaging. A concentration of 48-51% HF was used for etching with times ranging from 30 seconds-5 minutes. The etch rates of fused silica have been well studied and this should correspond to etching depths of 500nm-5 microns. Etching with concentrated HF was successful in exposing the semiconductor feature but was found to have significantly faster etch rates than expected with the higher etch times causing features to be completely lost. In

addition to the higher etch rates, contaminated particles were found present on samples with high quantities of carbon and fluorine detected with EDS.

Alleviation of these problems was accomplished by removing the polishing step and mounting cleaved samples directly as well as altering the etch chemistry to a more dilute solution to slow the etching of the glass. Etching with a 10:1 HF solution (10 H_2O:1 49% HF) allowed for a more controlled etch down to a rate of 26nm/min[40] and also eliminated fluorine contamination being detected by EDS.

1.6.2 Optical Transmission Characterization

Optical transmission tests were performed to determine the effects of the nanowire array on light. The first step in optical testing involved developing a method to reliably join these samples into traditional optical fiber setups and successfully couple light into and out of these samples. Samples were butt coupled to lead fibers and aligned by using a fused quartz capillary tube with ID 150µm OD 250µm. This allowed for tolerances with the size of the samples while providing adequate alignment.

Initial tests were completed with MMF with a core of 50µm for the lead-out fiber and both SMF with an 8µm core and MMF were tested as the lead-in fiber. The MMF was chosen to provide the highest intensity of light across a range of wavelengths and to provide the best chance of capturing any light from the sample. The SMF was also tested due to its small core size that was smaller than the average core size of 10µm in samples. Light was provided by a broad-spectrum halogen white light source. The spectrum was then analyzed using an Ando AQ6315 Optical Spectrum Analyzer with wavelength range 400-1700nm. Samples were cleaved to lengths

ranging from 1-5cm to evaluate the maximum length of transmission possible. Transmission with the MMF lead-in was not visible in the 5cm sample but was visible in shorter samples with no change in the spectrum compared to the signal with no sample present. Transmission with SMF lead-in was not observable in any length of sample.

The observation of light only being visible when the MMF lead-in was used led to the determination that light was being carried outside of the core region in the glass cladding and not giving any useful information about the samples. To understand this phenomenon and confirm that is what is happening the optical setup was modified to provide analysis using a beam profiler. The modified setup for use with the beam profile is shown in Figure 0-5 below.

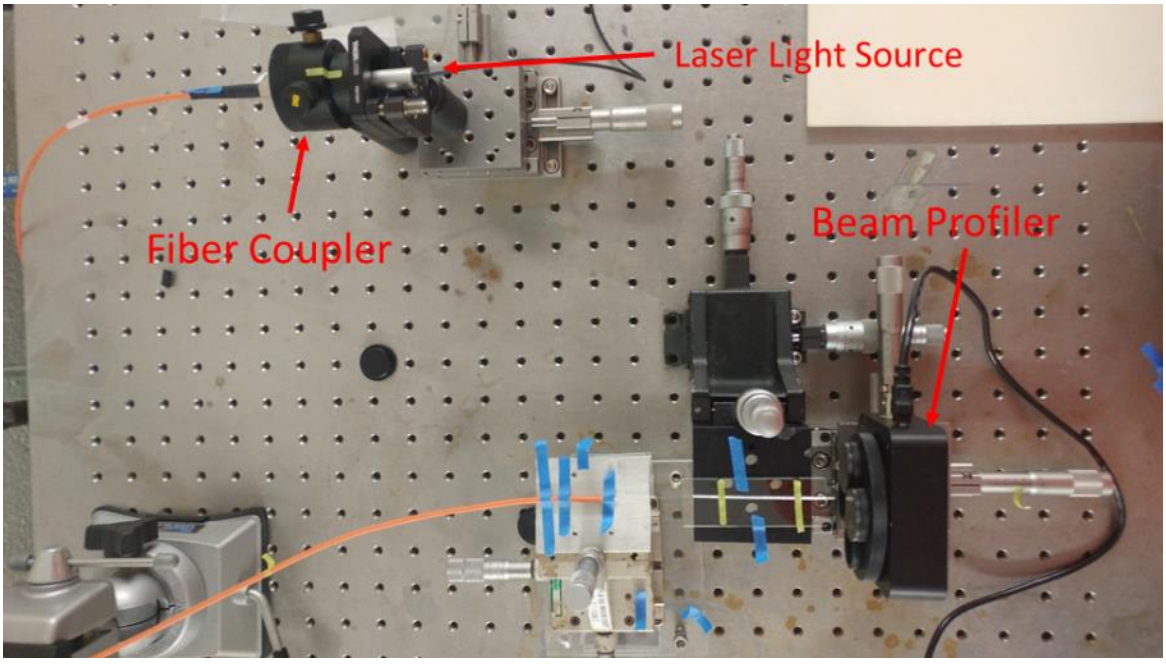

Figure 0-5: Optical Setup with laser light source and beam profiler for detecting the output

This setup removed the need for a lead-out fiber with the sample being closely positioned in front of the beam profiler for detection. The beam profiler, the sample and lead fiber were all place on 3-axis stages to allow for optimal lineup of the butt coupling between the lead fiber and

the sample as well as to align the output onto the detector of the beam profiler. The beam profiler also required the use of a monochromatic light source so the switch was made to use three different laser wavelengths provided from three Thorlabs Laser diodes at 532nm, 780nm, and 980nm. The use of the beam profiler allows for far field patterns to be observed since the detector is located more than 2 wavelengths of light away from the end of the fiber. The far field patterns allow for determination of the modal characteristics of a fiber. Based on the number of modes and the interference patterns it allows for complex patterns to be observed.

1.6.3 Electrical Properties Characterization

Electrical testing was done to evaluate if any electroluminescence was present in these samples and to determine if photocurrent was measurable when light was applied to these samples. The same setup is used for both tests with the only difference being the presence of a photodetector or light source located directly above the sample. The setup shown in the Figure 0-6 below

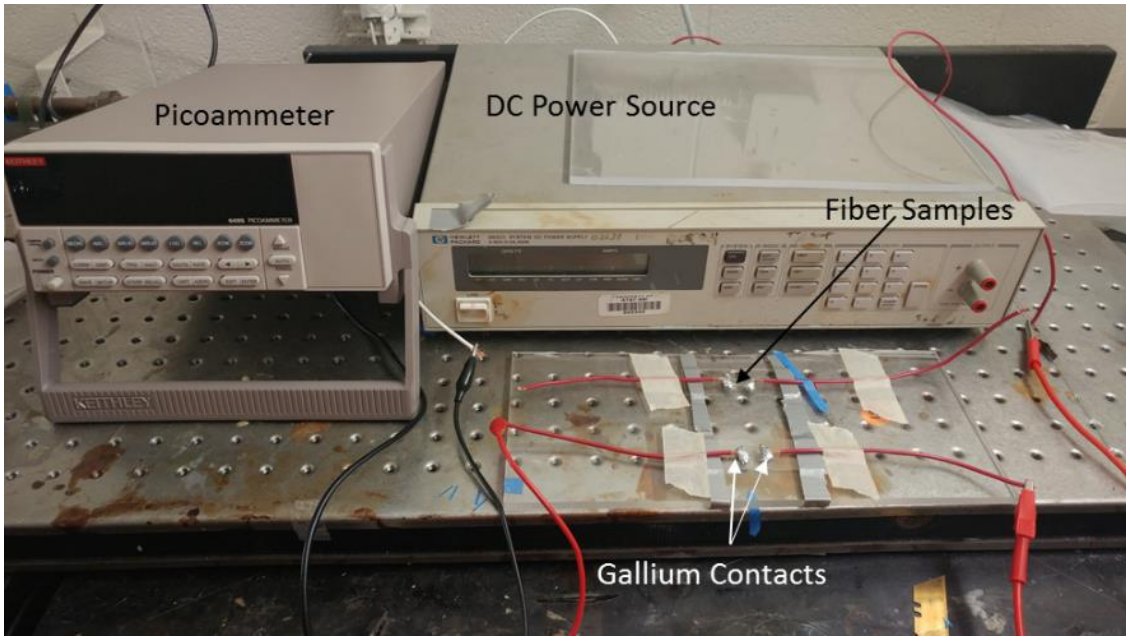

Figure 0-6: Electrical Setup for connecting fiber samples to DC power source

This setup was used to connect a group of fiber samples in parallel for testing. Each sample was tested using 15 sections of fiber 1.5cm in length with fresh cleaves at both ends. These samples were connected in parallel to copper electrical wires using gallium metal to provide the connection. Several materials were evaluated to provide the electrical interconnect. These consisted of silver paint, graphite paint, traditional Pb-Sn solder, Sn-Ab solder, gallium metal, and indium metal. The silver and graphite paint suffered from radically different results based on drying and delamination from the samples. The solders and indium metal while providing good electrical connections were difficult to handle and keep molten long enough to connect all of the fibers. The gallium metal provided a good electrical connection that did not change between its liquid and solid states and with its near room temperature melting point stayed liquid long enough to correctly and easily place all 15 fibers for a sample.

The overall electrical setup shown in Figure 0-6 was used for all experiments though depending on the test, the hardware used differed. For the electroluminescence tests, the power supply used was a Kepco APH 2000M DC source providing up to 2kV. Monitoring current and voltage in this high voltage setup was done via an Agilent 34405A multimeter. The photodetector used was a Thorlabs PDA10DT InGaAs with a wavelength range 0.9-2.57μm connected to an oscilloscope for output. The detector is held approximately 1cm from the samples during testing to get it as close as possible during the test. This photodetector was chosen as it provided a large wavelength range over which to detect any light generation. Testing was done in a dark room to eliminate as much interference as possible.

The setup was then changed to a lower output power supply for better control in the low range for photoconductivity measurements. These measurements were carried out on different samples

than the electroluminescence to ensure no changes occurred after having a high voltage applied. The power supply used then was a HP 6633A which is capable of providing 0V-50V DC. Since the photocurrent was expected to be small, a Keithley 6485 Picoammeter replaces the multimeter. For this testing the photodetector is replaced with a 100W halogen work light to provide a wide range of wavelengths to generate photocurrent.

In addition to the measured photoconductivity with the picoammeter, current data was collected from 0.014V-3V to allow for the understanding the I-V characteristics of the samples and allow for resistance to be calculated. This calculated resistance and estimated cross sectional areas of the semiconductor features allow for resistivity to be determined and compared to the literature values of the starting bulk materials.

Results and Discussion

1.7 Nanowires Characterization

Nanowires of a wide range of compositions of semiconductors and sizes were produced. As fibers produced moved from the small scale of less than a meter of the draw tower to continuous draws reaching over a kilometer in length on the draw tower several phenomena were observed that changed how the powders were processed to the sizes of tubes used in the preforms. The ability to detect fibers with nanowires present was improved as understanding of the draw conditions and the relationship to the fibers produced was gained.

1.7.1 Silicon Nanowires

Silicon nanowires were produced on both the lathe and draw tower and from a variety of compositions. Table 0-1 below summarizes the silicon samples produced that provided samples of nanowires. Fibers were produced from both undoped and doped silicon to determine any effects on drawing or glass behavior the dopants might have. The doped silicon powder was produced from on hand silicon wafers with p-type dopant boron and an unknown n-type doped wafer. The dilute quantities of dopants are not expected to have an effect on the drawing behavior though must be evaluated as oxides of the dopants are also some of the most common modifiers to silica glass.

Table 0-1: Table of Silicon Samples and the sizes of Preforms

Sample	Semiconductor Concentration (wt. %)	Particle Size (Si) µm	Particle Size (SiO_2) µm	Preform ID (mm)	Preform OD (mm)
Silicon Lathe 1	15	<20	125-150	3	8

Silicon BO 1	5-20	<20	<20	3	14.4
Si p-type	30	<45	<45	3	19.6
Si n-type	30	<45	<45	3	19.6
Si PN fiber	15	<45	<45	4	23.75

Fibers were successfully produced from these preforms with a variety of feature shapes and sizes. Fibers produced with silicon nanowires from work on the lathe suffered from short lengths and unpredictable results from draw to draw. These fibers were successful in producing some features below the target size of 100nm but suffered from size variation inconsistency. The results for these are shown below in Figure 0-1.

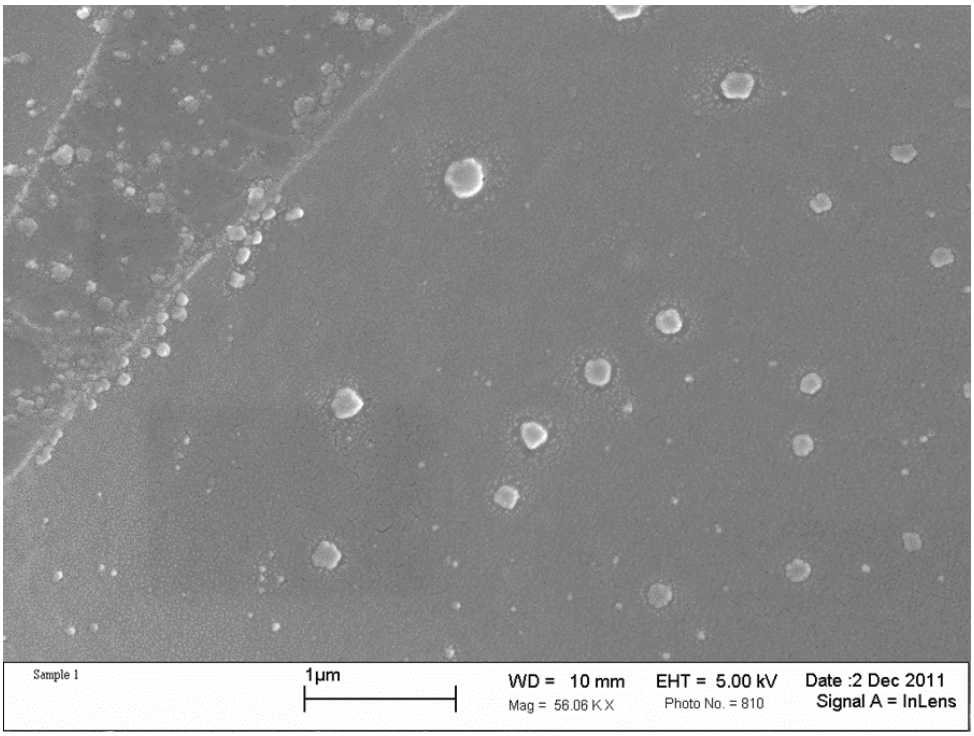

Figure 0-1: Silicon nanowires from fiber produced on lathe.

These fibers had short sections with the nanowires located in between large void spaces. These wires were limited to approximately 80nm in diameter at their smallest and were irregularly shaped. The larger than optical fiber standard size of 125µm made cleaving of these fibers

difficult and polishing was required to get smooth surfaces for analysis. The polishing and etching led to significant contamination around the nanowires. This greatly contrasts to fibers produced on the tower, which were produced in lengths up to a kilometer from a single preform with uniform diameters ranging from 100-150µm. The uniformity and sizes of these fibers allowed for traditional cleaving to be used for sample preparation, removing the contamination present in polished fibers.

The move to the draw tower allowed for hundreds of meters of fiber to be produced with much higher consistency than previously capable. Fibers produced on the tower still contained regions of collapsed glass and voids in addition to the regions with nanowires. This presented the challenge of determining a method to evaluate fiber samples and determine the presence of nanowires without taking them to the SEM. The larger preforms and continuous drawing allowed for the variation of the composition of the core region along the length of the preform. SiBO1 was the first preform attempted with the percentage of silicon powder in the mixture being increased through the preform. Figure 0-2 below shows schematically the grading of silicon powder through the preform.

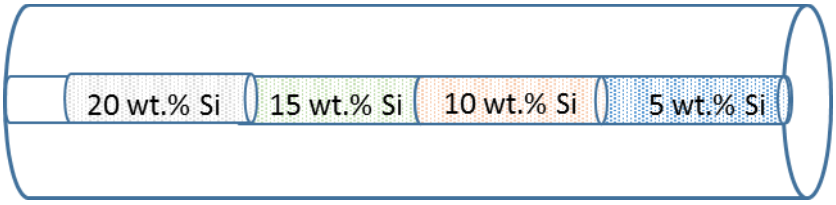

Figure 0-2: Schematic of preform SiBO1 showing step index of powder mixture along length of preform.

Optical microscopy was used to provide this screening method as well as providing a method to observe light interactions with the samples. Figure 0-3 below shows the core region of SiBO1 from the low concentration area of the sample imaged using reflected light. Fibers with nanowires were found to have unique core regions that despite the very small nature of the features were visible in an optical microscope. The fibers in SiBO1 were found to have very small core regions 4-6µm in diameter showing up as bright regions in the image. The core region was found to be non-uniform with bright and dark spots present.

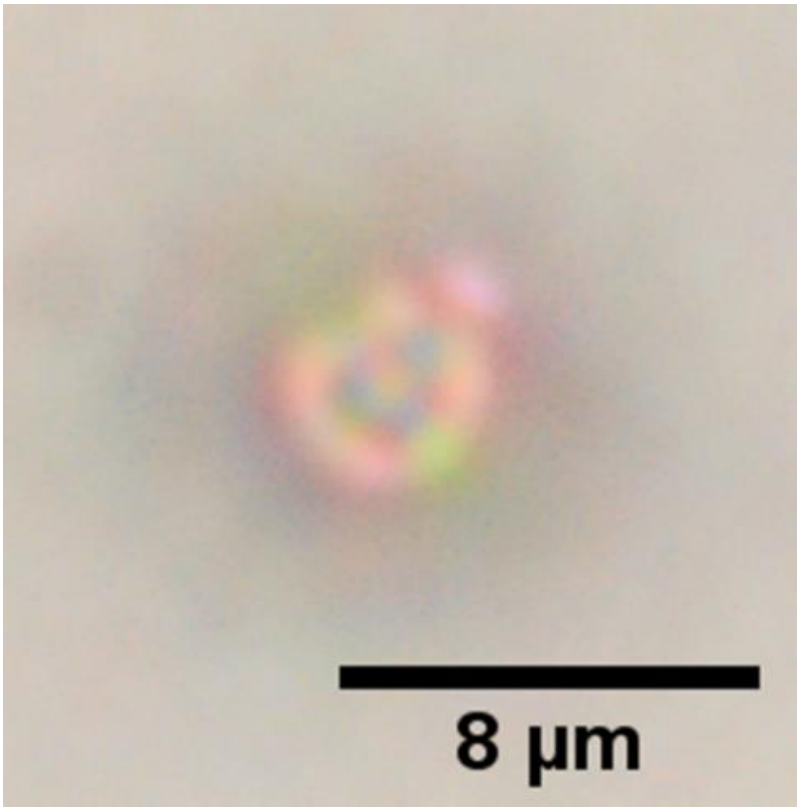

Figure 0-3: Core Region of Fiber Drawn from SiBO1 preform taken in reflected light microscopy showing few small features.

Fibers were also examined in transmission mode (through the samples) using the condenser lens to focus the light into fibers approximately 1.5cm in length and shown below in Figure 0-4.

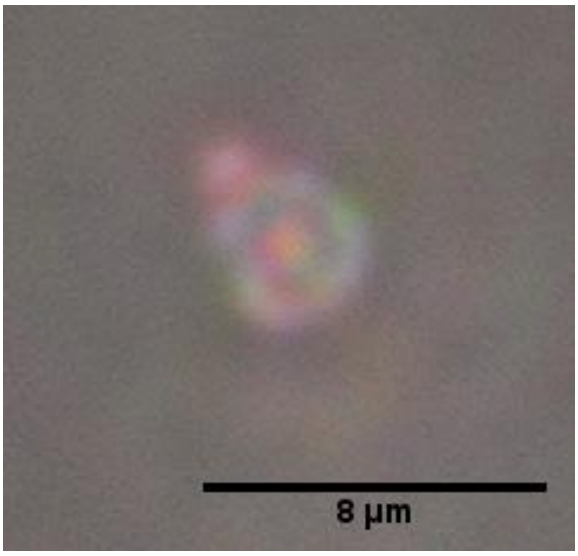

Figure 0-4: Core Region of Fiber drawn from SIBO1 preform taken using transmitted light microscopy.

Fibers when viewed in transmission showed very similar features matching those taken with reflected light. Unexpectedly however, the bright and dark regions are the same whether taken in transmission or reflected light conditions, indicating a region that has complex interactions with light. An SEM micrograph is shown below in Figure 0-5

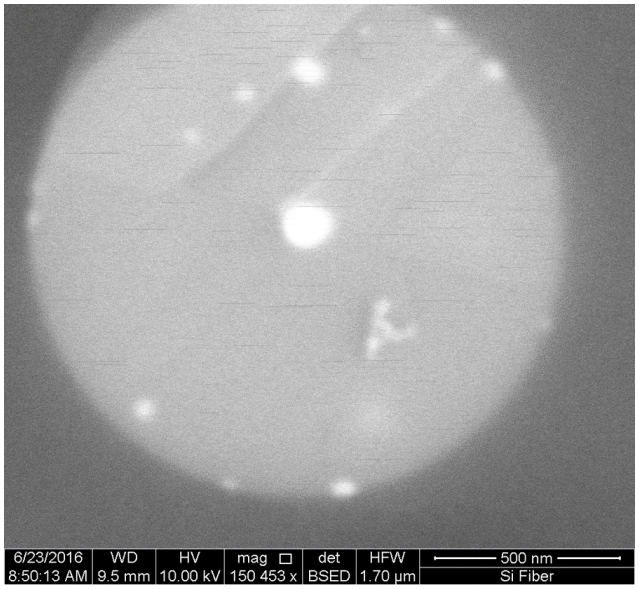

Figure 0-5: SEM taken with BSE showing several SiNW in a showing variation in chemistry from the surrounding cladding region.

The SEM results were taken using the backscatter detector to provide atomic number contrast. The core region was found to consist of a brighter well-defined region with semiconductor nanowires present in small numbers. EDS analysis showed that the only elements present in the sample are silicon and oxygen shown by the spectra in Figure 0-6 below.

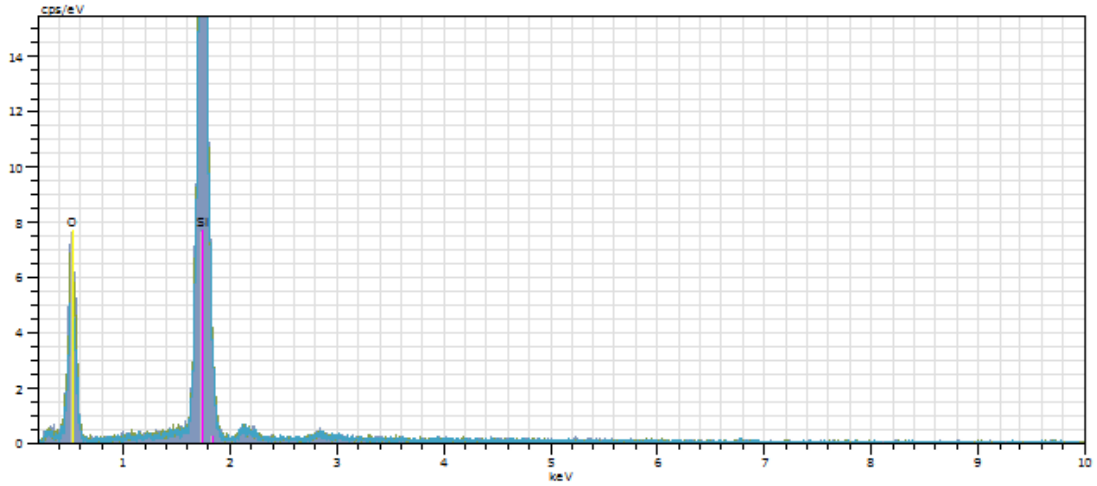

Figure 0-6: EDS spectra of the core and cladding regions of the fiber shown above in Figure 0-5

The core region was found to have a higher concentration of silicon than the fused quartz cladding region. In addition to the region shown above, samples from higher concentration sections of the preform showed more of an array of nanowires and are shown below in Figure 0-7. Higher quantities of nanowires were present with sizes ranging from 50-100nm.

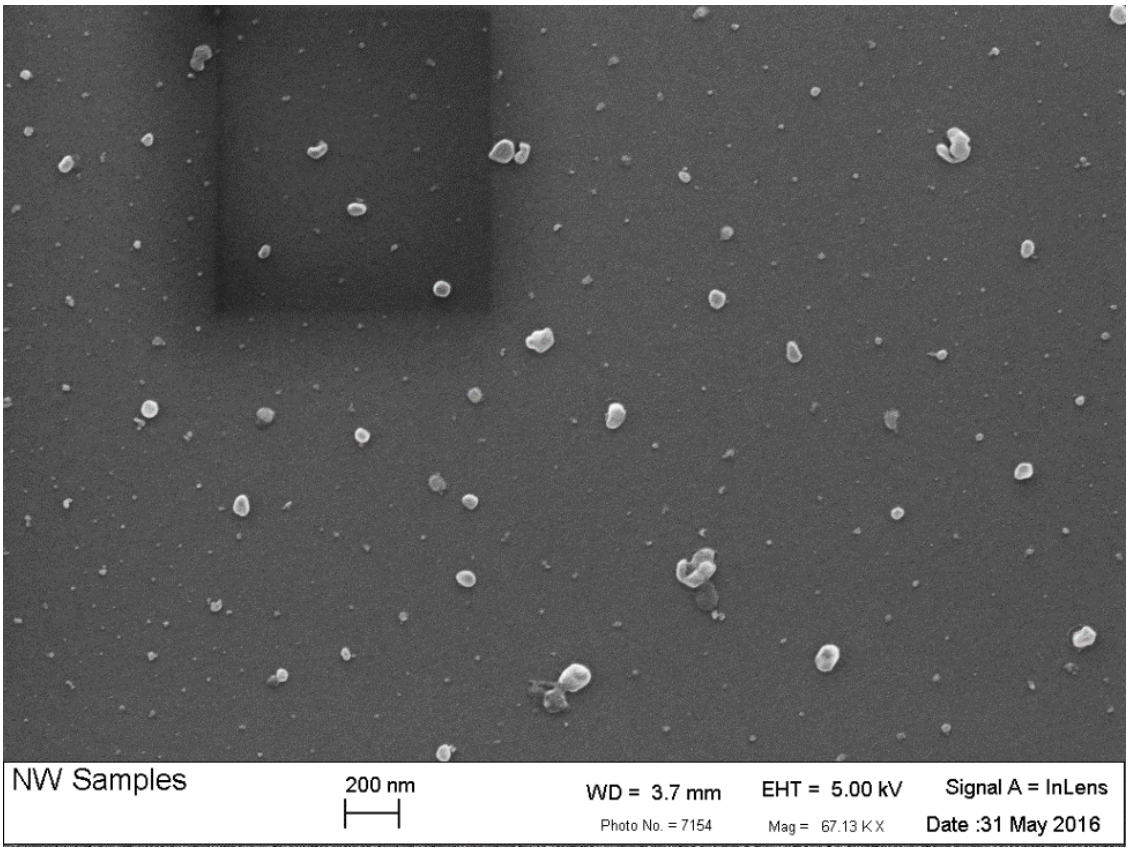

Figure 0-7: Region of SiNW from SiBO1 preform shown sticking out of the surface after HF etch.

The next two preforms, Si p-type and Si n-type, were varied to look at using doped fibers as well as looking at larger particles present in the powders. The powders were produced in the same grinding process and time but were sieved to allow the presence of particles of both glass and semiconductor up to 45µm in size. The overall size of the preform was also increased to allow for higher draw down ratios as well. Due to the inconsistency and difficulty of finding regions with wires present in SiBO1, the weight percentage of semiconductor was also increased.

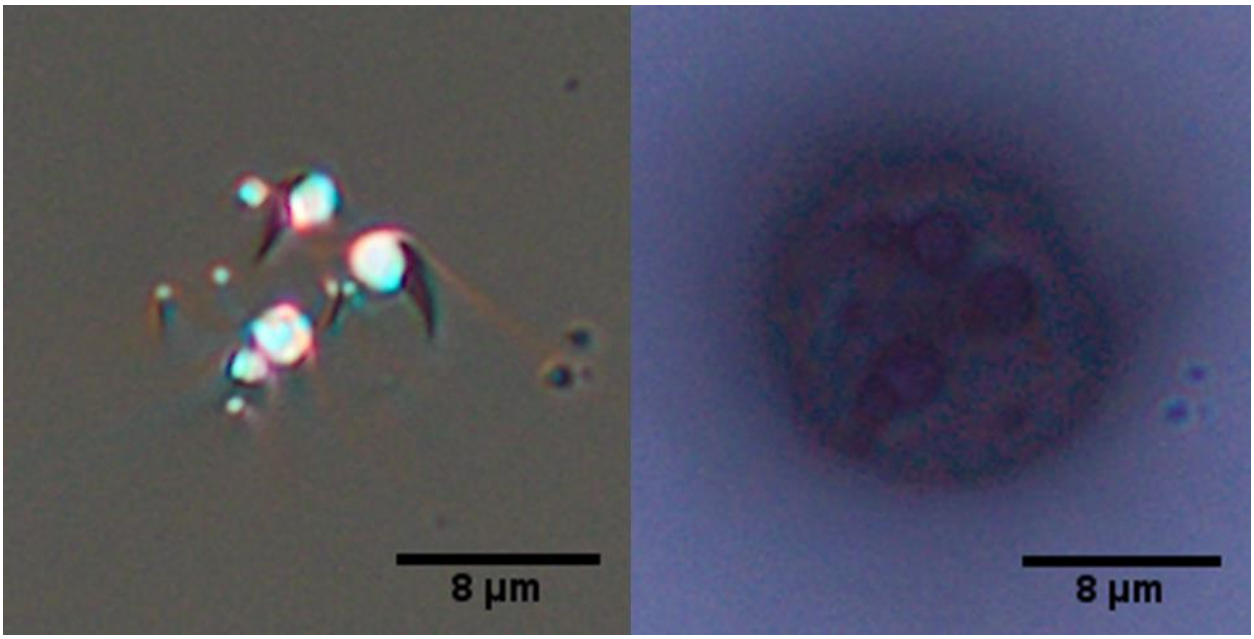

Figure 0-8: Core of fiber from Si P-type preform showing the same region in reflected (left) and transmission (right) with several microwires present.

Figure 0-8 and Figure 0-9 show fibers drawn from the Si p-type and Si n-type preforms. These fibers had core regions 8-12 microns in diameter with a small quantity of microwires. Optical microscopy showed these fibers to have different appearances in reflected and transmission. In reflected a small quantity of wires were present and easily measurable. In transmission the microwires were capable of blocking light being transmitted but the rest of the core region still allows passage of some light.

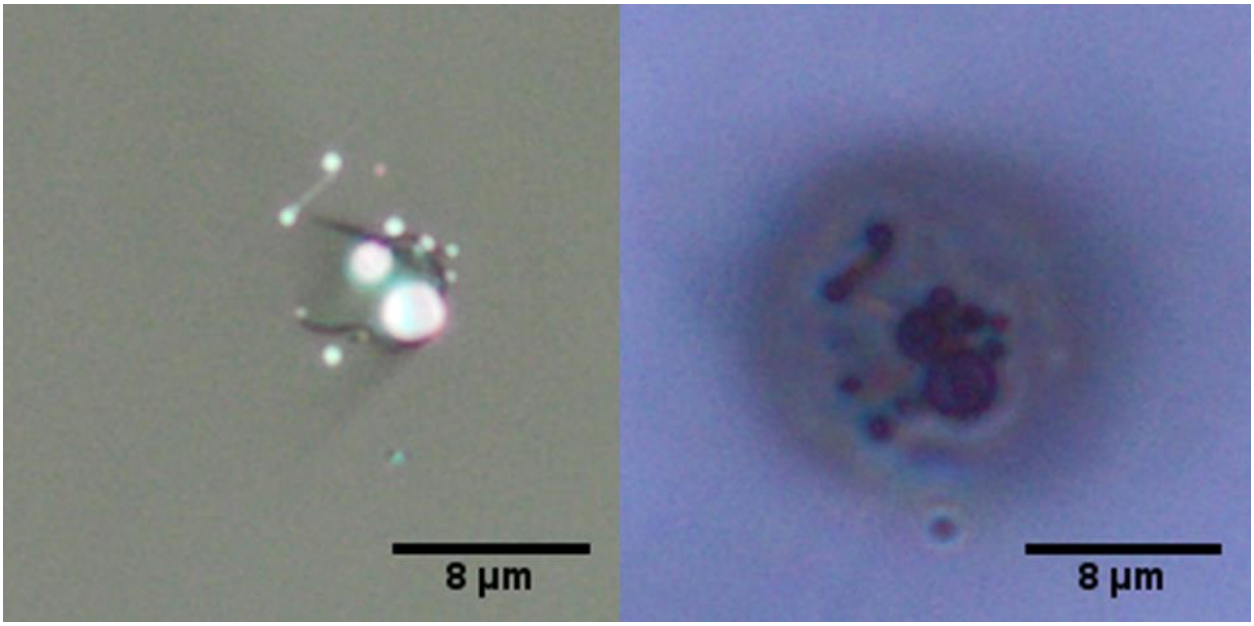

Figure 0-9: Core of fiber from Si n-type preform showing the same region in reflected (left) and transmission (right) with several microwires present.

The difference in transmission of light in the core suggests that while microwires are the primary feature present in these samples it is possible that some nanowires are also present. SEM was carried out on these samples to determine the presence of any smaller features and is shown below in Figure 0-10. The fibers were found to have sub-micron features with the smallest found in most fibers to be 250nm in diameter. These submicron features were few in number and very few were found in samples below the desired 100nm diameter. The draw down ratios of these larger preforms is estimated to be 130. This should result in the largest particles at 45µm being drawn to below 500nm in diameter. As significantly larger features are shown in the fibers it is concluded that the higher concentration of semiconductor powders is the primary cause of the micro features and not the larger particle sizes of the powders being used.

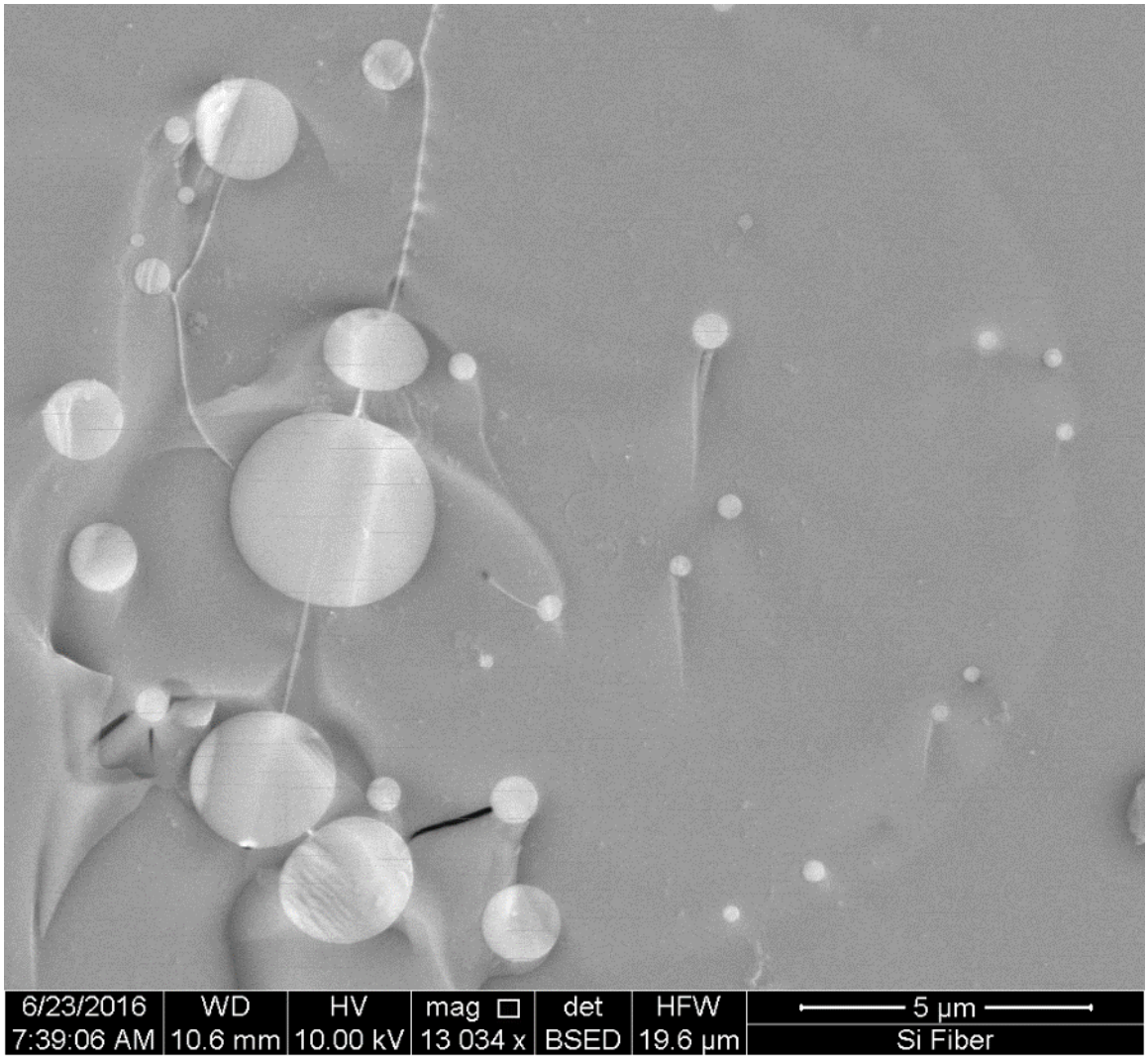

Figure 0-10: SEM of SiNW produced from Si n-type preform with largely microwires present.

Analysis of the size and distribution of the wires was carried out using ImageJ. Samples with few wires are easily measured and counted by observation while samples with many wires were counted and measured using the "analyze particles" feature of ImageJ. This technique is useful in determining rough sizes and close estimate of number of particles. It is limited when analyzing very small particles on lower magnification images due to the small number of pixels making up each particle. Wire sizes are reported on a histogram binning the number of wires in size ranges

with the maximum of each bin shown below it. Figure 0-11 below shows a histogram for the Si n-type shown in Figure 0-10.

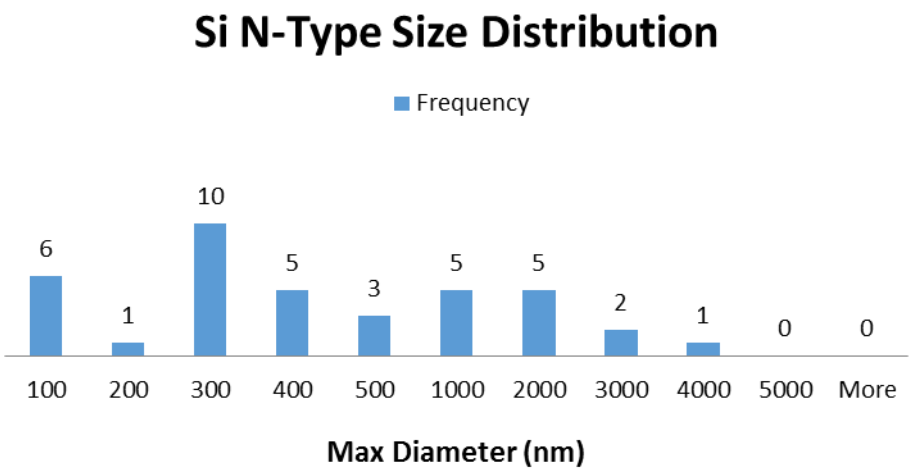

Figure 0-11: Histogram bin labeled for max size of NW from Si n-type preform.

Wires in the Si n-type preform were shown to have a few nanowires with 24 of the 38 wires being in the 100-1000nm size.

The SiPN preform was produced in a step composition manner similar to that shown in Figure 0-2 with the first half consisting of p-type silicon powder and the second half of the preform containing n-type silicon powder. The inner and outer diameters of the preform were also increased to provide a higher draw down ratio. The powder size was maintained at the larger size while the concentration was lowered to 25 wt.%. A sample fiber from the Si PN preform is shown below in Figure 0-12. The samples produced during this draw were successful in producing much smaller features than previous draws and reducing the number of microwires observed.

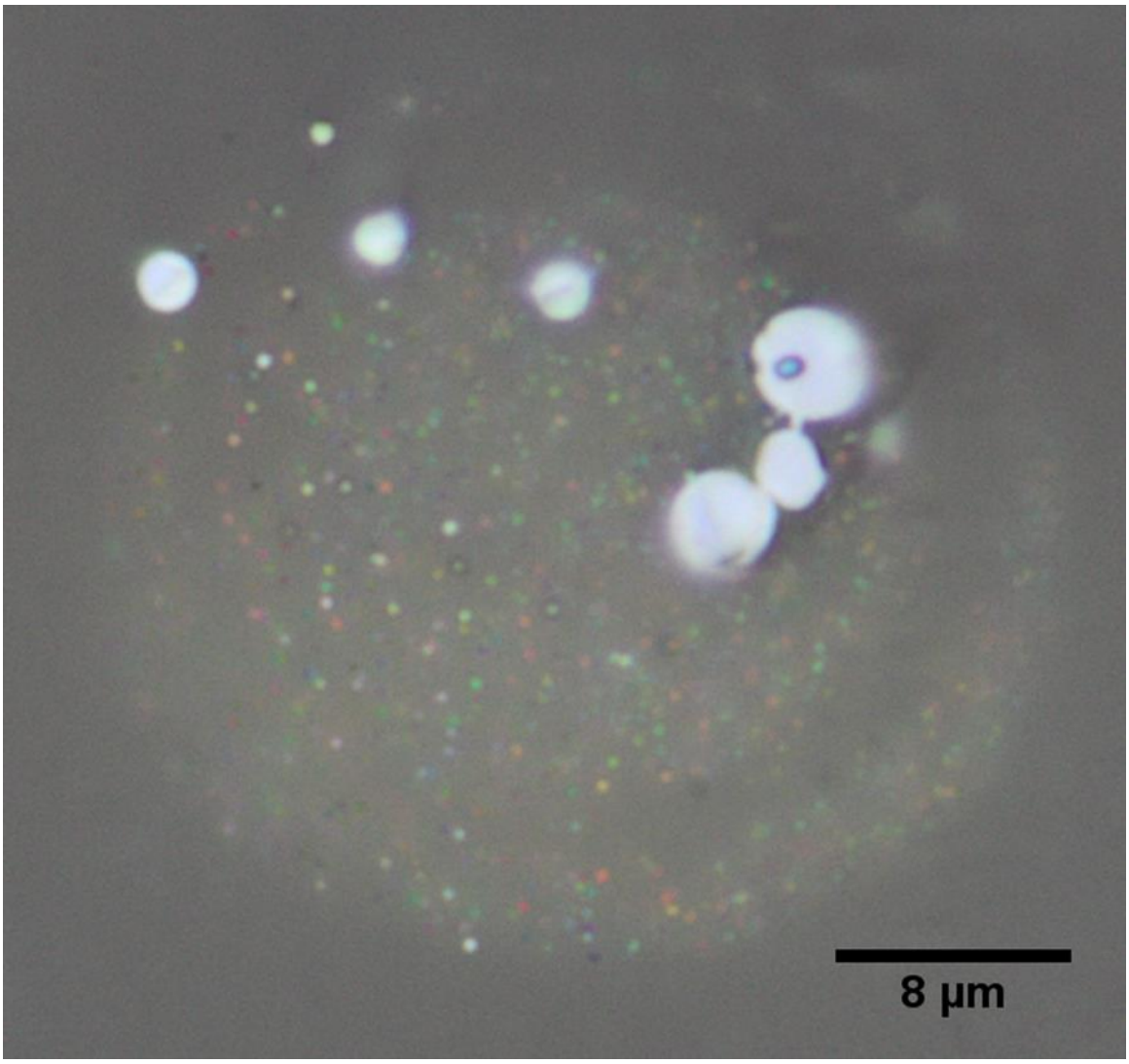

Figure 0-12: Core of fiber from Si PN preform showing core in reflected (left) with a high quantity of submicron features visible.

The core region of these fibers was found to be larger ranging from 25-30µm with hundreds of submicron features visible with reflected light. The core region showed several distinct regions distinguishable in optical microscopy with regions of glass without features appearing darker. SEM analysis of these fibers is shown in the sample fiber below in Figure 0-13.

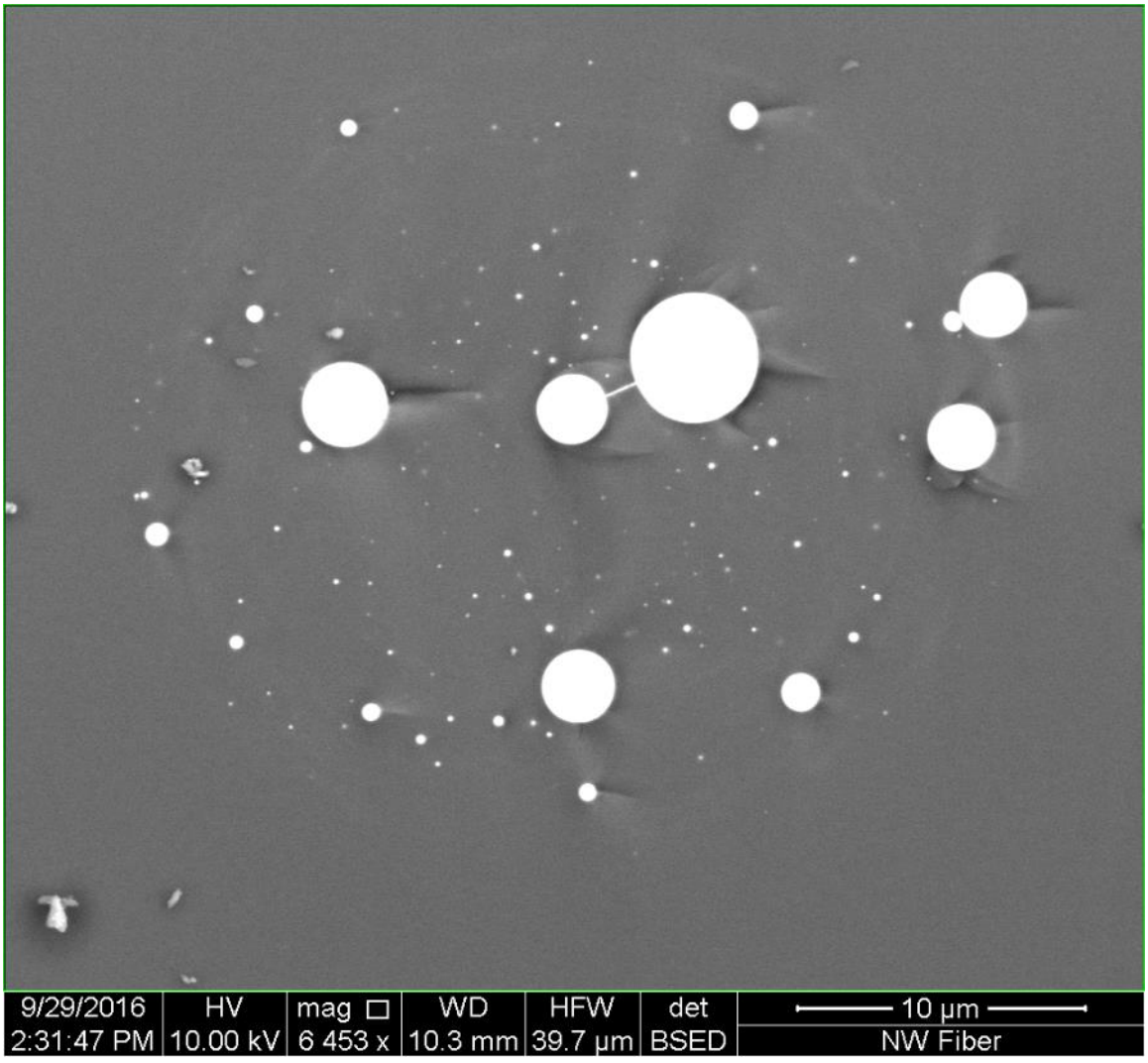

Figure 0-13: SEM of from SiPN preform with high quantity of nanowires and a few microwires.

The figure above confirms the presence of nanowires located throughout the core region with a small quantity of microwires dispersed in the region. Figure 0-13 is taken in backscatter mode, which provides high contrast for the semiconductor features. Also present is regions in the core being slightly lighter than the cladding region. This is similar to the effect observed in Figure 0-5 though to a lesser degree. This difference is attributed to a lower oxygen content in the glass regions near the semiconductor features. Analysis of the particles using ImageJ on Figure 0-13 provides additional information on the wires present. By adjusting the threshold of the image, it

allows for easy counting of particles and rough analysis of their size. The adjusted image is shown below in Figure 0-14 and is in black and white, showing the features observed in the core region.

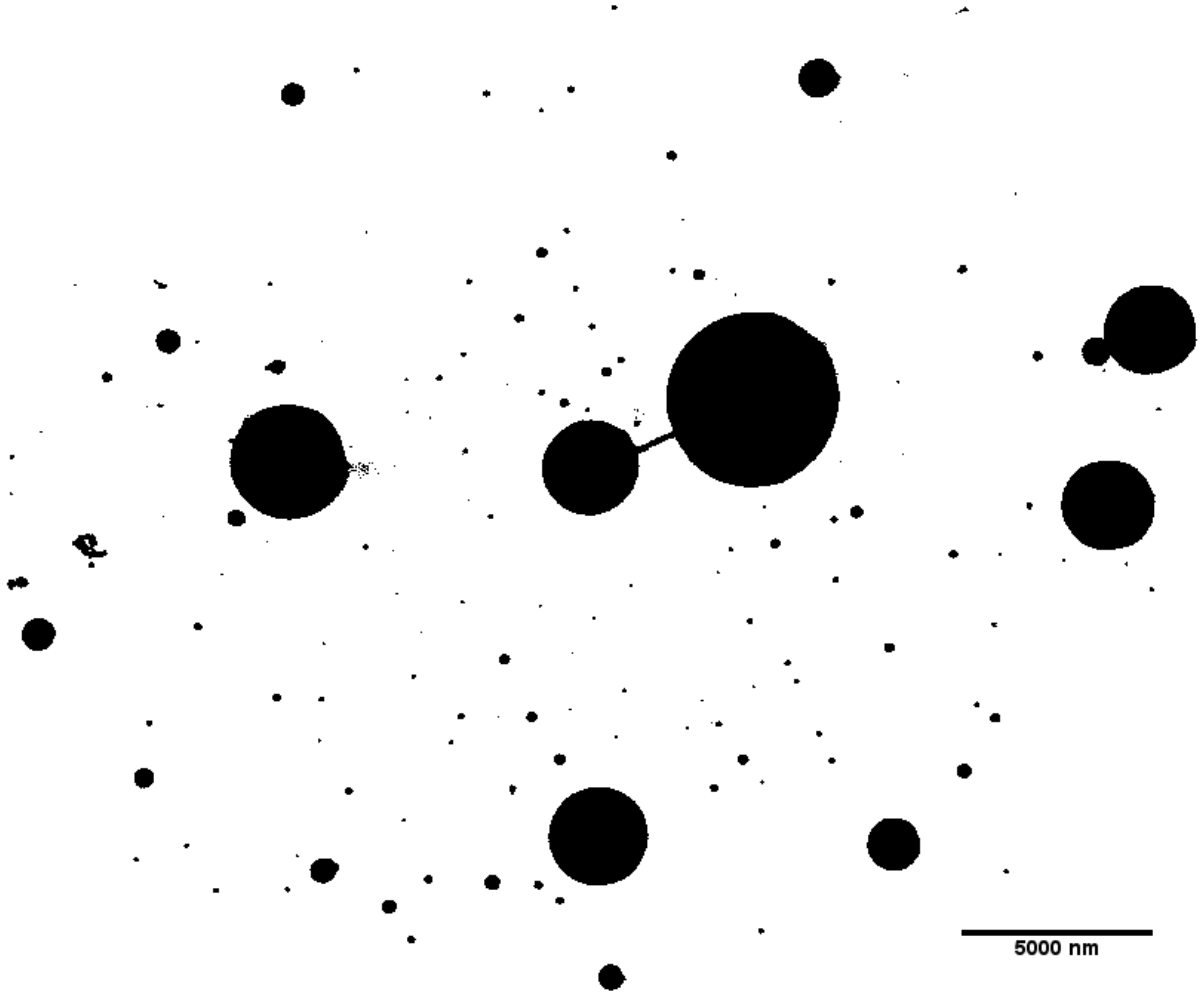

Figure 0-14: Image from Figure 0-13 modified using ImageJ to count and measure particles.

The results of the ImageJ analysis are summarized in the histogram below providing sizes and distribution for the wires.

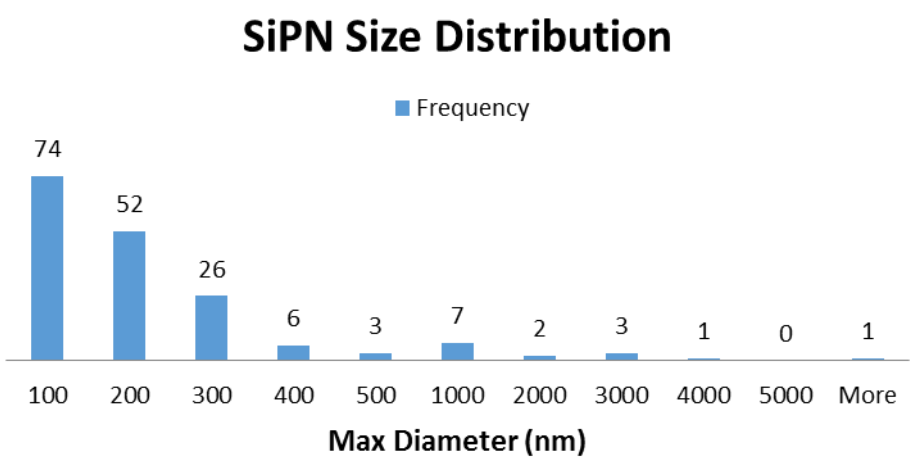

Figure 0-15: Histogram bin labeled for max size of SiPN Fiber showing distribution of wires.

The number of wires in the SiPN preform was found to be increased over the previous p-type and n-type preforms. The histogram in Figure 0-15 shows that 74 wires below 100nm in diameter were found more than double the total wires found in the previous samples.

Higher magnification of nanowires from these samples is shown below in both Figure 0-16 and Figure 0-17. These images were taken using the Inlens detector of the FESEM, which provides the highest resolution analysis possible of the scopes available at this time.

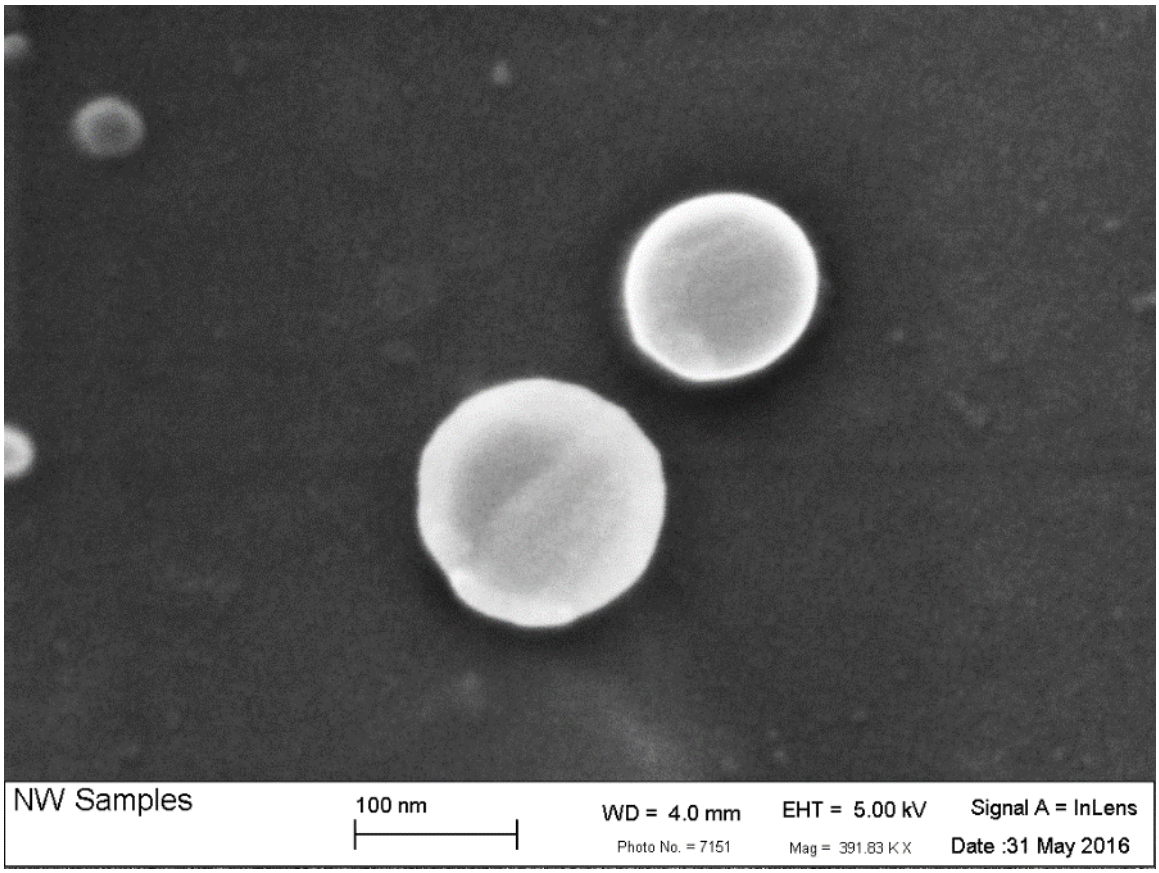

Figure 0-16: SEM of two SiNW approximately 100nm in diameter.

The above figure shows two nanowires protruding from the glass matrix. These wires are extending an estimated 100nm from the surface of glass matrix based on the etch rates reported by Williams[40]. The wires are shown to be circular in shape and located in the region of the core. In some instances, the wires produced in these fibers exhibited a different structure from the common circular shape. This structure is shown below in Figure 0-17 and shows the common circular wire structure with diameter of 100nm and additional structure protruding radially from the wire. This protrusion was measured to be approximately 20nm across and several hundred nanometers in length. The limited information into the depth of this structure prevent the determination of whether the structure is wire or plate like.

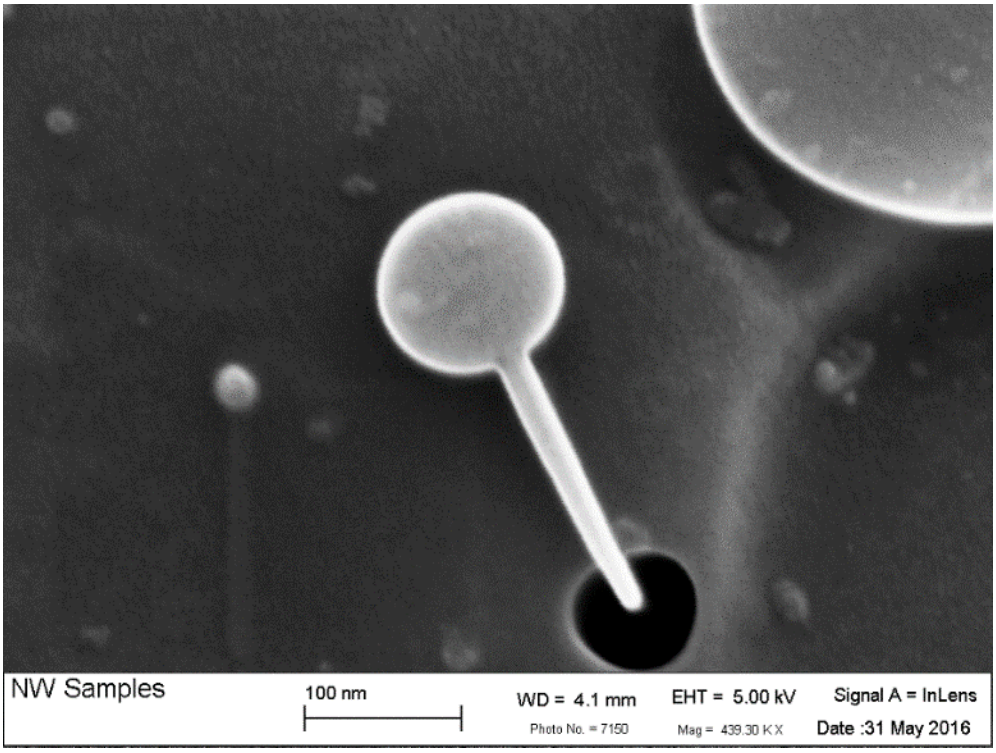

Figure 0-17: SEM of SiNW with 100nm wire with plate like structure protruding from wire.

Silicon nanowires were produced using a variety of different preforms and concentrations. The presence and size of wires was found to be highly dependent on the amount of semiconductor powder present in the core. At low concentrations of 5 wt.% the presence of wires was irregular with large sections of fiber containing only glass or void space. The regions that contain nanowires were found to interact with light allowing submicron features to be visible in optical microscopy. These regions were found to consist of a core with an oxygen deficient region with few semiconductor nanofeatures present. As the concentration of the semiconductor powder is increased up to 25 wt.% the probability of nanowires being present increases with fewer regions of voids present. When the concentration increases to 30 wt.% the presence of nanowires greatly decreased and consolidation to microwires occurs. EDS analysis of the larger microwires was possible and confirmed the wires as pure silicon. EDS was unable to detect the dopants in either

the n-type or p-type silicon though this was expected due to the detection limits of EDS at approximately 1000ppm and the available detector limitation of not being able to detect elements with an atomic number below carbon. Drawing of these doped semiconductors showed no differences in drawing behavior and confirmed no major differences to the produced fibers resulting from composition. Glass in core regions of some fibers was found to differ in appearance in both optical microscopy and SEM with backscatter detectors. Backscattered electrons provide contrast based on atomic number suggest these different regions are a different composition than the glass cladding. EDS confirmed the presence of only silicon and oxygen in these samples. The atomic concentration was found to be different from the cladding regions with lower oxygen content but was highly variable point to point. The close proximity of clear silicon features located within the cubic micron region of detection for EDS makes it difficult to determine the exact atomic ratio of silicon to oxygen in these regions.

1.7.2 Germanium Nanowires

Germanium nanowires were also produced due to the similarities of silicon with germanium as well as its own usefulness in photonic applications. Germanium has a smaller bandgap and has been shown in previous sections to have very useful photonic properties on a nanoscale. These preforms were prepared in a similar manner to the silicon based preforms and drawn on both the lathe and draw tower. Preforms are mixed based on a mass basis with silicon and quartz having similar density but germanium having higher density. Germanium's density is 5.323g/cm^3, more than double the density of silicon's 2.329 g/cm^3. Germanium preforms are mixed to the similar wt.% as their silicon counterparts and it is expected that due to the higher density that there are less than half as many semiconductor particles to be drawn down. The blowout problems

experienced in all preforms prior to the burn out treatment were the most severe for the germanium based preform causing limited success on fibers produced on the lathe. Figure 0-18 below shows germanium wires for the lathe-produced fiber with inset showing smaller sizes of wires observed.

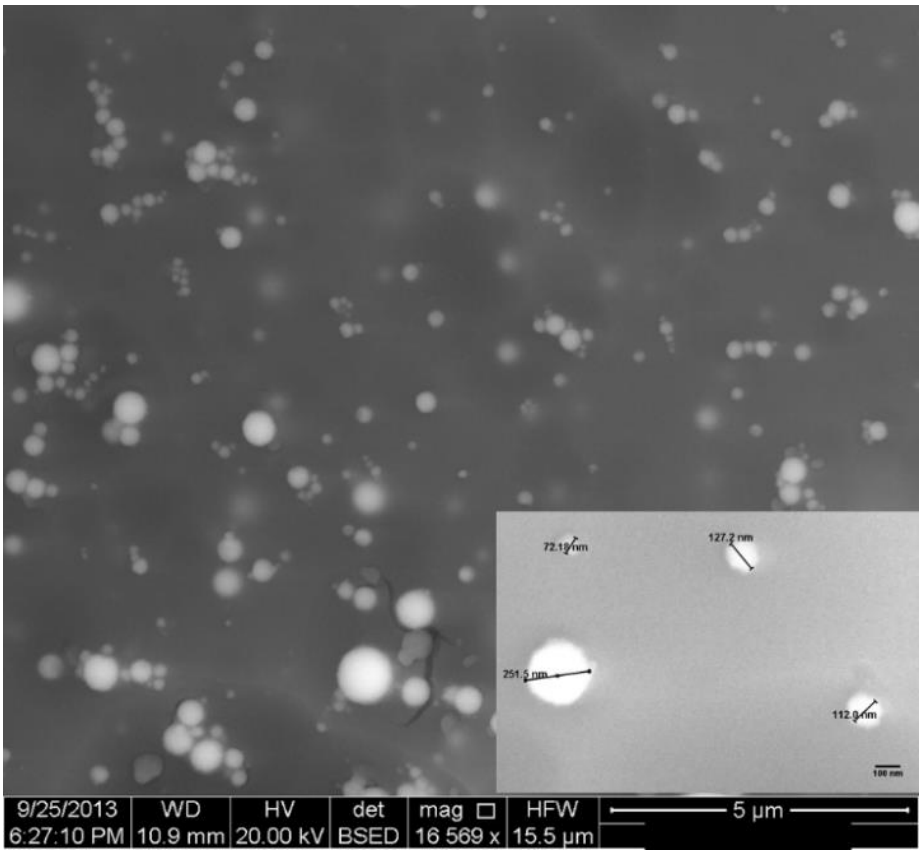

Figure 0-18: SEM of GeNW produced on the lathe showing high quantity of wires with inset showing measurements of a few.

Analysis of the particle distribution is shown below in the Figure 0-19.

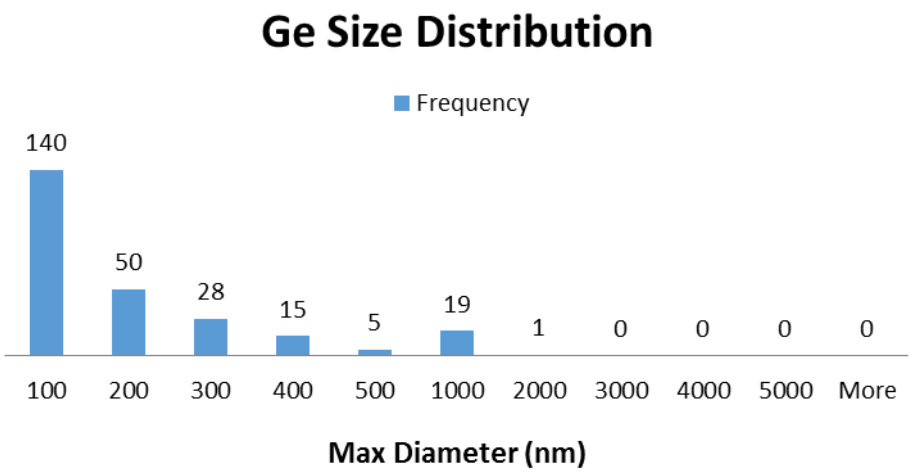

Figure 0-19: Histogram bin labeled for max size of the Ge particle distribution from lathe produced fiber.

Germanium based samples were found to have very few larger wires with only one wire in the analyzed fiber exceeding 1000nm in diameter. Just over half of the NW were below the desired 100nm in diameter.

The lathe produced fibers were successful in producing large quantities of wires but were extremely erratic with less than 1 in 10 fibers being produced with wires and at very short lengths of a couple of centimeters prior to blowout stopping the draw. Blowout was eliminated with the furnace treatment and germanium produced fibers on the draw tower produced a long continuous drawn section of fiber in this work with nearly 2km of fiber being produced.

The GeBO1 preform was produced with 20 wt.% Ge in a tube with ID 3mm OD 14.4mm. While extremely long lengths of fiber were produced from the germanium preform, the fiber was found to have not fully collapsed with holes present in a large majority of the samples. Examples of this structure are shown below in Figure 0-20 and Figure 0-21. These figures show the fiber in optical microscopy and SEM. Differing from the behavior of the SiNW samples in optical

microscopy, these fibers showed holes present in most and a few small features clearly visible with reflected light. SEM analysis showed that the features present were submicron in most samples and some features as small as 100nm.

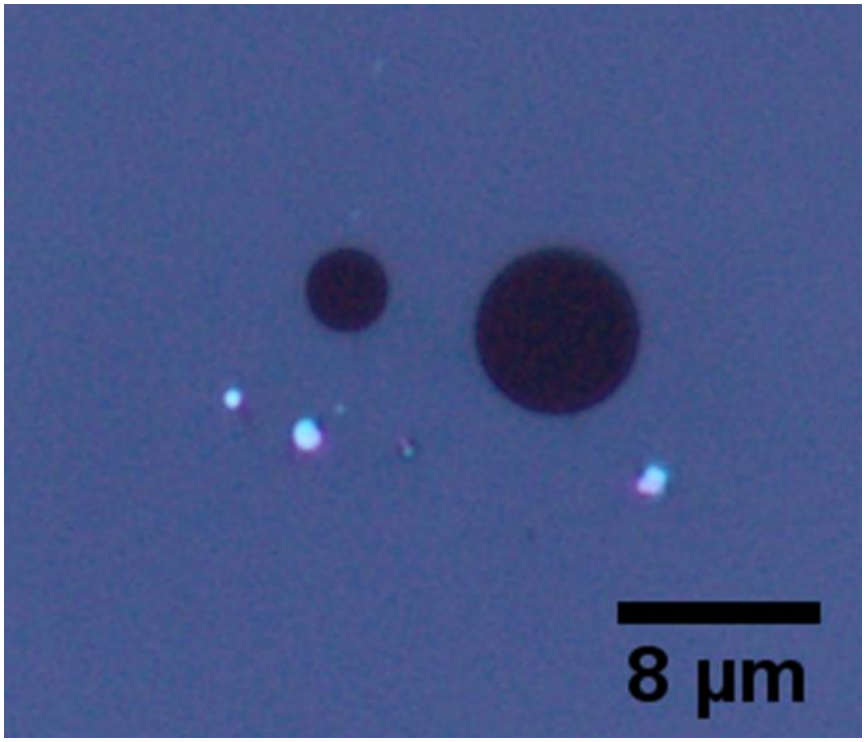

Figure 0-20: Core of fiber from GeBO 1 preform showing holes and sub-micron wires present.

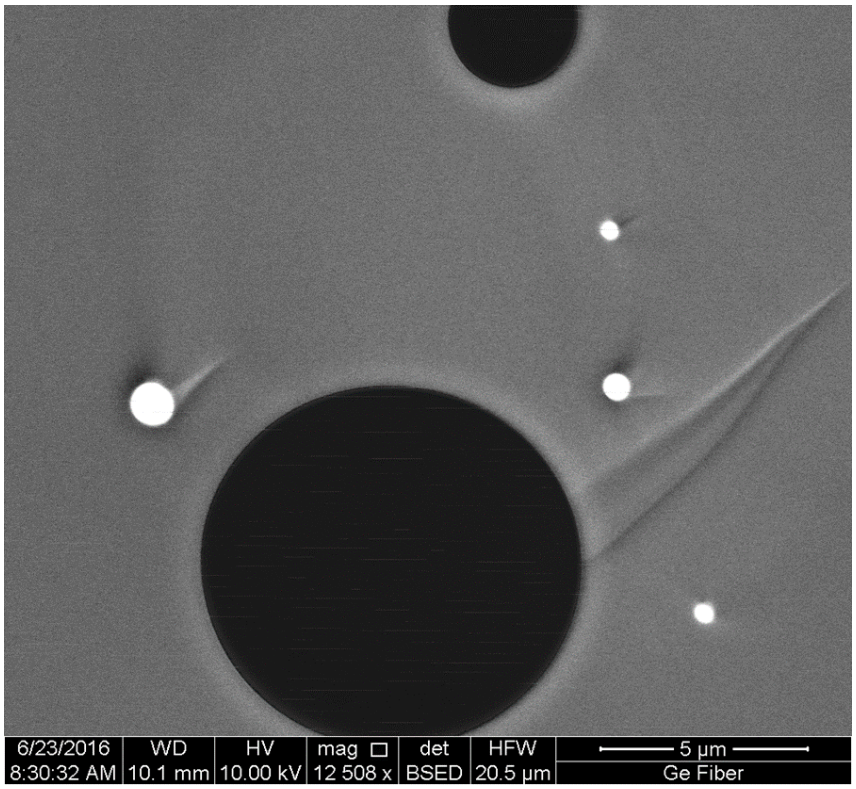

Figure 0-21: SEM of GeNW from preform GeBO1 with a small quantity of wires located near several holes.

While the hole-based regions were the predominant feature of the GeBO1 fibers, there were regions that fully collapsed and produced a solid fiber. These regions were found to have no features resembling wires but a region appearing to consist of multiple compositions and is shown below in Figure 0-22.

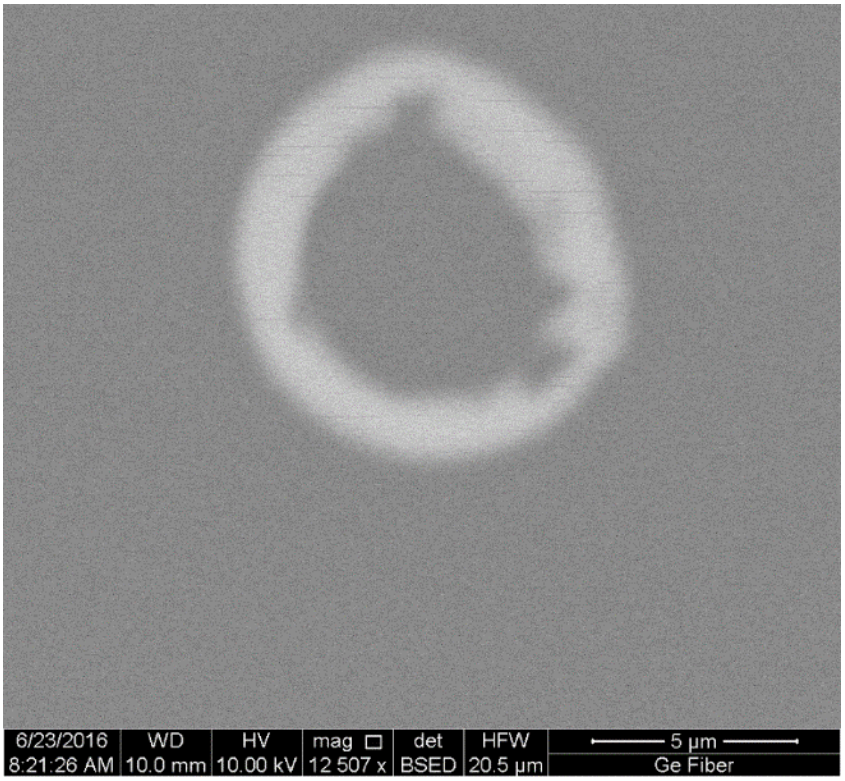

Figure 0-22: SEM of GeBO1 fiber taken with BSED showing distinct ring shape of composition difference in core region.

EDS taken of the regions in the fiber found the bright region to be composed of silicon, germanium, and oxygen with the darker regions being composed of only silicon and oxygen and is shown below in Figure 0-23.

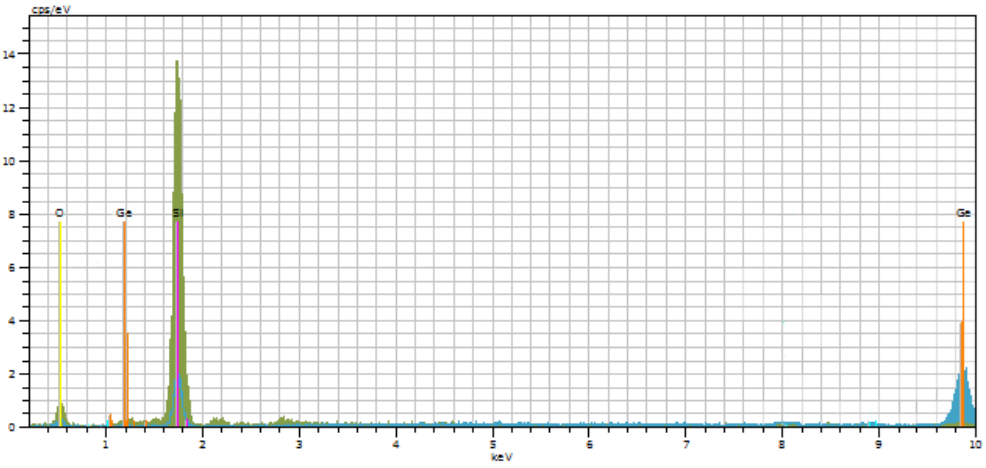

Figure 0-23: EDS Spectra of fiber from Figure 0-22 with the green spectra showing the darker cladding region absent of germanium and the blue spectra from inside the brighter region.

This region is thought to be the result of oxidation of the germanium particles and the diffusion of the germanium dioxide into the silica. The reduced presence of wires and the existence of the ring structure in fibers produced on the tower compared to the lathe is a result of germanium becoming oxidized prior to reaching the drawing region. Fibers produced on the lathe are produced with a highly localized heat source from the torch and the powder undergoes very little heating outside of the drawing region. In contrast, 18-20cm of preform are located in the furnace above the drawing point and exposed to elevated temperatures prior to melting allowing oxidation to occur.

1.7.3 Silicon-Germanium Alloy Nanowires

Silicon and germanium preforms were produced initially and used to develop an understanding of the particle sizes and compositions necessary to produce nanowires as well as the optimal drawing conditions. The desire to be able to produce SiGe alloy-based features comes from the tunable nature of electronic properties in the alloys. Discussions in section 2 referenced the variable nature of properties including the bandgap across the compositional range of silicon-germanium. The phase diagram also showed that a solid solution is formed across the entire compositional range allowing any composition to be made. The goal of this work was to be able to produce these alloy features in fiber from a mixed powder preform. The silicon and germanium powders for this experiment were made from the same sources as the individual silicon and germanium preforms. Based on the results observed during the silicon and germanium preforms the mixture of 25 wt.% semiconductor was chosen for the alloy experiment to provide a high quantity of wires while minimizing the presence of microwires. The structure of the preform is shown below in Figure 0-24. In this preform, the total semiconductor

concentration was made the same though the %Ge in the powder was varied along the length of the preform.

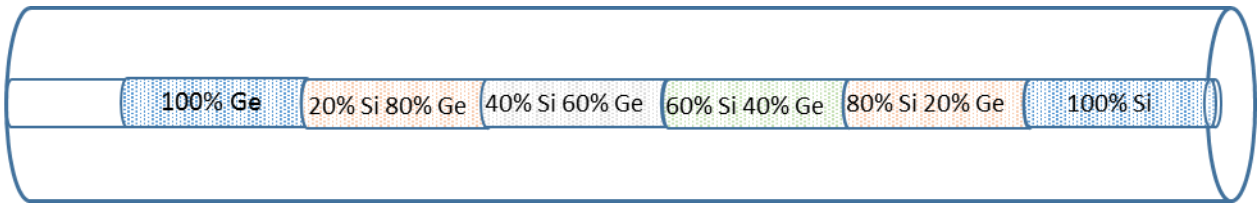

Figure 0-24: Schematic showing step composition of SiGe preform with each composition being 5cm in length.

This variation allows for the determination of producing alloys from a variety of compositions as well as the possibility of varying composition along length without issue. The tube chosen for this draw was OD 14.4mm ID 3mm. All powders were milled and sieved to -20µm. Drawing of this preform provided a high quantity of fiber due to the long nature of the preform. This also required the draw to last several hours, during which time a break in the fiber occurred and the draw had to be restarted in the process. The restart of the draw causes a large section of preform to be lost 2-3cm resulting in a sizable quantity of the 60% Si 40% Ge region to be lost. A sample of fiber observed in optical microscopy is shown below in Figure 0-25.

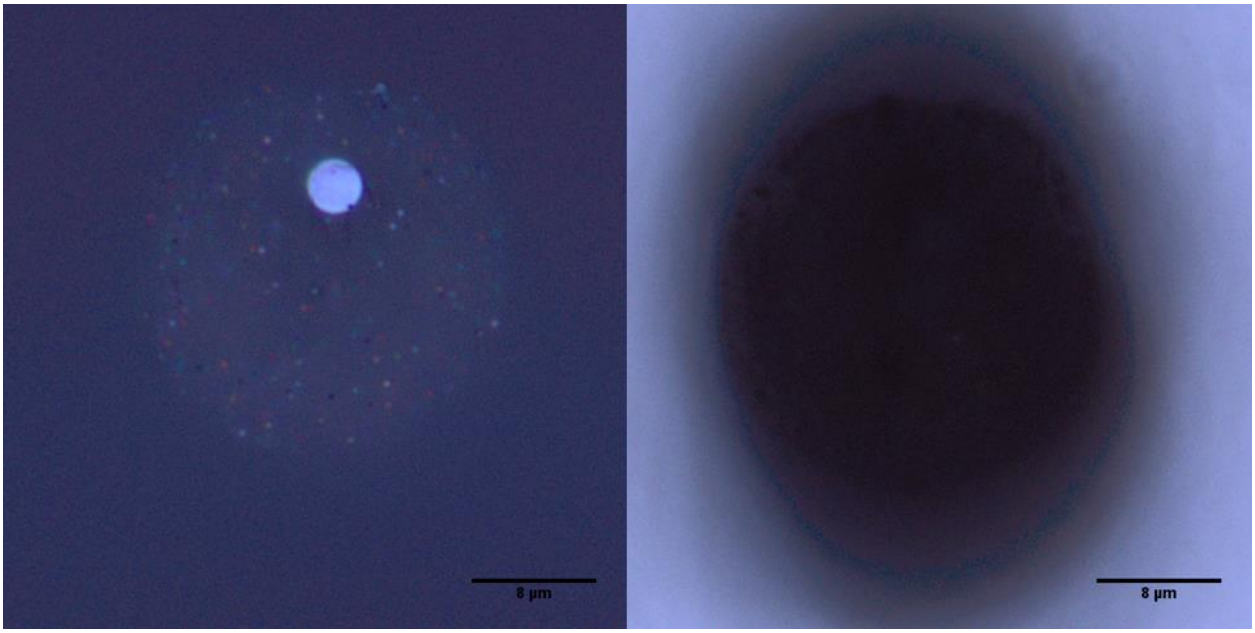

Figure 0-25: Core of fiber from SiGe preform showing the same region in reflected (left) and transmission (right) with several microwires present.

The SiGe samples were characterized by very few microwires and clearly visible submicron features in reflected light. A noticeable difference was observed using transmitted light with the core absorbing and blocking nearly all light from passing through. This dramatic increase in light blocked is caused by the larger quantity and more even distribution of features through the core region. Figure 0-26 below shows a region from SiGe that possessed more microwires that was etched to provide a better understanding of aspect ratios of these features. This etching was done with concentrated 49% HF and was done for 2 minutes to provide approximately 2-3µm semiconductor sticking out of the fiber matrix. The image shows however that the etch rate was much greater in regions around the wires causing deep etch pits and many of the smaller features to be completely lost from the fiber. This deep etching allowed for a wire 100nm in diameter and several microns in length to be observed shown in Figure 0-27

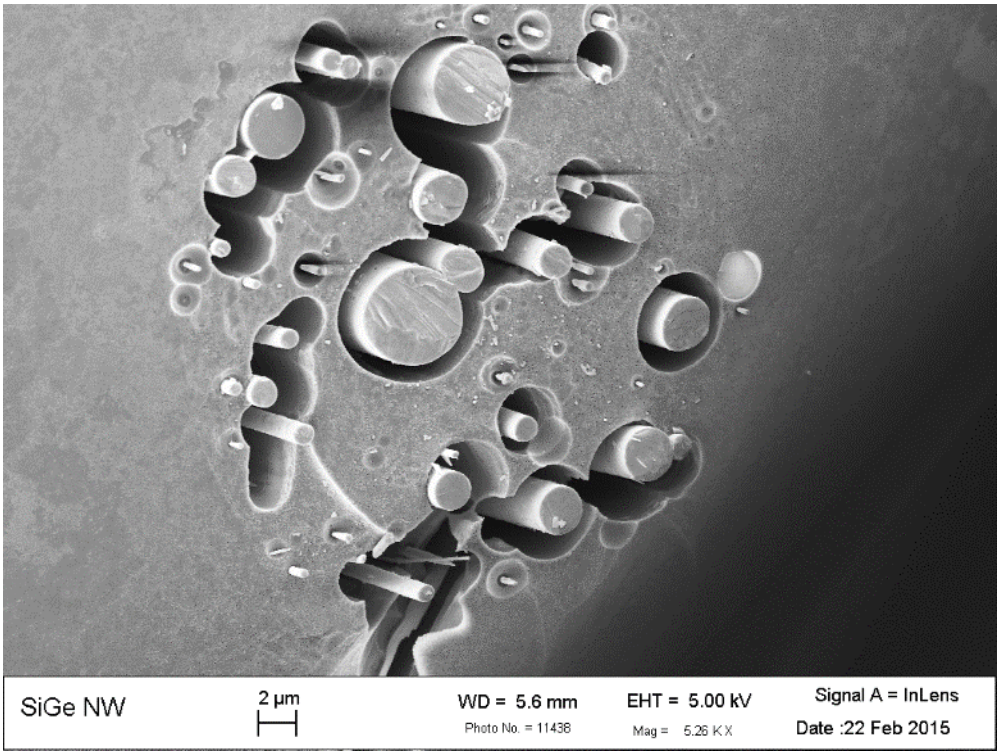

Figure 0-26: SEM of SiGe fiber after etching tilted 15° to help show length.

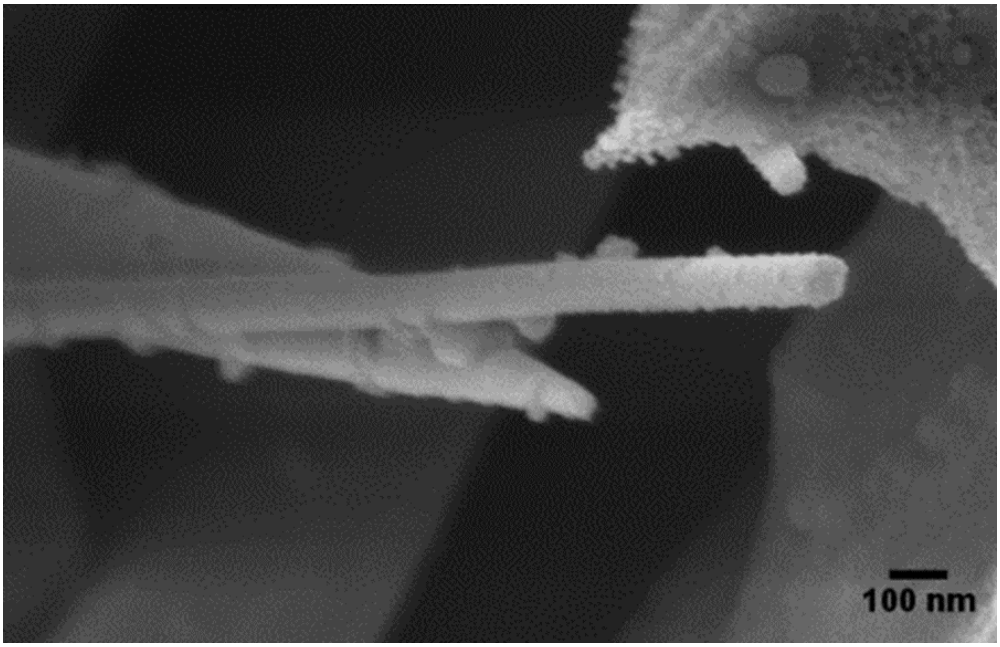

Figure 0-27: SEM close up of small wire from Figure 0-26 showing nanowire sub 100nm diameter microns in length.

The large quantity of fibers produced during this draw required a method to easily screen and sort fibers to aid in finding fibers with the nanowires present. Based on the light absorption observed in these samples it allowed for fibers to be easily sorted by examining them over the surface of a flashlight. Fibers were easily divided into two groups; those with a dark core region and those that appeared to be predominately clear. Samples from these two groups were examined in SEM and found that the samples with the dark region had high quantities of nanowires present. Samples that appeared clear had nanowires present in low quantities and were present in a small fraction of the samples. As the preform was drawn, fibers were separated into composition groups based on the starting size of the region and calculated based on the feed speed of the preform when a new composition was reached. The break in the middle of the draw and subsequent restart resulted in some error to these regions being divided. Fibers from the 100% germanium region were largely binned as having no visible features and few wires were found in the samples. The remaining 4 regions of compositions all had large quantities of fibers with features visible and were analyzed in SEM to determine sizes and distribution of nanowires. In addition to analysis of the end faces of these fibers, nanowires were removed from the glass matrix entirely by etching and collected via filter paper. Based on the highly rapid severe etching observed using concentrated HF, a dilute 5:1 HF solution was used to better control etching and minimize any features lost. Thirty sections of fiber approximately 5cm in length were placed in containers for etching and 250mL of 5:1 HF solution was added to ensure adequate quantity to etch the entire glass matrix. After etching, the acid solutions were filtered using vacuum filtration through hardened filter paper with very fine particulate retention (~1μm). The removed wires were then rinsed with DI water to help remove any remaining HF residue and then placed in a

desiccator box and allowed to dry before being placed in the SEM. The results from the four regions are shown in the figures below and summarized in Table 0-2. Compositional analysis was done on several wire sections using EDS to compare to the target compositions. These points were selected along several of the larger wire and had variance of 1-2 atomic percent on a given sample, which is reported as the average here.

Table 0-2: Summary of Fiber Regions analyzed from SiGe preform

Sample	Target Composition (wt.)	EDS Measured Composition
SiGe 1	100% Si	100% Si
SiGe 2	80% Si-20% Ge	85% Si-15% Ge
SiGe 3	60% Si-40% Ge	Section lost during restart
SiGe 4	40% Si-60% Ge	20.5% Si-79.5% Ge
SiGe 5	20% Si-80% Ge	14.2% Si- 85.8% Ge
SiGe 6	100% Ge	Very few wires found

Samples from the silicon rich side of the preform, taken prior to the fiber break and subsequent restart of the draw, agree well with the target compositions. The samples measured after the break did not agree with the expected target composition. This is likely caused by human error separating the fibers and the estimated point of fiber break and the amount of preform lost during the restart. Additional analysis on remaining fiber sections would likely find samples closer to the other target compositions.

Figure 0-28 below shows the core region of fibers from SiGe 1 with wires produced of pure silicon. Micro and nanowires were both visibly present in the sample. Slight variations in the contrast of the glass regions around the wires was observed similar to that observed in the pure silicon based preforms.

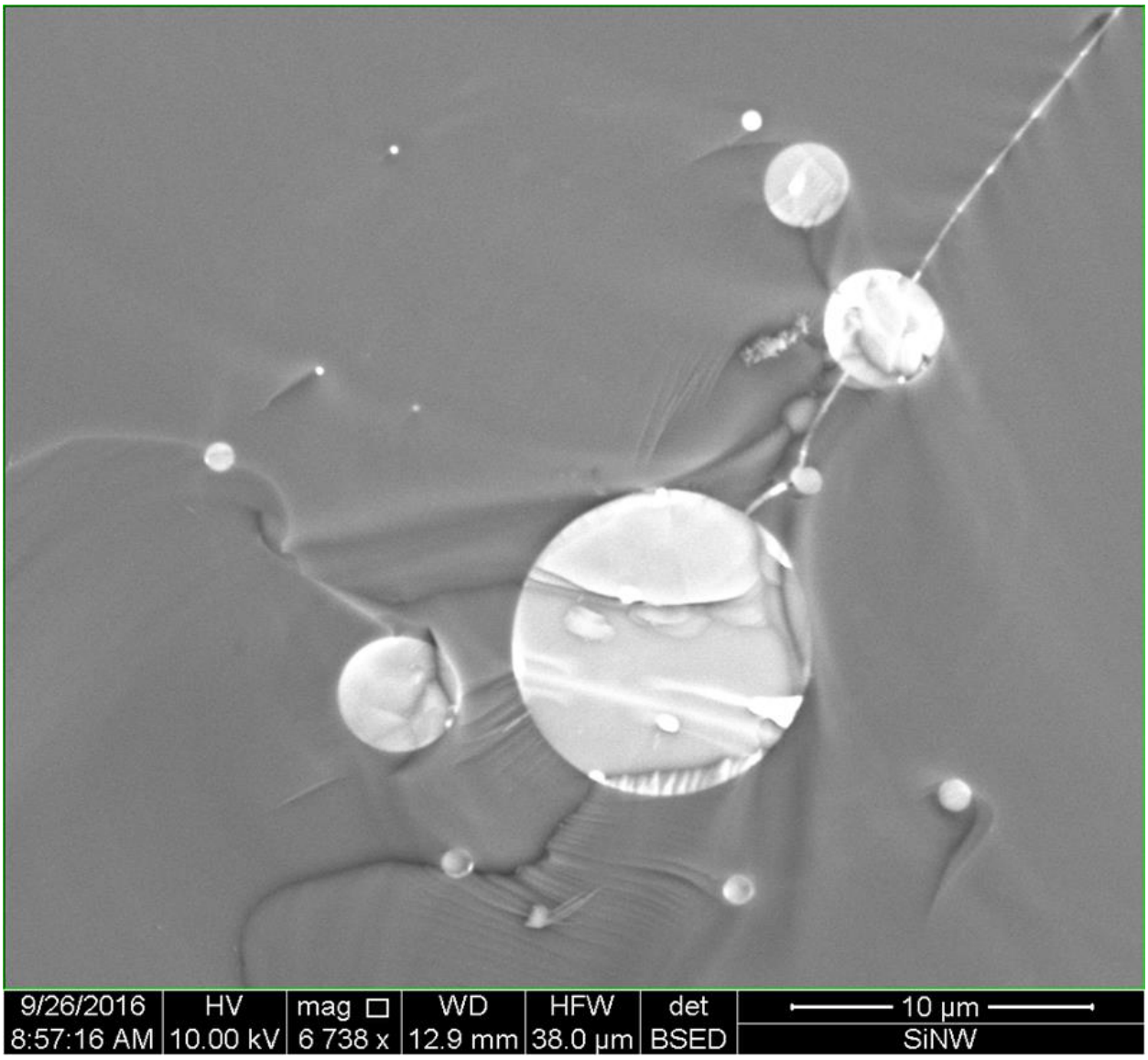

Figure 0-28: SEM of SiGe #1 fiber from region with measured composition of 100wt. % Si.

Removal of wires from these fibers was accomplished and were recovered via the filter paper. SiGe 1 showed few wires visible to the naked eye on the surface of the filter paper. Analysis of these wires was accomplished by two methods. The first method consists of direct mounting of small sections of filter paper to SEM stubs using graphite paint around the edges and coating the sample with iridium. The second method involves using carbon mounting tape to pick up the

wires from the filter paper surface and collect as many as possible then coating with iridium. Figure 0-29 below shows wires recovered directly on the filter paper.

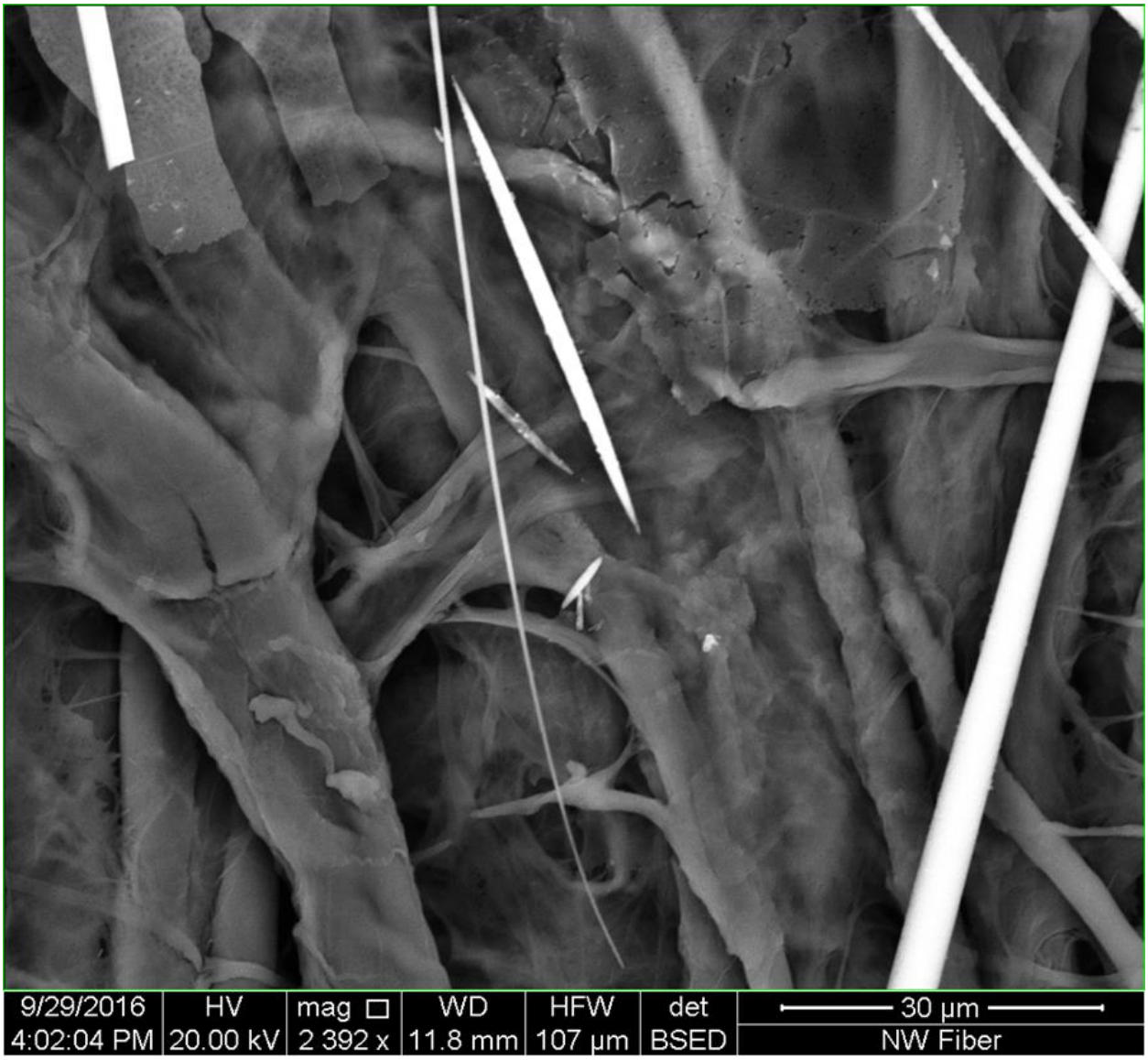

Figure 0-29: SEM of SiGe 1 (100 wt.% Si) NW removed from fiber via etching.

The recovered wires were limited for SiGe 1 and consisted primarily of microwires. The only nanowires found for these samples were found down in holes of the filter paper and near the edges of the paper suggesting that the smaller wires may have washed off the filter paper and

been lost. The center wire shown in Figure 0-28 measured hundreds of microns in length with a diameter at ~100nm, demonstrating the capability to produce very high aspect ratio nanowires.

Figure 0-30 shows the core region of fiber from SiGe 2. This region was found to have more nanowires present than the pure silicon region that preceded it.

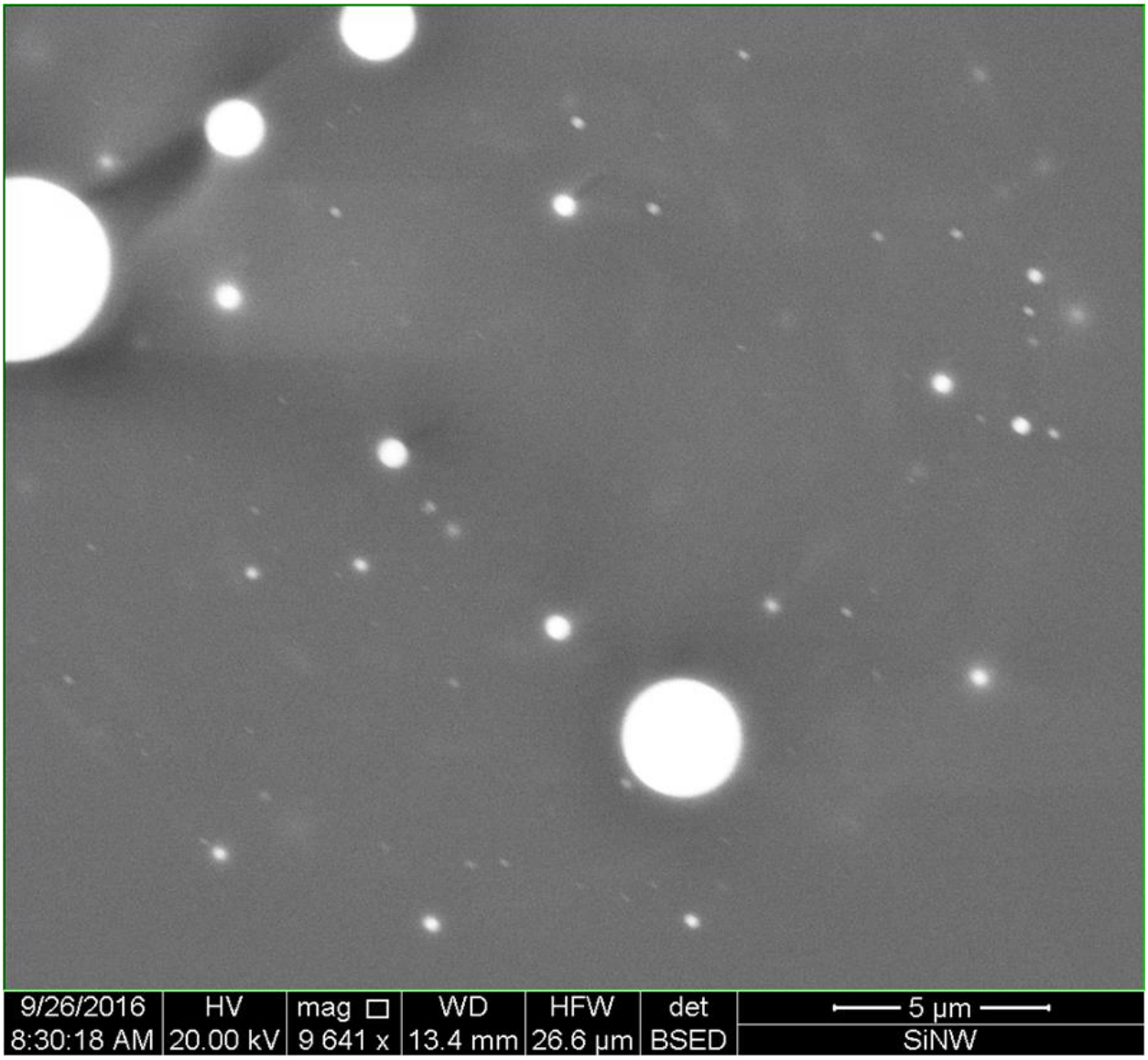

Figure 0-30: SEM of SiGe #2 fiber from region with measured composition of 85 wt.% Si/15 wt.% Ge.

Figure 0-31 shows nanowires recovered after being removed from the matrix with etching. The left image shows a large selection of wires recovered from filter paper using carbon tape.

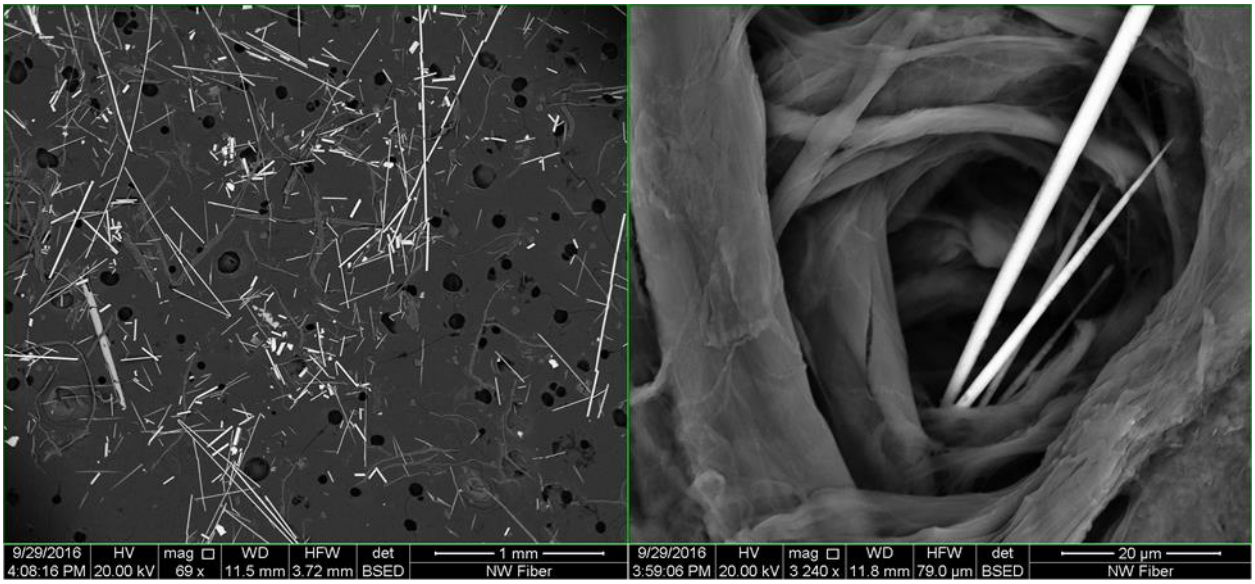

Figure 0-31: SEM of SiGe 2 (85 wt.% Si/15 wt.% Ge) NW removed from fiber via etching collected on carbon tape (left) and in the pore of the filter paper (right).

The right image of Figure 0-31 shows a few of the smallest nanowires found trapped in a pore of the filter paper. A large quantity of wires was present on the filter paper but predominately consisted of those 500nm and larger in diameter. Similar to the wires recovered from the sample 1 fibers the wires recovered were few and were located towards the edges of the filter paper with the smallest wires being found only in the pores of the filter paper.

Figure 0-32 shows the end face view from SiGe 4. In contrast to samples from the silicon rich regions a hole was observed in the core region. The quantity of nanowires observed was significantly higher than the number of wires observed in SiGe 1 and SiGe 2. Variations in the contrast of the glass is still visible while the semiconductor features show up considerably brighter due to the presence of germanium in the sample.

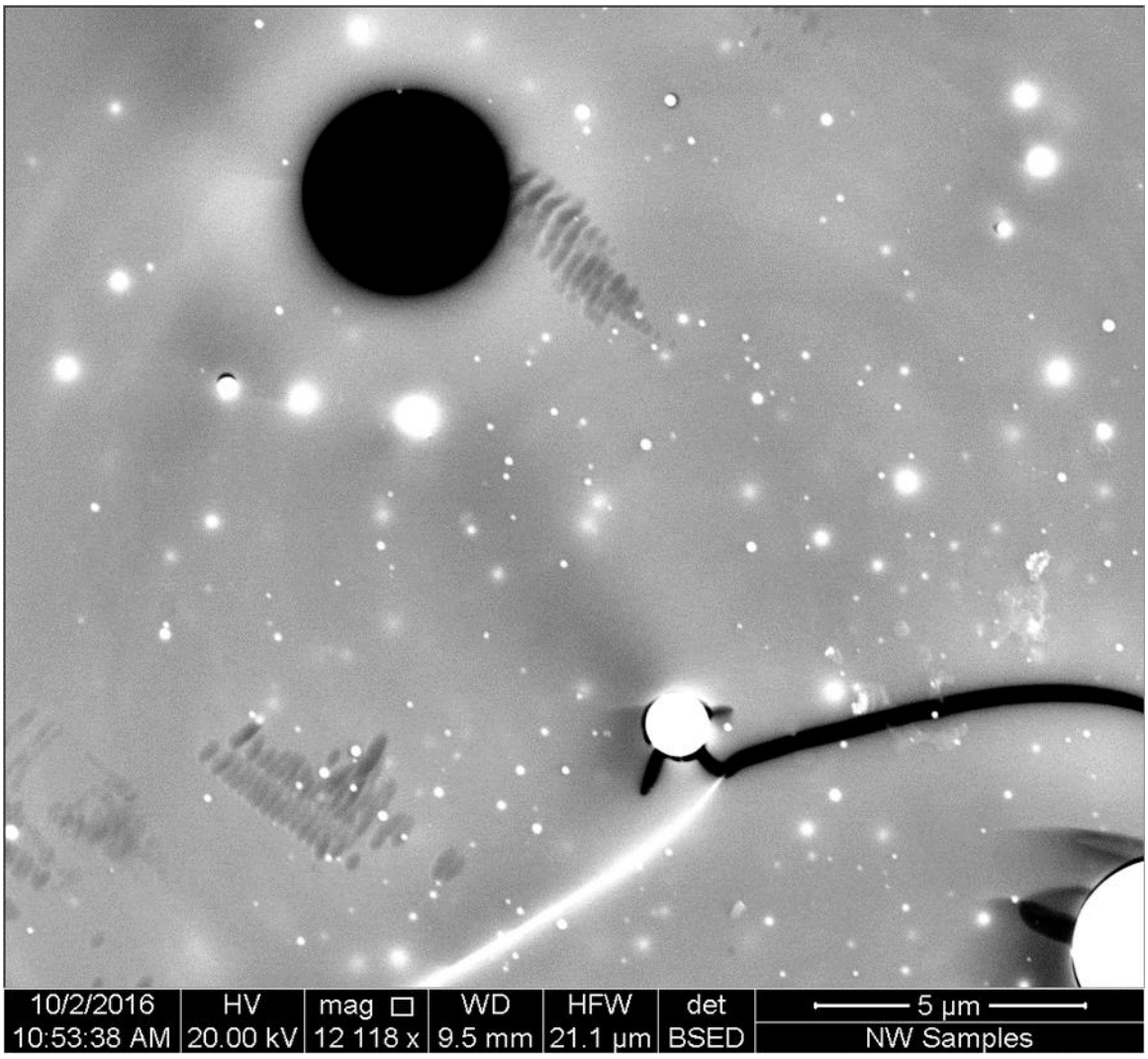

Figure 0-32: SEM of SiGe 4 fiber from region with measured composition of 21 wt.% Si/79 wt.% Ge.

Figure 0-33 shows high magnification of the wires after removal from the glass. SiGe 4 and SiGe 5 differed from SiGe 1 and SiGe 2 with significantly higher quantities of wires being visibly present on the filter paper. The wires can be separated into two groups with wires near a micron in diameter with lengths from tens of millimeters up to centimeters and much smaller wires near the surface with diameters below 100nm and lengths of several microns. These smaller wires are shown below and are characterized with surfaces appearing rougher than those from silicon rich regions.

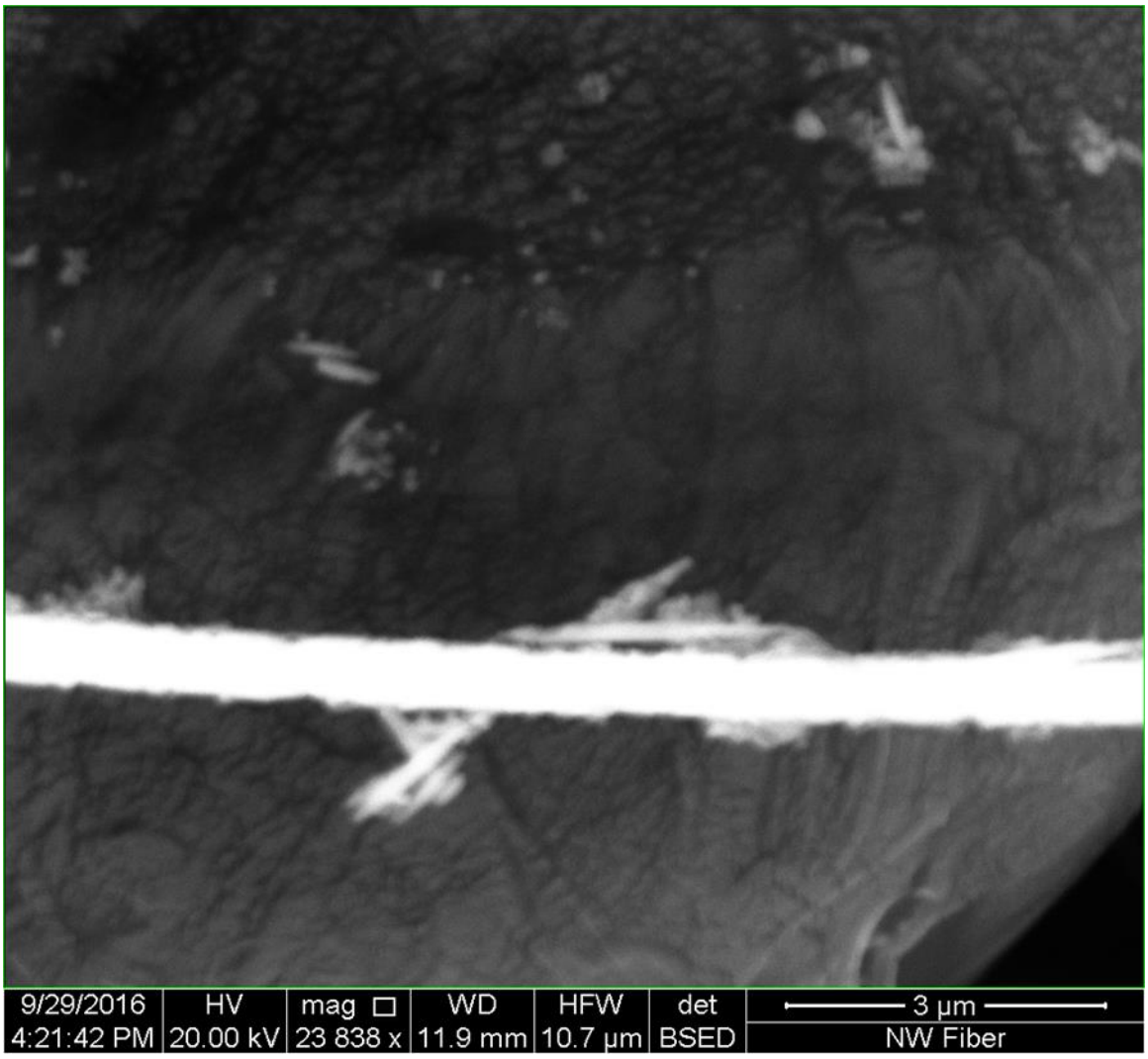

Figure 0-33: SEM of SiGe 4 (21 wt.% Si/79 wt.% Ge) NW removed from fiber via etching.

EDS analysis confirmed no unwanted contamination present on the samples even with the rougher appearance.

Figure 0-34 shows the end face results in backscatter of fibers from SiGe 5. These fibers appeared similar in appearance to those from SiGe 4, which is expected due to the similar composition discovered in EDS results. Fewer wires were present in these samples with the

microwires still being present in most fibers examined. While not shown in the figure several fibers still demonstrated holes present in the core region.

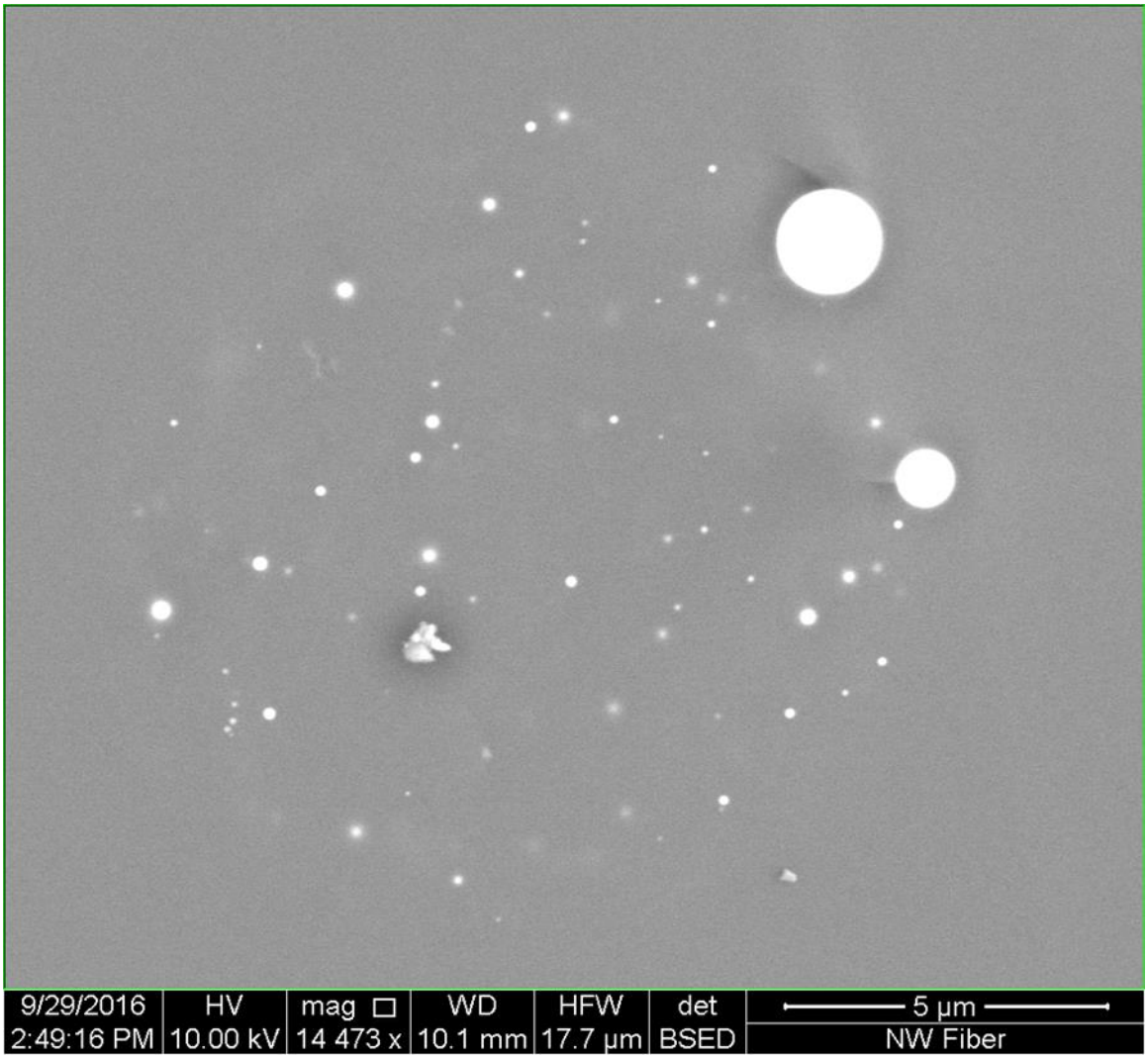

Figure 0-34: SEM of SiGe 5 fiber from region with measured composition of 14 wt.% Si/86 wt.% Ge.

Wires removed from this sample strongly resembled those from SiGe 4 in both size and shape. Some wires appeared to show the rougher structure that was present though EDS confirmed no contaminant elements in the samples. Wires removed from these samples are shown below in Figure 0-35 and Figure 0-36.

Figure 0-35: SEM of SiGe 5 (14 wt.% Si/86 wt.% Ge) NW removed from fiber via etching.

The smaller wires were found in pores of the filter paper and based on the observed sizes it is likely that many of the smaller features were not trapped by the filter paper. Figure 0-36 shows low magnification images of wires recovered from SiGe 5. Hundreds of wires are shown from just a small section of filter paper, while the wires can be recovered and drastically consolidated by using carbon tape to collect them.

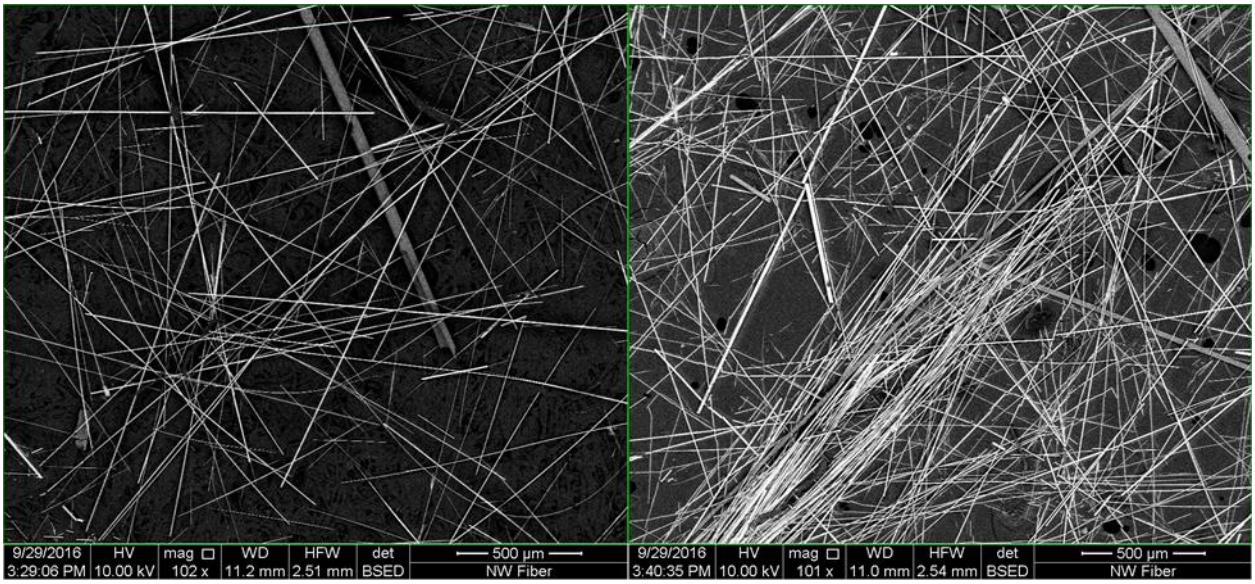

Figure 0-36: SEM at low magnification of SiGe 5 on filter paper (left) and collected on carbon tape (right) showing length and high quantity of wires recovered from fiber.

Semiconductor nanowires in the SiGe alloy system were successfully produced with varying compositions from a single preform. These alloys were produced from mixing high purity silicon and germanium powders in the core. EDS analysis confirmed that wires could be produced using this method with the alloy composition within 1 wt.% of the mixed powder composition. Analysis of the particle sizes and distributions was carried out using ImageJ. Figure 0-37 below shows histogram comparisons of the four compositions of the SiGe preform that were shown in the figures above.

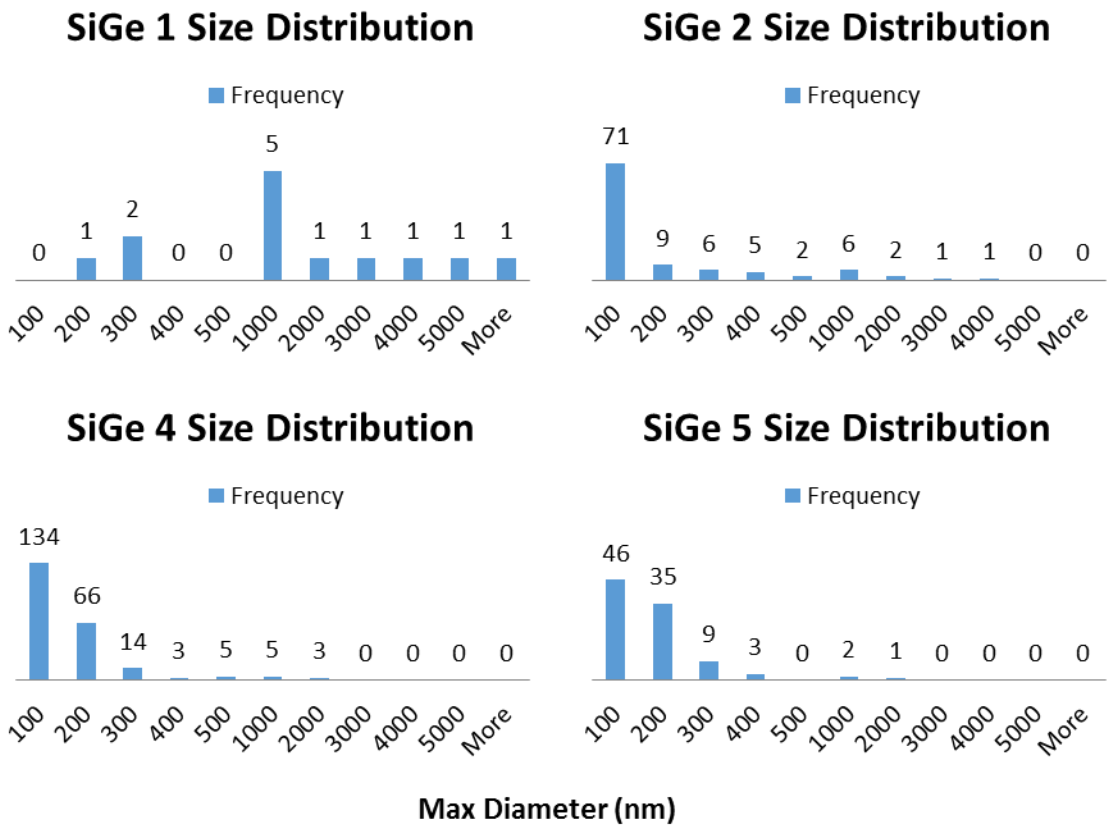

Figure 0-37: Histograms bins labeled for max size of the four SiGe compositions showing the wire sizes and distributions produced.

Wires produced in the silicon rich alloy regions were found to have fewer wires, only thirteen in SiGe 1 sample. The shift in composition from pure silicon in SiGe 1 to 85 wt.% silicon in SiGe 2 showed radical change in quantity, 13 to 103, and distribution from 0 percent to 70 percent of the wires below 100nm diameter. SiGe 4 and SiGe 5 had similar compositions and similar wire distributions though showed different quantities of total wires. The difference in wire quantities from the histograms and the observed lengths in the removed wires shows that the quantity of wires varies along the length and radically different numbers of wires can be found in nearby samples. Wires recovered from etched samples were significantly fewer in this region of

compositions but nanowires that were recovered were found to have higher aspect ratios. The quantity of nanowires was observed to be significantly higher in the germanium rich regions. In addition to the higher quantity of nanowires, void spaces were also found in the core regions of fibers in the germanium rich region. These void spaces were fewer but similar to those found in the fibers produced in the pure germanium samples. Fibers produced from these preforms were similar to those produced in both the pure silicon and pure germanium samples with regions of nanowires and regions of solid glass fiber varying along the length of the fiber. Differing from previous draws fibers with nanowires present were easily distinguished by a dark core region observable to the naked eye. Fibers that contained few or no nanowires appeared to be completely clear when viewed from the side. This allowed for quick screening and sorting of fibers to increase the chance of getting a sample with nanowires present.

In addition to producing fibers of varying alloy compositions these samples provided an understanding into differing etch behavior based on the strength of the HF acid used for etching.

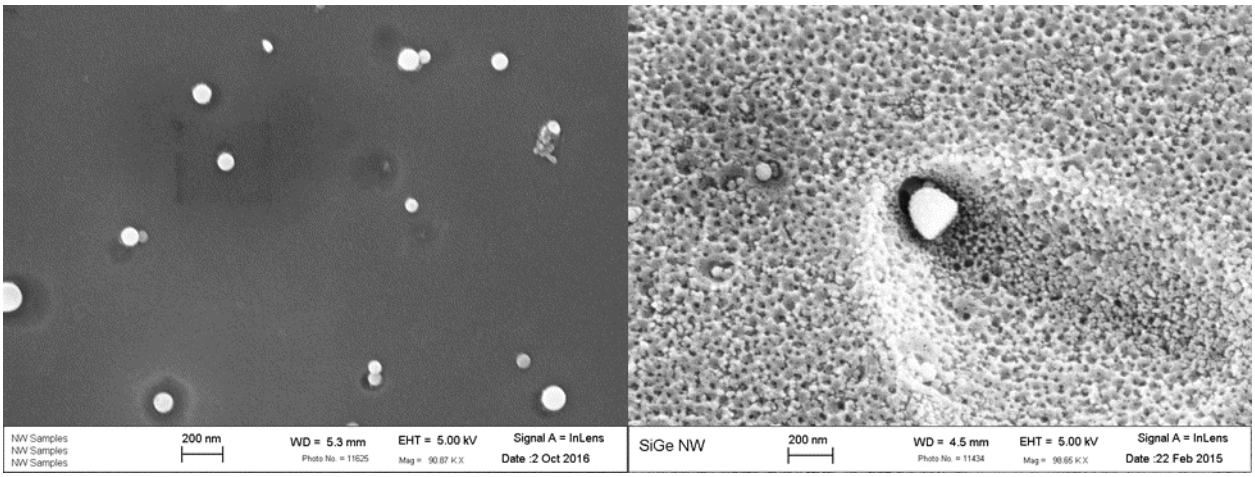

Figure 0-38: Comparison of SiGe samples using dilute 5:1 HF (left) and concentrated stock 49% HF (right).

In Figure 0-38 above two samples are shown from the SiGe preform etched using varying concentrations of HF acid. The sample in the left of the figure was etched for 5 minutes using 5:1

HF while the one on the right was etched 3 minutes in 49% HF. Drastically higher etch rates are expected with the concentrated acid though etch rates in both cases were higher than the reported values. Regardless of etch concentration, faster etching occurs at the interface of the semiconductor features with pits forming around them. When concentrated HF was used however, a preferential etch was observed in the glass region of the core. This glass structure strongly resembles porous structures found in phase separable glasses and has not been observed in other samples during this work. Understanding the mechanism causing this phenomenon is beyond the scope of this work though merits further work due to the potential use of nanoporous silica.

1.7.4 Microstructured Fiber

In addition to the direct fiber draws performed in this work, a 2-step draw was employed to show that the regions of semiconductor features could be controlled and integrated with traditional optical features. This 2-step process is similar to the process used to produce photonic crystal fibers. In this process, a traditional preform such as those used in the silicon, germanium, and alloy work is drawn on the draw tower down to only a thickness of approximately 1-3mm. This thicker structure called cane is then stacked in another glass tube that allows for control of the location and provide further draw down of the size. This preform was produced using cane from the SiPN preform with 14 sections of cane stacked around a traditional Ge-doped core rod in a fused quartz tube. This preform, after the draw was completed, is shown below in Figure 0-39.

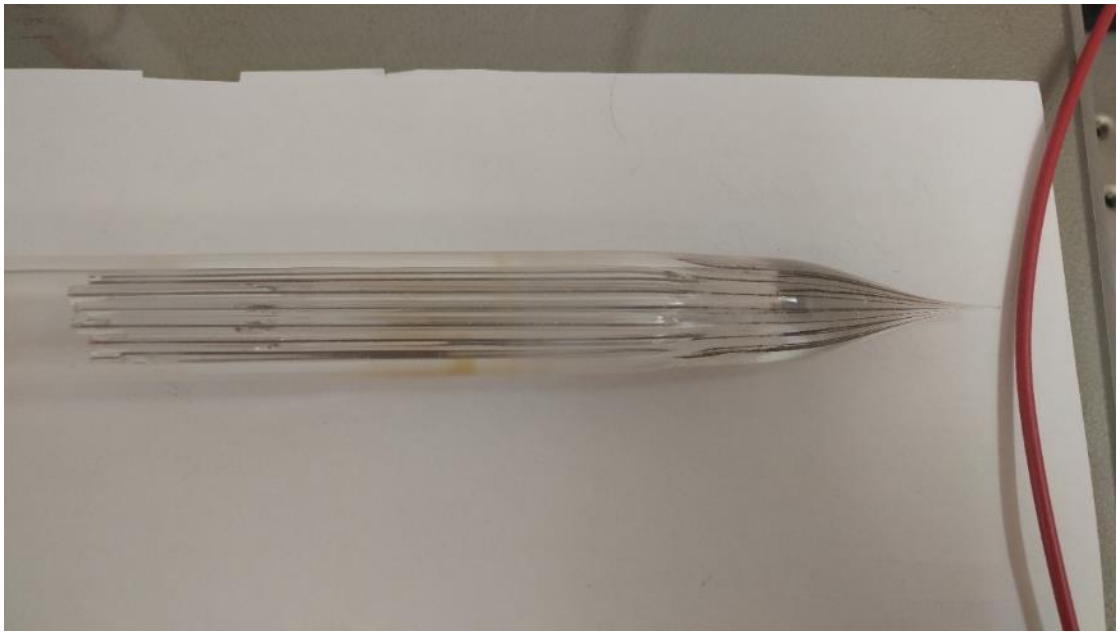

Figure 0-39:SiMF preform after drawing showing collapse of void space and draw down of features around core.

The preform was loaded on the draw tower and vacuum applied to assist in removal of the void spaces in between the various stacked rods. The right side of the preform where the neck down region is located clearly shows no void spaces and clear glass around 14 distinct dark semiconductor regions. Figure 0-40 below shows the fiber produced from this preform in optical microscopy viewed in transmission. With light shining through the fiber, the doped core is clearly visible carrying a high quantity of light.

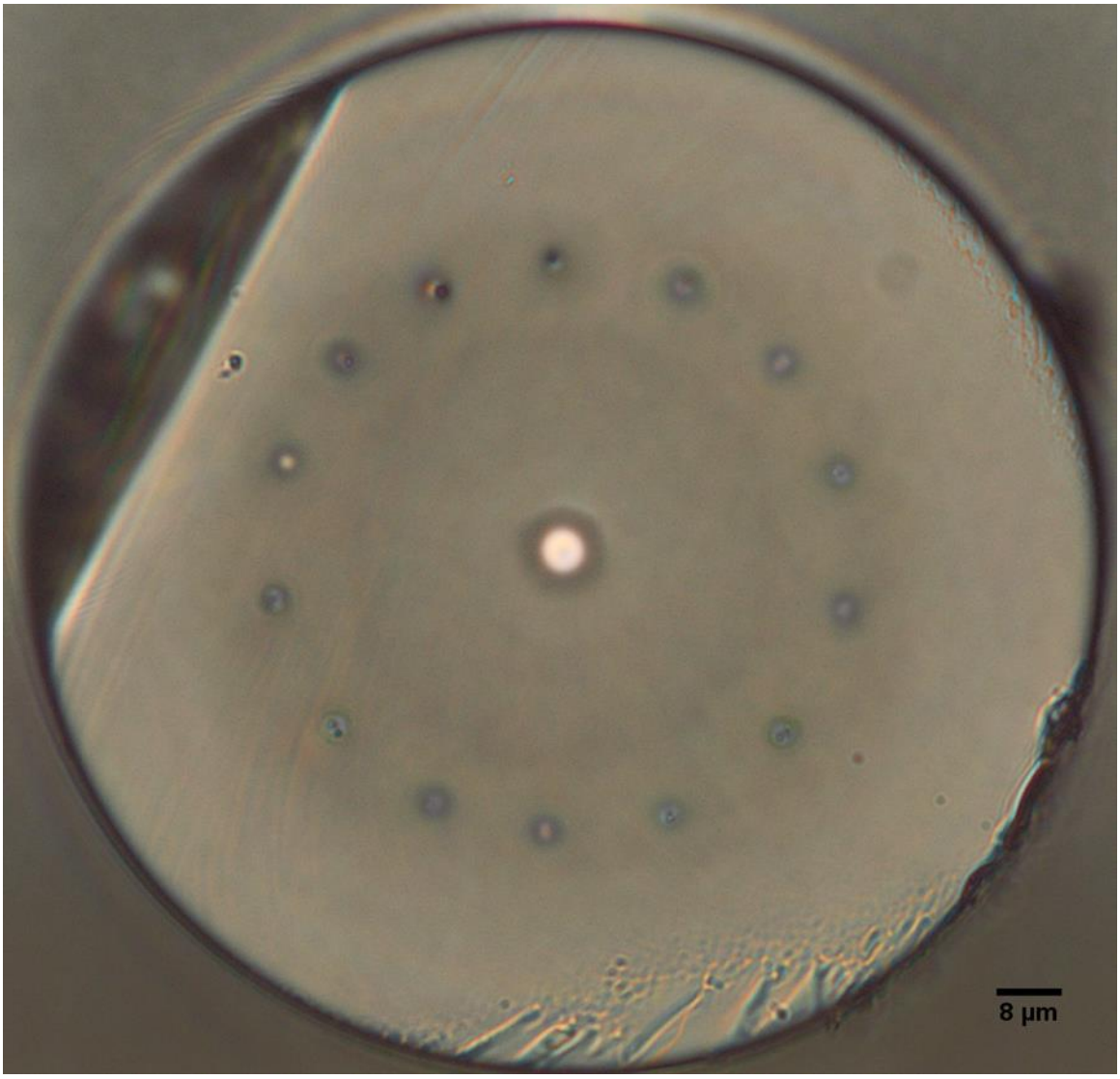

Figure 0-40: Fiber produced from SiMF preform with single mode core present surrounded by 14 semiconductor features.

Surrounding the core are 14 distinct spots reacting with the light being transmitted through the fiber sample. SEM analysis was carried out on the fiber to determine the type of features and sizes present at those locations. Figure 0-41 shows the SEM image.

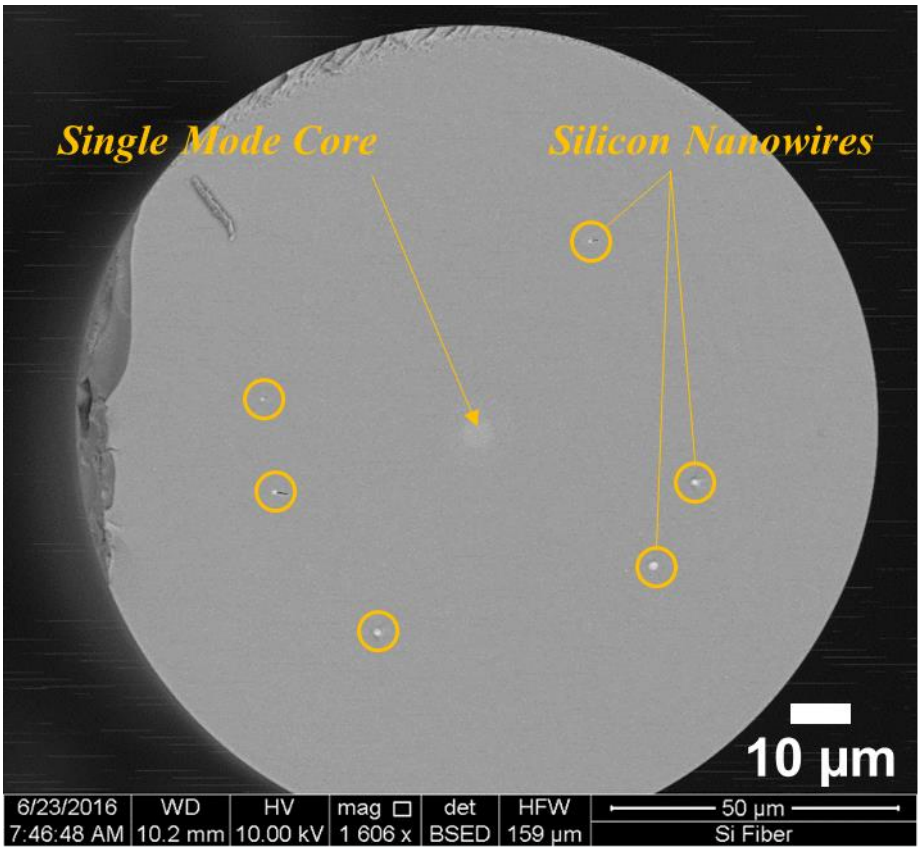

Figure 0-41: SEM of SiMF fiber with nanowires shown in area around single mode core.

SEM showed that instead of regions of nanowires present at the locations individual nanowires were present at the locations observed in optical microscopy. Features were clearly visible at six of the 14 expected locations. The absence of clear features at the other locations may indicate that the features are not consistently present and it is likely that some of the features diffused and formed regions of differing composition capable of interacting with light allowing them to be visible in optical microscopy but not showing up in SEM.

1.8 Analysis of Stress Created by Semiconductor Drawing

Semiconductor fibers were produced over long length scales during this research. Cracking was observed in a variety of fibers with differing sizes and compositions. Understanding the stress

condition that is created when the wires are drawn is necessary to provide the mechanical limits of wire sizes producible. As previously stated the strength of fused silica glass is extremely high, in the gigapascal range, when defects are ~~controlled..~~controlled. The surface produced at the interface with the semiconductors is expected to be extremely high quality with few to no defects indicating that the stress created by the solidifying semiconductor is extremely high.

The stress in the glass can be estimated by assuming that the glass around each semiconductor can be approximated as an independent open-end thick-walled cylinder that doesn't interact with its neighbors. This assumption is made because this is the worst-case scenario for the highest stress at the inside surface of the glass. The stress in the glass for this assumption is governed by the Lamè equations shown below as Equation 5 for the hoop stress and Equation 6 for the radial stress.

$$\sigma_\theta = \frac{r_i^2 P_i - r_O^2 P_O}{(r_O^2 - r_i^2)} + \frac{(P_i - P_O) r_i^2 r_O^2}{(r_O^2 - r_i^2) r^2} \tag{5}$$

$$\sigma_r = \frac{r_i^2 P_i - r_O^2 P_O}{(r_O^2 - r_i^2)} - \frac{(P_i - P_O) r_i^2 r_O^2}{(r_O^2 - r_i^2) r^2} \tag{6}$$

Where r_i and r_o and P_i and P_o represent the inner and outer radii and the internal and external pressures respectively. With the assumption of no external pressure the equation can be simplified and are shown below in Equation 7 and Equation 8.

$$\sigma_\theta = P_i \left[\frac{r_i^2 + r_O^2}{r_O^2 - r_i^2}\right] \tag{7}$$

$$\theta_r = -P_i \tag{8}$$

This stress state indicates that the glass will experience a radial compressive stress equal to the internal pressure while there will be a tensile hoop stress dependent on the tube dimensions.

The relative stress induced by the pressure is graphed below in Figure 0-42.

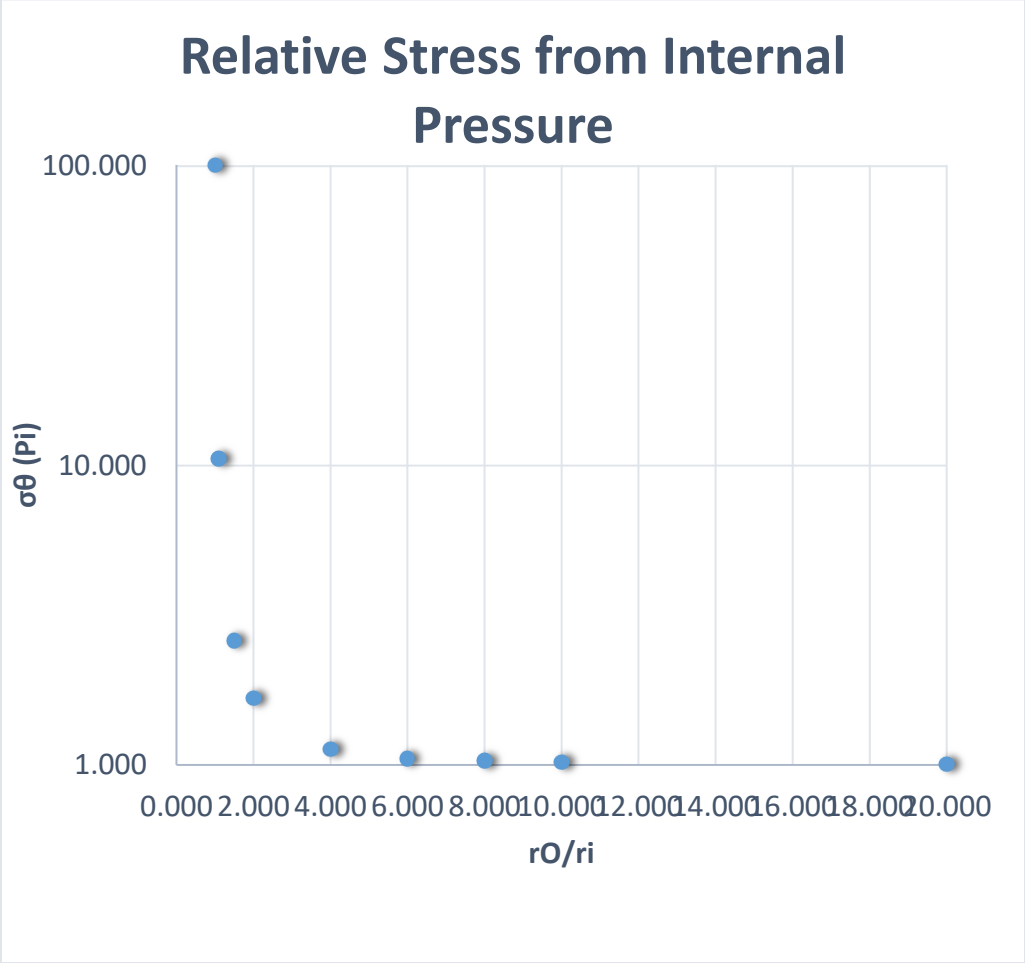

Figure 0-42: Relative stress induced in a thick-walled cylinder from an internal pressure.

This graph provides an easy to see trend in the increase in stress as the glass thickness decreases. The stress caused by the pressure is observed to have an exponential increase and in the case of a very thick tube the stress is equal to the internal pressure.

The internal pressure caused the solidifying semiconductor can be calculated using the elastic constants for silicon and germanium and the known volumetric increase. The elastic constants of silicon and germanium have been previously studied and are readily available.[42, 43] These elastic constants can be used in combination with the Hooke's Law to calculate the stress generated by the volumetric expansion that occurs at solidification. The Young's modulus and Poisson's ratio are 159GPa and 0.228 for silicon and 129GPa and 0.213 for germanium. Combining these values with the volumetric change leads to an estimated pressure generated of 9.8GPa for silicon and 3.7GPa for germanium. These stresses are on the same order of magnitude as the expected strength of the fused silica. These values explain the presence of more cracks in silicon-based samples and high amounts of stress being generated in the glass. These stress values are then expected to reduce as the fiber cool due to the higher thermal expansion values of the semiconductors compared to the glass

1.9 Light Transmission through NW Fibers

Characterization of the fibers by optical microscopy provided some insight into the optical properties of these samples. Samples with microwires were found to be easily visible and provide minimal interference when light was transmitted through the samples. The presence of nanowires in the core were observed to be highly visibly when light was shined on the surface despite being significantly smaller than the wavelength of light incident on the surface. In transmission these nanowires were found to be highly effective at blocking all light transmitted through the core region. Initial attempts to further understand the effects of the wires were accomplished using a traditional optical setup with a broad-spectrum white light source and an optical spectrum analyzer to try to provide a thorough understanding of the optical effects.

Samples for optical testing were 5cm in length and butt-coupled to lead-in fibers for testing. Light can be injected into these fibers with two available lead-in fibers. A SMF with 8μm core or MMF with 50μm. Based on the analysis carried out and shown above, fibers produced in this work have cores ranging from 6-30μm. The MMF fiber is the preferred choice because it is capable of carrying higher power over a much wider wavelength range than the single mode fiber. The limitation of the MMF comes from the size being larger than the sample cores. The short nature of the samples being used allows for a considerable amount of the light to be carried through the plain quartz glass surrounding the core region. Optical transmission testing using the OSA with MMF using both a monochromatic laser light source as well as the white light source showed the signal unchanged whether a sample is present or not. This required all further testing to use the SMF to ensure that the light being observed is only being transmitted through the core. OSA testing with a SMF showed power loss but no spectrum changes with samples, with mostly microwires present, while those samples with nanowires blocked all signal from reaching the detector.

Confirmation of these optical results as well as better understanding of light interactions required the setup shown in Figure 0-5. The Thorlabs Beam Profiler provides the ability to take far field images of samples, which can be used to determine the number of modes transmitted by an optical sample. These samples are not expected to show transmitted modes like a traditional optical fiber though the beam profiler provides useful intensity location maps of the light output from the sample. Fibers from SiGe compositions were selected for optical testing with the beam profiler due to the large quantity of wires and differing sizes present. Figure 0-43 below shows the far field pattern obtained when using MMF as the lead-in fiber.

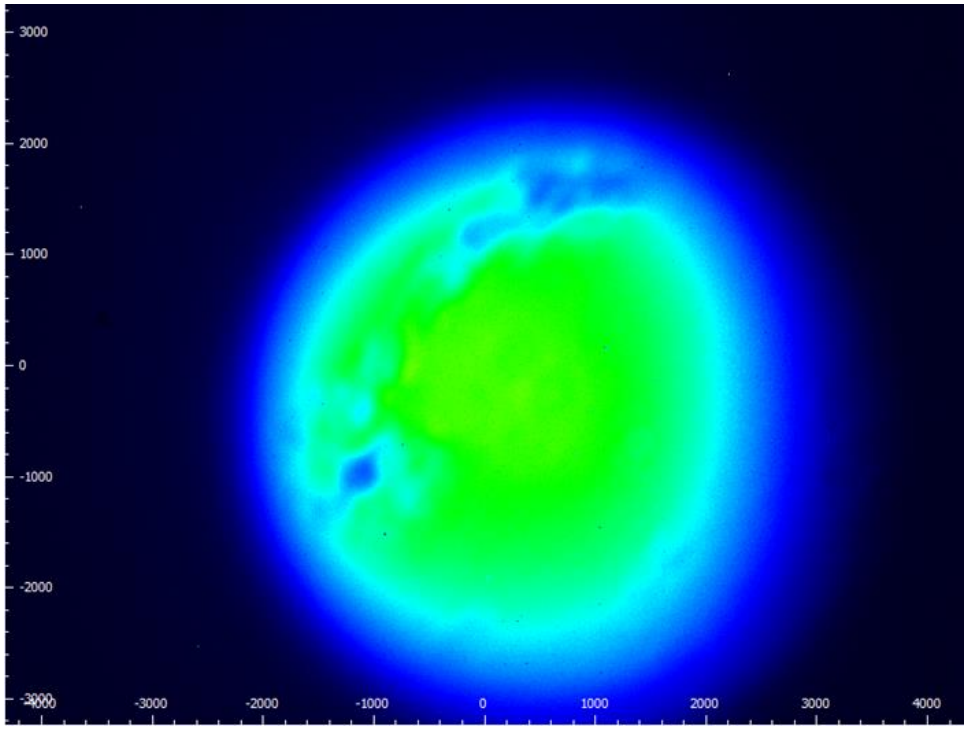

Figure 0-43: Far-Field image from Beam Profiler using MMF to provide light on SiGe sample.

The high intensity of the 532nm laser used in the MMF showed a single intensity spot indicating a lack of higher modes that would normally create a characteristic speckled pattern. No features were visible in the sample while the MMF was used as the lead-in fiber. This confirms the results observed during the testing with OSA showing significant quantity of light transmitting around the core and negating any effects provided by the features in the core.

Figure 0-44 shows the far field image obtained from a fiber from SiGe 2. The fiber had a structure similar to that shown in Figure 0-30.

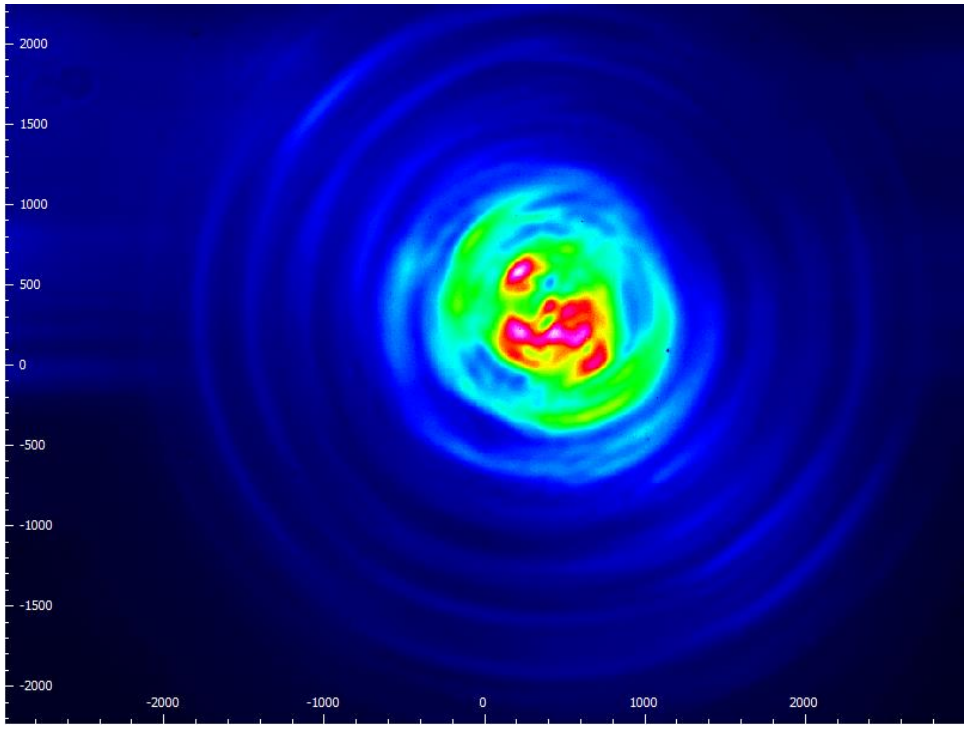

Figure 0-44: Far-field image of SiGe sample from the silicon rich region with few nanowires and higher quantity of microwires.

The far field pattern observed from the silicon rich region of the sample is consistent with the presence of more than a single mode of light with regions of high intensity indicating a possible modal pattern. This pattern is similar to a SMF fiber shone at distance to the Beam Profiler. This signal also indicated that less modes are transmitted through these samples than those from the germanium rich region shown below. This pattern and correlation to semiconductor features makes it difficult to determine the exact effect of the wires on light transmission through the fibers. Figure 0-45 shows the far field image taken from SiGe 4 similar to that in Figure 0-32. The far field image showed drastically different results compared to that of the samples with fewer nanowires. Samples with microwires and few nanowires exhibited areas of high intensity transmission, which was not present in fibers with high quantities of nanowires.

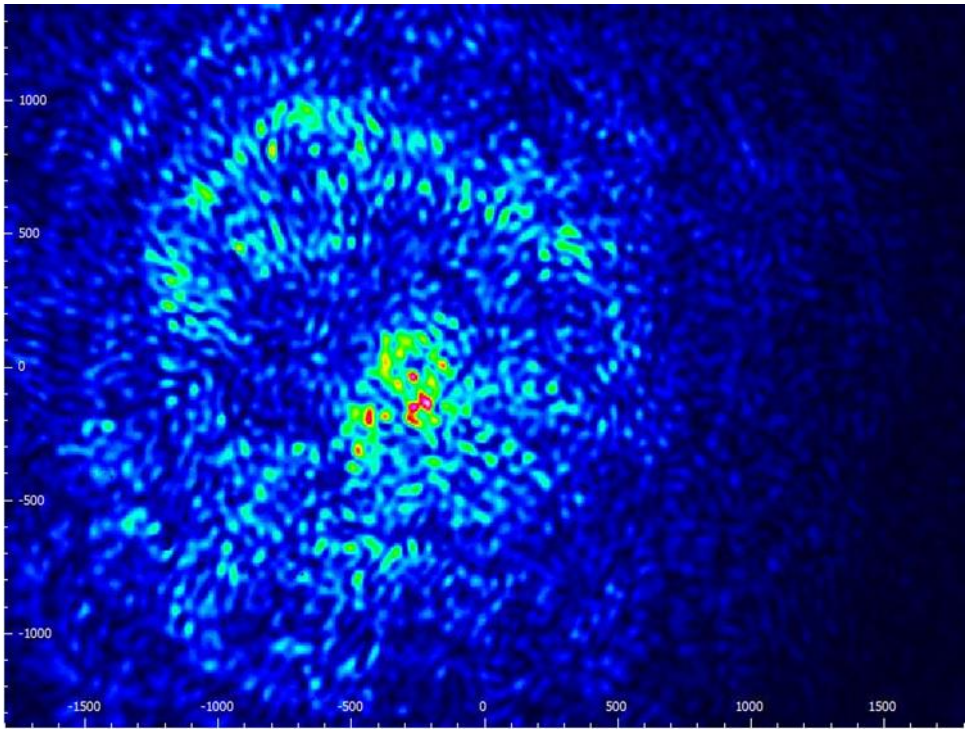

Figure 0-45: Far-field image of SiGe sample from the germanium rich region with high quantity of nanowires present.

The highly speckled pattern of higher intensity is consistent with a far field image with a high number of modes present causing an interference pattern. This could indicate that light has been successfully transmitted through the fiber and has had a strong increase in the number of modes present from the SMF used to inject light into the sample. The correlation of the intensity pattern to the presence of the wires makes it difficult to separate any interaction light may have with the wires and the higher modes of light transmitted in the sample.

The results from the far field images strongly agreed with the observations from optical microscopy. Different behavior was clearly observed from the germanium and silicon rich samples that were tested. The far field patterns suggest that the transmission of light through the samples is possible with the interference pattern suggesting higher modes present in the samples from the germanium rich sample which contained significantly more nanowires. The pattern

from the silicon rich region showed a pattern consistent with fewer modes being transmitted by the fiber. The interference patterns of the modes plus the correlation of the intensity spots to wire locations makes it impossible to determine the exact optical transmission characteristics of the fibers.

The use of the beam profiler and far field patterns has shown that transmission of light through the samples is possible. This information combined with the observations of these samples in optical microscopy indicate complex interactions occurring with light. Transmission has been clearly observed while absorption and scattering have been observed in optical microscopy. Transmission mode analysis with optical microscopy showed clear dark regions on SiGe samples indicating that the semiconductor features are capable of blocking a majority of light coming through the core through a combination of absorption and scattering. Reflected light in optical microscopy confirms that scattering is occurring with size having an effect. The samples are illuminated with white light and yet different size particles clearly appear as different colors demonstrating a size dependent effect on what wavelengths are scattered.

1.10 Electrical Characterization of Fibers

1.10.1 Light Generation in Fibers

Determining the potential for light generation in these semiconductor features was done using an applied voltage. The extremely small cross-sectional area of conductive materials required that several fibers be connected in parallel to allow for a measurable resistance. It was found by trial and error that for all samples those measurable values were obtained using 15 sections of fiber. Applied voltage tests were carried out on samples from the Si BO1, Si PN, and SiGe preforms.

Fibers were selected and viewed using optical microscopy to ensure wires were present in all sections prior to testing. The fibers were placed on a glass slide and connected to copper wires using liquid gallium. The photodetector was then placed approximately 1 cm above the samples, the closest possible while avoiding electrical contact. Testing was done in a dark room and a background signal was recorded for each sample. Voltage was then powered on and increased from 50-2000V while monitoring the output of the photodetector. In the case of all samples, no change in signal was observed from the photodetector.

Measuring no signal from the samples does not eliminate light being produced in the fiber samples. Multiple factors in the semiconductor features could lead to no light being measured. Light has been successfully generated in arrays of silicon nanowires in the work by Huo (2004) in the range of 600nm.[18] Difference between these wires that successfully generated light and those produced in this work are present in both the diameter and lengths of the wires produced. The wires produced in this work were predominately sized in the 20-100nm and larger with lengths in the hundreds to thousands of microns. This differs greatly from the approximately 5nm diameter wires with lengths less than ten microns used to generate light. These factors indicate that wires produced in this work are not ideal for light generating applications without additional process controls to further control the wire sizes. It is likely that the primary cause is due to the very limited surface area of semiconductor present in the fibers for enough light to be generated and then successfully transmitted through the glass cladding.

1.10.2 Measurement of Photocurrent

In the opposite direction of generating light using electrical sources, light was used to generate electrical current in the samples. The very small features of the semiconductor require the ability

to measure extremely small currents so a picoammeter was used for the measurements. Photocurrent measurements were carried out on the four sample regions taken from the SiGe preform as well as SMF to provide a "control" comparison to glass fibers. These fibers were selected for this experiment due to having the smallest wires and highest quantities of wires. The fibers were aligned in the same manner with fifteen sections parallel on a glass slide connected using gallium metal to copper leads. The fibers were then connected to the low power DC power supply capable of supplying voltage down to 14mV with the picoammeter connected in series behind the sample arrays. The minimum voltage was applied and the current measured with the picoammeter. The voltage was then turned off and the current allowed to decay to a stable level. The light for measurement is then applied via 100W halogen light. The current is then recorded. The increase current is the measured photocurrent. Table 0-3 below summarizes the voltage and measured current of the samples.

Table 0-3: Summary of measured photocurrent from SiGe samples.

Sample	$V_{Applied}$(V)	$I_{Measured}$(nA)	$I_{Power\ Off}$ (nA)	$I_{Light\ Applied}$ (nA)	$I_{Photocurrent}$ (nA)
SMF Fiber	0.014	0	0	0	0
SiGe #1	0.014	2070	2.5	10.8	8.3
SiGe #2	0.014	355	2.1	3.9	1.8
SiGe #3	0.014	120.5	2.5	4.2	1.7
SiGe #4	0.014	42.5	1.8	3.4	1.6

After removal of the light source, the current quickly decayed back to the previously measured value. This experiment was repeated multiple times to ensure no chance of random measurement error being the source of the photocurrent.

The measured photocurrent was found to vary across the varying compositions from the SiGe preform. The samples providing the highest measured current were those from the 100% silicon

with all of the mixed compositions having approximately a fourth of the photocurrent. In addition to this difference, the silicon samples were found to have an order of magnitude lower resistance than the other samples.

Based on the semiconductor properties of silicon and germanium this trend of lower resistance and higher current from the silicon samples compared to those with higher germanium concentrations is unexpected. The much lower resistivity of germanium should allow for much lower resistance with equal surface areas present. This indicates that the difference observed in the samples is a not due to the composition of wires but due to the number of wires participating in conduction. The wires observed after removal from fibers showed smaller wires both in length and diameter in those from the germanium samples. The cause of the higher resistance and lower photocurrent is caused by fewer wires participating in the conduction in the samples. Composition has a distinct effect on the photocurrent generated by the sample but the effect is from the extrinsic properties of the wires rather than the intrinsic properties of a given composition. It is clear that germanium rich regions produce higher quantities of wires at smaller sizes compared to the silicon rich regions. This results in a lower total cross-sectional area of semiconductor to participate in the electrical testing combined with observed shorter lengths after etching results in higher measured resistance despite a lower intrinsic resistivity.

1.10.3 I-V Characteristics of SiGe Samples

The picoammeter was used to measure the minute currents in the samples of the SiGe samples over a range of applied voltages to allow for the resistance of those samples. Figure 0-46 below shows the I-V curves collected from the SiGe samples.

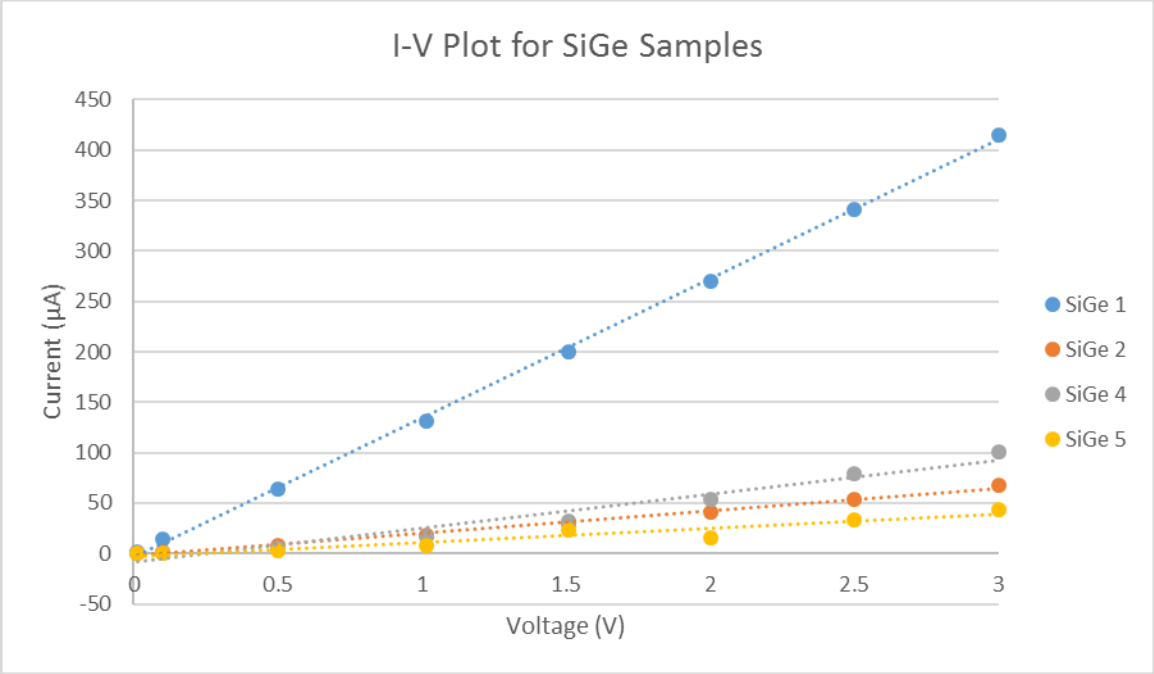

Figure 0-46: I-V curves and fitted lines for the four SiGe samples.

The mixed compositions were found to have very similar behavior while the pure silicon samples showed radically different behavior. In the case of all four samples the I-V relationship was clearly linear with the fits all having R^2 values above 0.9. With the observed linear relationship between current and voltage it allows us to use Ohm's law to calculate the resistance. The resistance values are obtained as the inverse of the slope of the fit lines on the I-V plot. The calculated values from the bulk resistivity as well as the measured resistance from the I-V plots are summarized in Table 0-4 below.

Table 0-4: Summary of Resistances and Resistivity of SiGe alloy samples.

Sample	**Bulk Resistivity (Ω-m)[1, 44, 45]**	**Estimated Resistance (Ω)**	**Measured Resistance (Ω)**	**Calculated Resistivity (Ω-m)**
SiGe 1	2300	1.332E+10	7251.106	0.000850357
SiGe 2	1954.96	8.287E+10	29756.591	0.000702021
SiGe 4	471.85	4.477E+10	44877.261	0.000472938
SiGe 5	326.99	6.950E+10	72400.811	0.000344661

The table above summarizes bulk values of the resistivity for the compositions of the SiGe alloys. The values for the alloys were interpolated based on the reported literature values of silicon and germanium and the linear relationship of properties of these alloys. The estimated resistance was then calculated based on the resistivity values and an estimated cross-sectional area of the samples and the measured length of the samples. The cross-sectional area was estimated using the "analyze particles" feature of ImageJ that results were already presented in the previous section. The feature calculates the area of the wires of the sample fibers shown in the previous sections. The fibers used in these tests had similarly observed features as to those in the sample images. The calculated area is then multiplied by fifteen, the number of fibers used in these tests to provide a total estimated cross-sectional area. With this same cross-sectional area and length, the resistivity of the material was calculated based on the measured resistance of the samples.

The estimated resistance was found to be in the giga-ohm range and up, high enough to impede any current flow. This information directly contradicts the successfully measured current in all samples even at very low applied voltages. This provides us with the understanding that these nanowires have unique properties that radically differ from the bulk values. The resistivity values calculated from the measured resistance were found to be six to seven orders of magnitude lower than those of the bulk values. This resistivity is plotted against composition in Figure 0-47 below.

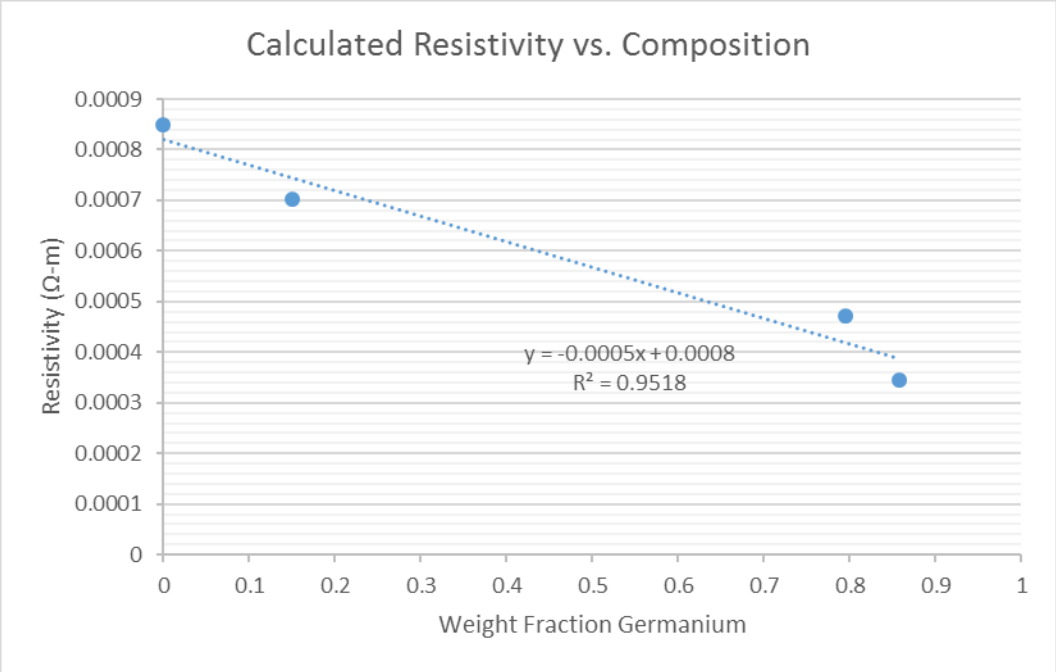

Figure 0-47: Calculated resistivity from measured resistance vs germanium concentration with linear fit line.

This calculated resistivity was found to still have a nearly linear relationship with respect to composition. This value while orders of magnitude lower has the exact same relationship as resistivity in the bulk alloys. This value is much closer to the reported resistivity of 0.0085 Ω-m calculated from a single undoped silicon nanowire.[28] That work suggested that the much lower resistivity was due to surface conduction and a thin layer of surface silicon dioxide passivating the surface This surface conductivity is speculated to be the cause of lower resistance rather than electrical conduction through the bulk of the nanowire. All nanowires produced in this work are inherently surrounded by silicon dioxide and it is likely this mechanism is allowing for decreased resistivity in these samples as well. The measured values still resulted in values an order of magnitude lower but error is likely in both the length and estimated area used in the calculations. The length and area assume that all wires participate and extend the full length of the fiber which

does not agree with the lengths of wires observed after removing with etching. The estimated area has error caused by the limitation of the resolution of the lower magnification images used to calculate the area of all wires in the core regions.

Conclusions

In this research, a mixed powder method previously used by Ayers (1993) to produce arrays of microwires was modified to allow for an inherently safe and reliable method to manufacture semiconductor nanowires. This research worked to develop an understanding of the preform and drawing conditions necessary to reliably produce fibers of sizes used in traditional fiber optic applications with unique nanofeatures. A discussion of the current semiconductor nanowire methods is given with limitations and issues involved. The benefits of using silicon and germanium nanowires was discussed with emphasis on the change of properties from their bulk properties. The benefits of improved absorption and shift to the more useful direct bandgap structure was discussed. Optical and electrical testing of these nanowires was unable to confirm the transition from the bulk indirect band gap behavior to the more useful direct behavior but a clear difference from the bulk properties was observed. In addition to the production of pure elemental semiconductor features, this work was able to produce SiGe alloy wires in optical fiber. An analysis of the optical and electrical properties of these in fiber produced wires was carried out to evaluate the use of these structures to provide useful interactions between light and electricity in fibers. A method for removing these wires from the glass matrix and recovering them was developed using etching.

Fibers ranging from 100-200μm were reliably produced with a variety of core compositions. Silicon and germanium features, which had previously been produced as single features on a microscale, were produced in large quantities at much smaller sizes than previously reported. Wires were also produced over a range of compositions of SiGe alloy from a mixture of the two powders for the first time in an optical fiber.

Size and composition of the source mixed powders have a direct effect on both the quantity and sizes of the wires produced. An upper and lower limit of semiconductor concentrations capable of producing nanowires was determined. A thorough analysis of wire sizes and shapes was carried out using SEM and optical microscopy. Analysis of the wire distributions provided a clear understanding of the sizes produced in relation to the composition of the wires being made. Samples made of pure germanium and from the germanium rich end of SiGe samples produced high quantities, more than 75, with diameters below 100nm. Samples from the pure silicon preforms and the silicon rich regions were found to have fewer small wires and larger microwires more frequent. Wire size was found to be dependent more on powder concentration than the maximum powder particle size. Fibers produced with more than 25 weight percent semiconductor were found to show fewer wires, less than fifty wires while those produced with the same powders but at concentrations at or below 25 weight percent were found to have over 150 wires and half of them below the desired 100nm diameter.

A method of producing a preform and successfully drawing fiber that includes a light guiding core as well as semiconductor nanowires was developed. This method allows for precise control of semiconductor nanowire locations and integration with other features in an optical fiber. Fiber was produced with a small light guiding core with 14 distinct semiconductor features in the cladding.

The optical properties of these wire arrays were measured using a variety of techniques to provide an understanding of possible uses and applications of these wires. Nanowire samples were found to have complex interactions with light with absorption, scattering, reflection, and transmission all being observed in these samples. Microwires were found to clearly reflect

incident light in microscopy. Samples from the SiPN and SiGe fibers with high concentrations of nanowires were found to be successful at absorbing light and limiting transmission when exposed to white light from the microscope. Scattering was observed in these samples when viewed in optical microscopy with reflected light. Submicron features were visible and appeared as different colors indicating a clear dependence of size and the light scattered by those features. Use of the beam profiler and far field patterns allow for us to observe transmitted light and different modal behavior depending on the size and distribution of the wires.

Electrical testing was done to understand possible interactions between light and electricity for photonic applications of these structures. Photocurrent was successfully measured from a variety of SiGe nanowire structures in an optical fiber for the first time. Electrical testing allowed for collecting current data with applied voltage and I-V plots to be made. This information allowed for calculating the resistance of the SiGe samples used in the electrical testing. The intrinsic resistivity was found to be more than five orders of magnitude lower than the bulk reported values of resistivity. This drastic increase is conductivity is speculated to be caused by surface conductivity at the semiconductor-silicon dioxide interface.

The new contributions to the body of literature in this field of semiconductor nanowires and photonics are summarized below:

- Expanded on the previously used mixed powder method for a novel way to produce high quantities of highly oriented high aspect ratio nanowires in an inherently safe way.
    - Determined the optimized range of the powder sizes and concentrations necessary to reliably produce wires below the target 100nm size.

    - Development of a method that allows for nanowires to be produced completely encapsulated in glass greatly reducing exposure to nanoparticles.
    - Developed preforms that allow for the composition of wires to be changed over the length of the fiber
- Production of SiGe alloy nanowires in an optical fiber for the first time
    - Wires produced across a wide compositional range from pure silicon to pure germanium.
    - Determined size and distribution relationship with composition
- Produced a structured fiber allowing precise control of semiconductor feature regions and integration with traditional optical fiber structures.
    - Fiber successfully produced with 14 semiconductor features around a small light guiding core.
- Developed understanding of the optical and electrical properties of these arrays.
    - Determined the effects of both nanowires and microwires on the transmission of light through these arrays.
    - Successfully measured photocurrent from nanowires isolated in glass fibers for the first time.
    - Obtained I-V plots for SiGe alloy wires and calculated intrinsic resistivity based on the measured resistance.
    - Observed resistivity to have a linear behavior across the silicon germanium composition range.

    - Electrical resistivity was found to be orders of magnitude lower than the expected value calculated with bulk values
- Developed an understanding for use of HF acid etching to remove wires from the glass matrix and recover them.
    - Determined necessary concentrations to remove both silicon and germanium wires from the glass matrix and recover the wires.
    - Observed higher etch rates and differing etch behavior based on presence of wires and concentration of HF.

Future Work

This work was successful in producing a wide variety of semiconductor nanowires in using optical fiber drawing techniques. The wires produced were found to have numerous interactions with light and present several interesting photonic application opportunities. Future research opportunities made available by this research are below:

- Optimization of powder shape and size distribution to further eliminate microwires and produce higher quantities of nanowires.
- Possible integration into solar cell applications due to photocurrent generation.
- Exploration of high optical absorption of nanowires for use in optical fiber sensors.
- Evaluation of strain states in structure to modify the electrical properties of the semiconductor wires present.
- Extension of the drawing process to produce nanowires of other materials such as copper, nickel, metglas.

References

1. Kasap, S.O., *Principles of Electronic Materials and Devices*. 2002: McGraw-Hill.
2. Law, M., J. Goldberger, and P. Yang, *Semiconductor nanowires and nanotubes.* Annu. Rev. Mater. Res., 2004. **34**: p. 83-122.
3. Ballato, J., et al., *Advancements in semiconductor core optical fiber.* Optical Fiber Technology, 2010. **16**(6): p. 399-408.
4. Scott, B., et al., *Fabrication of silicon optical fiber.* Optical Engineering, 2009. **48**(10): p. 100501-100501-3.
5. Scott, B., et al., *P-Type Silicon Optical Fiber.* Advances in Synthesis, Processing, and Applications of Nanostructures: Ceramic Transactions, 2012. **238**: p. 103-107.
6. Scott, B.L. and G.R. Pickrell, *Silicon optical fiber diameter dependent grain size.* Journal of Crystal Growth, 2013. **371**: p. 134-141.
7. Scott, B.L., K. Wang, and G. Pickrell, *Fabrication of n-type silicon optical fibers.* IEEE Photonics Technology Letters, 2009. **21**(24): p. 1798-1800.
8. Ayers, J.D., *Glass fibres with fine conducting cores.* Journal of Materials Science, 1993. **28**(9): p. 2337-2346.
9. Kawamura, Y., et al., *Direct-gap photoluminescence from germanium nanowires.* Physical Review B, 2012. **86**(3): p. 035306.
10. Nolan, M., et al., *Silicon nanowire band gap modification.* Nano letters, 2007. **7**(1): p. 34-38.
11. Harris, C. and E. O'Reilly, *Nature of the band gap of silicon and germanium nanowires.* Physica E: Low-dimensional Systems and Nanostructures, 2006. **32**(1): p. 341-345.
12. Abstreiter, G., *Chapter 2 Band Gaps and Light Emission in Si/SiGe Atomic Layer Structures*, in *Semiconductors and Semimetals*, J.L. David, Editor. 1997, Elsevier. p. 37-76.
13. Menéndez, J. and J. Kouvetakis, *Type-I Ge/Ge 1-xy Si x Sn y strained-layer heterostructures with a direct Ge bandgap.* Applied physics letters, 2004. **85**(7): p. 1175-1177.
14. Lockwood, D.J., *Chapter 1 Light Emission in Silicon*, in *Semiconductors and Semimetals*, J.L. David, Editor. 1997, Elsevier. p. 1-35.
15. Yang, J.-E., et al., *Band-Gap Modulation in Single-Crystalline Si1-x Ge x Nanowires.* Nano letters, 2006. **6**(12): p. 2679-2684.
16. Nam, D., et al., *Electroluminescence from strained germanium membranes and implications for an efficient Si-compatible laser.* Applied Physics Letters, 2012. **100**(13): p. 131112.
17. Sánchez-Pérez, J.R., et al., *Direct-bandgap light-emitting germanium in tensilely strained nanomembranes.* Proceedings of the National Academy of Sciences, 2011. **108**(47): p. 18893-18898.
18. Huo, J., et al., *Electroluminescence from silicon nanowires.* Nanotechnology, 2004. **15**(12): p. 1848.
19. Yan, J.-A., L. Yang, and M. Chou, *Size and orientation dependence in the electronic properties of silicon nanowires.* Physical Review B, 2007. **76**(11): p. 115319.

20. Hong, K.-H., et al., *Strain-driven electronic band structure modulation of Si nanowires.* Nano letters, 2008. **8**(5): p. 1335-1340.
21. Zhang, F., V.H. Crespi, and P. Zhang, *Prediction that Uniaxial Tension along⟨111⟩ Produces a Direct Band Gap in Germanium.* Physical review letters, 2009. **102**(15): p. 156401.
22. Olesinski, R.W. and G.J. Abbaschian, *The Ge−Si (Germanium-Silicon) system.* Bulletin of Alloy Phase Diagrams, 1984. **5**(2): p. 180-183.
23. Jifeng, L., C.K. Lionel, and M. Jurgen, *Monolithic Ge-on-Si lasers for large-scale electronic–photonic integration.* Semiconductor Science and Technology, 2012. **27**(9): p. 094006.
24. Shiri, D., et al., *Strain induced change of bandgap and effective mass in silicon nanowires.* Applied Physics Letters, 2008. **93**(7): p. 073114.
25. Cheng, T.-H., et al., *Strain-enhanced photoluminescence from Ge direct transition.* Applied Physics Letters, 2010. **96**(21): p. 211108.
26. Hu, L. and G. Chen, *Analysis of optical absorption in silicon nanowire arrays for photovoltaic applications.* Nano letters, 2007. **7**(11): p. 3249-3252.
27. Cui, Y., et al., *Doping and electrical transport in silicon nanowires.* The journal of physical chemistry B, 2000. **104**(22): p. 5213-5216.
28. Bauer, J., et al., *Electrical properties of nominally undoped silicon nanowires grown by molecular-beam epitaxy.* Applied physics letters, 2007. **90**(1): p. 012105.
29. Hochbaum, A.I., et al., *Enhanced thermoelectric performance of rough silicon nanowires.* Nature, 2008. **451**(7175): p. 163-167.
30. Gu, G., et al., *Growth and electrical transport of germanium nanowires.* Journal of Applied Physics, 2001. **90**(11): p. 5747-5751.
31. Ballato, J., et al., *Silica-clad crystalline germanium core optical fibers.* Optics Letters, 2011. **36**(5): p. 687-688.
32. Romaniuk, R., *Tensile strength of tailored optical fibres.* 2000. **8**: p. 101-116.
33. Ballato, J., et al., *Glass-clad single-crystal germanium optical fiber.* Optics express, 2009. **17**(10): p. 8029-8035.
34. Keck, P.H. and W. Van Horn, *The Surface Tension of Liquid Silicon and Germanium.* Physical Review, 1953. **91**(3): p. 512-513.
35. Kaiser, N., et al., *Wetting angle and surface tension of germanium melts on different substrate materials.* Journal of Crystal Growth, 2001. **231**(4): p. 448-457.
36. Cröll, A., et al., *Wetting angles and surface tension of Ge1−xSix melts on different substrate materials.* Journal of Crystal Growth, 2002. **242**(1): p. 45-54.
37. Sazio, P.J.A., et al., *Microstructured Optical Fibers as High-Pressure Microfluidic Reactors.* Science, 2006. **311**(5767): p. 1583-1586.
38. Rahaman, M.N., *Ceramic Processing*. 2006: Taylor & Francis.
39. Nolan, G. and P. Kavanagh, *The size distribution of interstices in random packings of spheres.* Powder technology, 1994. **78**(3): p. 231-238.
40. Williams, K.R., K. Gupta, and M. Wasilik, *Etch rates for micromachining processing-Part II.* Journal of microelectromechanical systems, 2003. **12**(6): p. 761-778.
41. Williams, K.R. and R.S. Muller, *Etch rates for micromachining processing.* Journal of microelectromechanical systems, 1996. **5**(4): p. 256-269.

42. Hull, R. and INSPEC, *Properties of Crystalline Silicon*. 1999: INSPEC, the Institution of Electrical Engineers.
43. Wortman, J.J. and R.A. Evans, *Young's Modulus, Shear Modulus, and Poisson's Ratio in Silicon and Germanium.* 1965. **36**(1): p. 153-156.
44. Sze, S.M. and K.K. Ng, *Appendix F Properties of Important Semiconductors*, in *Physics of Semiconductor Devices*. 2006, John Wiley & Sons, Inc. p. 789-789.
45. Kasper, E., *Properties of strained and relaxed silicon germanium*. 1995: INSPEC, Institution of electrical engineers London.